

**PREPARATION OF ELECTROSPUN NANOFIBERS AND
MICROPARTICLES OF POLYLACTIDE
(CO)POLYMERS AND QUATERNIZED CELLULOSE**

BY

NARUMON JONGMANWATTANA

**A THESIS SUBMITTED IN PARTIAL FULFILLMENT OF
THE REQUIREMENTS FOR THE DEGREE OF MASTER OF
ENGINEERING (ENGINEERING TECHNOLOGY)
SIRINDHORN INTERNATIONAL INSTITUTE OF TECHNOLOGY
THAMMASAT UNIVERSITY
ACADEMIC YEAR 2016**

**PREPARATION OF ELECTROSPUN NANOFIBERS AND
MICROPARTICLES OF POLYLACTIDE
(CO)POLYMERS AND QUATERNIZED CELLULOSE**

BY

NARUMON JONGMANWATTANA

**A THESIS SUBMITTED IN PARTIAL FULFILLMENT OF
THE REQUIREMENTS FOR THE DEGREE OF MASTER OF
ENGINEERING (ENGINEERING TECHNOLOGY)**

SIRINDHORN INTERNATIONAL INSTITUTE OF TECHNOLOGY

THAMMASAT UNIVERSITY

ACADEMIC YEAR 2016

PREPARATION OF ELECTROSPUN NANOFIBERS AND MICROPARTICLES
OF POLYLACTIDE (CO)POLYMERS AND QUATERNIZED CELLULOSE

A Thesis Presented

By

NARUMON JONGMANWATTANA

Submitted to

Sirindhorn International Institute of Technology

Thammasat University

In partial fulfillment of the requirements for the degree of
MASTER OF ENGINEERING (ENGINEERING TECHNOLOGY)

Approved as to style and content by

Advisor and Chairperson of Thesis Committee



(Asst. Prof. Dr. Paiboon Sreearunothai)

Co-Advisor



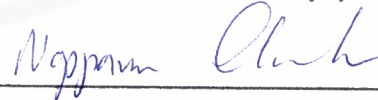
(Dr. Kittiwut Kasemwong)

Committee Member and
Chairperson of Examination Committee



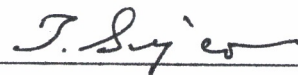
(Assoc. Prof. Dr. Pakorn Opaprakasit)

Committee Member



(Assoc. Prof. Dr. Noppavan Chanunpanich)

Committee Member



(Prof. Dr. Takeshi Serizawa)

MAY 2017

ACKNOWLEDGEMENTS

First and foremost, I would like to thank you to the Advanced and Sustainable Environmental Engineering of TAIST-Tokyo Tech program and Sirindhorn International Institute of Technology (SIIT), Thammasat University for providing me a valuable opportunity to doing the research.

I place on record, my sincere thank you to Assoc. Prof. Dr. Pakorn Opaprakasit for providing one of the most valuable opportunities in my life. I am extremely thankful to him for sharing his expertise, and valuable and sincere guidance, and all his supporting to extended my opportunities. I would like to express my sincerely thanks to my co-advisor Dr. Kittiwut Kasemwong, who is a researcher from National Nanotechnology Center, for all supports of my master study and related research, for his motivation, patience, and extensive knowledge. I could not have imagined having a better mentor for my general life and study. I would like to thanks to Prof. Dr. Takeshi Serizawa, my co-advisor from Tokyo Institute of Technology for providing me useful and informative comments. I would also like to acknowledge Assoc. Prof. Dr. Noppavan Chanunpanich. I was always appreciated that the door to her office were always open whenever I had questions or ran into trouble spots about my research. She steered me in the right direction whenever I needed. I would like to thank my advisor Asst. Prof. Dr. Paiboon Sreearunothai for his encouragement and comments, but also for some hard questions making me widen my research. My sincere thank goes to Dr. Atitsa Petchsuk, a researcher from National Metal and Materials Technology Center for providing me to access to laboratory facilities.

My special thanks go to Ms. Chonlada Suwanboon from King Mongkut's university of technology north Bangkok, and all staffs from Nano-Agro and Food Innovation laboratory in National Nanotechnology Center for stimulating discussions and for giving me spiritual supports over my years of study and my life in general.

Last but not the least, I would like to express my very deeply gratitude to my family and to my friends for giving me continuous encouragement and spiritual support over my years of study.

This achievement would not have been done without all of them. Thank you very much.

Abstract

PREPARATION OF ELECTROSPUN NANOFIBERS AND MICROPARTICLES OF POLYLACTIDE (CO)POLYMERS AND QUATERNIZED CELLULOSE

by

NARUMON JONGMANWATTANA

Master of Engineering (Engineering Technology), Sirindhorn International Institute of Technology, Thammasat University, 2017

Quaternized cellulose (QC) has been prepared by treating cellulose derived from de-starch cassava pulp with glycidyl trimethyl ammonium chloride (GTMAC) under semi-dry process at various GTMAC-to-anhydroglucose unit (AGU) molar ratios, ranging from 1 to 3. The QC at various GTMAC contents were then characterized to provide an optimal content of GTMAC at QC [2:1]. The optimal QC suspension introduced antibacterial activity against both Gram-positive and –negative bacteria. The QC aqueous suspension was further mechanically treated by passing through a microfluidizer to obtain optically transparent gel-like aqueous suspension of quaternized cellulose nanofibrils (QCNF). For specific use in biomedical applications, QC powder, QC and QCNF suspension were incorporated into polylactide (PLA) via various techniques, producing microparticles and nanofibers. Microparticles were successfully generated by a phase inversion emulsification (PIE) method and then passing through a microfluidizer. PLA nanofiber composites incorporated with QC and QCNF were produced by blend electrospinning of PLA/QC, and coaxial electrospinning of PLA/QCNF.

Keywords: quaternized cellulose, polylactide, electrospun nanofibers, microparticles

Table of Contents

Chapter	Title	Page
	Signature Page	i
	Acknowledgements	ii
	Abstract	iii
	Table of Contents	iv
	List of Figures	ix
	List of Tables	xiii
1	Introduction	1
	1.1 Background	1
	1.2 Objectives	3
2	Literature Review	5
	2.1 Antibacterial agents	5
	2.1.1 Lower molecular weight of inorganic and organic antibacterial agents	7
	2.1.2 Higher molecular weight of antibacterial agents	8
	2.2 Synthetic antibacterial polymeric materials	8
	2.2.1 Antibacterial polymers	8
	2.2.2 Antibacterial surface modification	9
	2.3 Cellulose	10
	2.3.1 Sources	10
	2.3.2 Structure and chemistry	11
	2.3.2.1 Degree of polymerization	13
	2.3.2.2 Crystalline index	13
	2.3.3 Reaction	13

2.3.3.1	General Consideration	13
2.3.3.2	Etherification	14
2.4	Nanocellulose	15
2.4.1	Cellulose nanocrystals	16
2.4.2	Cellulose nanofibrils	16
2.4.3	Bacterial nanocellulose	16
2.5	Microparticles	17
2.5.1	Microparticles from linear polymers	17
2.5.2	Microparticles synthesis from radical polymers	18
2.6	Phase inversion emulsification	21
2.7	Poly (lactic acid- <i>co</i> -glycidyl methacrylate) (PLLA- <i>co</i> -GMA) copolymers	21
2.8	Electrospun nanofibers	22
2.8.1	History of electrospinning	22
2.8.2	Fundamental Aspects	24
2.8.3	Parameter studies	25
2.8.4	Techniques of Electrospinning for controlling location of active agents	26
2.8.4.1	Blend electrospinning	26
2.8.4.2	Coaxial electrospinning	26
2.8.4.3	Emulsion electrospinning	27
2.9	Polylactic acid (PLA)	28
3	Experimental Approach	29
3.1	Materials	29
3.2	Methodology	30
<u>Section I</u>	Preparation and characterization of quaternized cellulose	30
(1)	Preparation of cellulose from de-strach cassava pulp	30
(1.1)	Alkali treatment	31
(1.2)	Bleaching treatment	31
(1.3)	Spray drying process	31

(2) Preparation of quaterized cellulose nanofibrils	32
(2.1) Optimization of GTMAC contents for preparation of quaternized cellulose under a semi-dry process	32
(2.2) Nanofibrillation of quaternized cellulose by a microfluidizer	33
(3) Characterization of DCP, cellulose and QC	33
(3.1) Fourier transform infrared spectroscopy	33
(3.2) Solid-state CP/MAS ¹³ C NMR spectroscopy	33
(3.3) X-ray diffraction analysis	33
(3.4) Nitrogen contents	34
(3.5) Antibacterial activity evaluation	34
<u>Section II</u> Preparation and characterization of microparticles of PLLA- <i>co</i> -GMA copolymers and quaternized cellulose	35
(1) Preparation of microparticles by a suspension curing process	35
(1.1) Microparticle formation	35
(1.1.1) Microparticle formation from QC powder via phase inversion emulsification method	35
(1.1.2) Microparticle formation from QC or QCNF suspension via phase inversion emulsification method and microfluidizer	36
(1.2) Washing process	37
(2) Characterization of microparticles	37
(2.1) Fourier transform infrared spectroscopy	37
(2.2) Scanning electron microscopy	38
(2.3) Laser scattering particle size distribution analyzer	38
<u>Section III</u> Preparation and characterization of electrospun nanofibers of polylactide and quaternized cellulose	38
(1) Preparation of electrospun nanofibers of neat PLA, and blending electrospun nanofiber composites of PLA and QC	38

(2) Preparation of coaxial electrospun nanofiber composites of PLA and QCNF	39
(3) Characterization of the nanofibers	40
(3.1) Fourier transform infrared spectroscopy (FTIR)	40
(3.2) Scanning electron microscopy (SEM)	40
(3.3) Water contact angle measurements	41
(3.4) Evaluation of antibacterial activity	41
4 Results and discussion	43
4.1 Characterization of quaternized cellulose (QC)	43
4.2 Characterization of microparticles of PLLA- <i>co</i> -GMA copolymers and quaternized cellulose	53
4.3 Characterization of electrospun nanofibers of polylactide and quaternized	58
5 Conclusions and recommendation	64
5.1 Research conclusions	64
5.1.1 Characterization of quaternized cellulose	64
5.1.2 Characterization of microparticles of polylactide (<i>co</i>)polymers and quaternized cellulose	64
5.1.3 Characterization of electrospun nanofibers of polylactide and quaternized cellulose	65
5.2 Recommendations	65
5.2.1 Microparticles of polylactide (<i>co</i>)polymers and quaternized cellulose	65
5.2.2 Electrospun nanofibers of polylactide and quaternized cellulose	65
References	67
Appendices	74
Appendix A Calculation of GTMAC-to-AGU molar ratio	75

Appendix B Proof equation of degree of substitution	76
Appendix C Crystalline indices from X-ray diffractogram	78
Appendix D Crystalline indices from NMR	81
Appendix E Particle size distribution of microparticles	84
Appendix F Measured diameters of nanofibers from ImageJ software	85
Appendix G Results of coaxial electrospinning of PLA-QCNF with various shell feed rates	88



List of Figures

Figures	Page
2.1 Action modes of various antibacterial agents on bacteria, spores, viruses and fungi	7
2.2 Common structure of quaternary ammonium compounds.	8
2.3 Structural composition of spruce wood	12
2.4 Molecular structure of cellulose	12
2.5 Positions in cellulose structure for chemical modification	14
2.6 Quaternization of cellulose	15
2.7 Cellulose nanocrystals and cellulose nanofibrils produced from a disintegration of cellulose microfibrils	15
2.8 Different routes to synthesize microparticles:	20
2.8(a) Solvent evaporation	20
2.8(b) Suspension or emulsion polymerization	20
2.8(c) Sedimentation polymerization	20
2.8(d) A SEM image of resulting microparticle via solvent evaporation	20
2.8(e) A phase contrast image of microparticles from suspension polymerization	20
2.9 PIE Pathway from W/O to O/W emulsion	21
2.10 Chemical structure of PLLA- <i>co</i> -GMA copolymer	22
2.11 Diameter comparison of nanofiber, protein, viruses and bacterial cells	23
2.12 Electrospinning of polymeric nanofibers	24
2.13 Schematic of electrospinning techniques controlling active agent location: (a) blend, (b) coaxial, and (c) emulsion electrospinning	27
2.14 Chemical structure of lactic acid isomers	28
3.1 Schematic of preparation of quaternized cellulose nanofibrils	32
3.2 Schematic of microparticle formation by PIE method	36
3.3 Schematic of microparticle formation from QC or QCNF suspension via PIE method and microfluidizer	37
3.4 Schematic of electrospun nanofibers of neat PLA, and blending electrospun nanofiber composites of PLA and QC	39

3.5	Schematic of coaxial electrospun nanofiber composites of PLA and QCNF	40
4.1(a)	Physical appearance of de-starched cassava pulp	43
4.1(b)	Physical appearance of cellulose products	43
4.2	FTIR spectra of de-starch cassava pulp, cellulose, and quaternized cellulose at various GTMAC-to-AGU molar ratios, from 1 to 3	44
4.3	XRD patterns of de-starch cassava pulp, cellulose, and quaternized cellulose at various GTMAC-to-AGU molar ratio, from 1 to 3	45
4.4(a)	¹³ C NMR spectrum of de-starch cassava pulp	46
4.4(b)	¹³ C NMR spectrum of cellulose	47
4.4(c)	¹³ C NMR spectrum of QC [1:1]	47
4.4(d)	¹³ C NMR spectrum of QC [2:1]	48
4.4(e)	¹³ C NMR spectrum of QC [3:1]	48
4.5	Effect of GTMAC: AGU molar ratio on the degree of substitution and the cationization reaction efficiency	50
4.6	Mechanism of antibacterial action of quaternized cellulose	52
4.7	Appearances of quaternized cellulose and quaternized cellulose nanofibrils suspensions	52
4.8(a)	SEM image of quaternized cellulose	53
4.8(b)	SEM image of quaternized cellulose nanofibrils	53
4.9	FTIR-ATR spectra of microparticles containing QC via different experimental approaches and their raw materials	54
4.10	SEM images of microparticles obtained from different experimental approaches	
4.10(a)	Microparticles from QC powder via PIE method	55
4.10(b)	Microparticles from QC suspension via PIE method	55
4.10(c)	Microparticles from QCNF suspension via PIE method	56
4.10(d)	Microparticles from QC suspension via PIE method and microfluidizer	56
4.10(e)	Microparticles from QCNF suspension via PIE method and microfluidizer	56

4.11	Particle size distributions of microparticles obtained from different experimental approaches:	57
4.11(a)	Microparticles from QC powder via PIE method	57
4.11(b)	Microparticles from QC suspension via PIE method	57
4.11(c)	Microparticles from QCNF suspension via PIE method	57
4.11(d)	Microparticles from QC suspension via PIE method and microfluidizer	57
4.11(e)	Microparticles from QCNF suspension via PIE method and microfluidizer	57
4.12	ATR-FTIR spectra of electrospun nanofibers of neat PLA, blend electrospun nanofiber composites of PLA-QC, and coaxial electrospun nanofiber composites of PLA-QCNF	58
4.13	FTIR spectra in transmission mode of electrospun nanofibers of neat PLA, blend electrospun nanofiber composites of PLA-QC, and coaxial electrospun nanofiber composites of PLA-QCNF	59
4.14	SEM images of electrospun nanofibers of neat PLA	60
4.15	SEM images of blend electrospun nanofiber composites of PLA-QC	60
4.16	SEM images of coaxial electrospun nanofiber composites of PLA-QCNF	61
4.17	Surface wetting behavior of electrospun nanofibers of neat PLA, blend electrospun nanofiber composites of PLA-QC, and coaxial electrospun nanofiber composites of PLA-QCNF	62
4.18	Apparent contact angle of electrospun nanofibers of neat PLA, blend electrospun nanofiber composites of PLA-QC, and coaxial electrospun nanofiber composites of PLA-QCNF over a duration of 30 min	62
C-1	X-ray diffractogram of DCP	78
C-2	X-ray diffractogram of cellulose	79
C-3	X-ray diffractogram of QC[1:1]	79
C-4	X-ray diffractogram of QC[2:1]	80
C-5	X-ray diffractogram of QC[3:1]	80
D-1	NMR spectrum of DCP	81

D-2	NMR spectrum of cellulose	82
D-3	NMR spectrum of QC[1:1]	82
D-4	NMR spectrum of QC[2:1]	83
D-4	NMR spectrum of QC[3:1]	83



List of Tables

Tables		Page
2.1	Classification of antibacterial agents	6
2.2	Chemical composition of different cellulose resources	11
2.3	Composition of a stirred solution and an additional solution for a different routes to synthesize microparticles	20
2.4	Electrospinning parameter affected fiber morphology	25
3.1	List of materials and chemicals used in the study	29
4.1	Results on the nitrogen contents of DCP, cellulose, and QC samples	50
4.2	Minimum inhibitory concentration and minimum bactericidal concentration of QC at molar ratio of 2 against <i>E. coli</i> (ATCC 8739) and <i>S. aureus</i> (ATCC 6538) for 24 hours of incubation period	51
4.3	Antibacterial activity and efficacy of electrospun nanofibers of neat PLA and coaxial electrospun nanofibers of PLA-QCNF against <i>S. aureus</i> (ATCC 6538) and <i>E. coli</i> (ATCC 8739), based on JIS Z 2801-2010	63
E-1	Summary of particle size distribution of microparticles via different experimental approaches	84
F-1	Measured diameter of electrospun nanofibers of neat PLA	85
F-2	Measured diameter of blend electrospun nanofiber composites of PLA-QC	86
F-3	Measured diameter of coaxial electrospun nanofiber composites of PLA-QCNF	87
G-1	Results of coaxial electrospinning of PLA-QCNF with various shell feed rates	88

Chapter 1

Introduction

1.1 Background

Antimicrobial agents have attracted vast interest from research community and industry, as these can be used in various applications. However, there are problems of residual toxicity of the agents, even the agents are used in a suitable amount. Also, their protection lifetime is relatively short, due to poor potential to control diffusion rate in various area, such as medical devices, healthcare productions, water purification systems, hospitals, dental office equipment, food packaging, food storage, and household sanitation. The use of non-leaching microbicidal surfaces treated with polymeric antimicrobial agent have been designed, in order to restrict bacterial colonization without releasing antimicrobial agents into the environment. Therefore, their service time can be prolonged and their efficiency and selectivity can be enhanced. Moreover, polymeric microbial agents are non-volatile and chemically stable and do not permeate into skin. These can reduce probability of loss associated with volatilization, photolytic decomposition, and transportation.

Due to their several advantages, there have been increasing effort during the last two decades to synthesize polymeric antibacterial agents via chemical or physical bindings of low-molecular weight biocides to polymeric materials. Such polymeric microbial agents provide long-term durability in an environmentally-friendly route (Kenawy et al., 2011). Among them, deposition or grafting of cationic polymers, such as quaternary ammonium salts, phosphonium salts, pyridinium cations, or quaternized polymers, on material's surface has been investigated to exhibit antimicrobial activity, utilizing electrostatic attractions between negative charges of the bacterial membrane and positive charges of material's surface. The negative charges of bacteria hold cationic ions as their counter ions. When the bacteria are adsorbed on the cationic surface, the negative charges of the bacterial envelope can be compensated with the cationic charges of the material's surface, leading to the loss of natural counter ions of bacteria. The release of these counter ions triggers the bacterial death. However, the penetration of cationic polyelectrolyte segments grafted on the

surface into bacterial cells also provides another possible mechanism of antimicrobial activity of the surface grafted with cationic polymers (Puoci et al., 2008).

Quaternary ammonium salts are well known as antiseptics and disinfectants used in a board range of applications, especially in biomedical field. Since antimicrobial activity of benzalkonium chloride was discovered in 1935, quaternary ammonium salts with several structures have been identified as disinfectants. These salts have some advantages over other antimicrobial agents, including excellent cell membrane penetration properties, low mammalian toxicity and sensitivity, good environmental stability, low corrosivity, and extended residence time and biological activity (Park et al., 2010). According to a survey on 500 US EPA (Environmental Agency), registered disinfectant products for household use consisting of quaternary ammonium salts are the most popular, which is applied in 57.8% of formulation. In 2004, the global consumption of quaternary ammonium salts was reported as 0.5 million tons (Xue et al., 2015).

As the most abundant bio-based polymer available today worldwide, cellulose has been very attractive because of its low cost, unique functionality, hydrophobicity, biocompatibility, recyclability, and biodegradability (Li et al., 2015). Therefore, modification and utilization of cellulose as biocompatible materials for use in various biomedical applications is particular attractive.

Recently, there have been increasing numbers of using synthetic biomaterials in medical applications, as using injectable bio-based polymeric materials (i.e. drug-loaded microparticles which can be formed in spherical or irregular shaped particles). Microparticles are particles with an average size ranging from 1 to 1,000 μm . Due to the variation in sizes of these particles, there are a wide range of applications, ranging from medical field, biochemical science application as carrier materials for purposes of purification, to use as flow indicators. (Saralidze et al., 2010)

Poly (lactic acid-co-glycidyl methacrylate) (PLLA-*co*-GMA) copolymers, biocompatible and biodegradable copolymer with curable properties, can be synthesized by ring-opening polymerization. The copolymers have high potential for use in biomedical fields, as they possess many excellent properties, e.g. biocompatibility, degradability, and high strength (Petchsuk et al., 2012).

In recent years, there has been a number of research about materials with complex microstructures for use in various applications, such as microelectronics, tissue engineering, and superhydrophobic surfaces. Among these, one attractive technique for production of controllable microstructures is electrospinning, in which nanofibers are produced (Brettmann et al., 2012). This offers material with high surface area with wide range of opportunity for further modification for specific use.

Electrospinning is a versatile method to produce two-dimensional nanofiber mats. Since patented design by Morton in 1902 (Brettmann et al., 2012), electrospun nanofibers have been significant materials in biomedical applications, due to large area-to-volume ratio, high interfiber porosity with adjustable pore size, low hindrance for mass transfer, flexible handling, tunable morphology, and good mechanical strength (Yu et al., 2015).

One attractive approach in electrospinning is adding other materials to the polymeric solution and embedded into electrospun polymeric nanofiber in order to form composite nanofibers. This is a promising technique for fabrication of nanocomposites, as the additional materials can be well distributed along the nanofibers. Examples of the materials electrospun along with polymer filaments are small molecules that can be dissolved in the solution (e.g. drug and ceramic precursors) as well as larger particles present in suspension systems (Brettmann et al., 2012).

Polylactic acid or polylactide (PLA) is one of the most attractive biodegradable polymer, which is derived from renewable resources, e.g. corn starch. It is a thermoplastic which not only possesses good mechanical properties (i.e. high strength and modulus), but is also biocompatible and degradable for use in textiles, industrial packaging, and medical applications (Huda et al., 2005).

1.2 Objectives

In this work, cellulosic material with antibacterial property will be developed. The materials are then incorporated with biocompatible PLA by various techniques to enhance its property for specific its property for specific use in biomedical applications. The objectives of this work can be divided into 3 aspects, as follows:

(1) To prepare and characterize quaternized cellulose at various glycidyl trimethyl ammonium chloride content, ranging from 1 to 3 via semi-dry process

(2) To prepare and characterize microparticles of polylactide (co)polymer and quaternized cellulose by a phase inversion emulsification technique

(3) To prepare and characterize of electrospun nanofiber of polylactide (co)polymer and quaternized cellulose.



Chapter 2

Literature Review

Microbial contamination is a great concern in water purification systems, hospitals, animal feed and food. Annually, approx. two million cases of microbial infections are reported in the USA, which more than 90,000 patients die from bacterial infections.

Typically, Gram-positive bacteria are less antimicrobial resistant, compared to Gram-negative bacteria. This is mainly because of different structure of cell walls, and a resistance not specific toward a certain antibacterial agents. Also, organisms can be resistant to antibacterial agents through enzyme productions to inactivate the agents, down alteration (regulation) of genes to encode a channel of outer protein membrane, efflux pumps to remove the agent from cell, or through alteration of the cell walls. In a rare case, an antibacterial agents is degraded and serves as source of energy.

Attractive routes have been goaled to control and minimise a progression of multi-drug resistant microorganisms. As a result, an effective control and prevention of microbial infections is an increasingly vital part in medical procedure. (Bshena, 2012)

2.1 Antibacterial agents

Classification of antibacterial agents is divided following their action modes, as presented in Table 2.1. Most agents are applied as fungicides or bactericides, and their purposes are mostly infection treatments. Recently, antibacterial agents have been improved via combining high and low molar mass compounds. Additionally, they have been modified chemically to introduce specific antibacterial properties. Figure 2.1 summarize action modes of various antibacterial agents on bacteria, spores, viruses and fungi.

Table 2.1 Classification of antibacterial agents. (Bshena, 2012)

Term	Definition
Antibiotic	A natural or synthetic organic chemical compounds in a diluted form are utilized to prevent growth of bacteria or kill microorganisms.
Antiseptic	Agents causes biocidal or static activity on living tissue to prevent bacteria growth.
Bacteriostat	Agents can prevent bacteria growth; however, they cannot necessarily kill bacteria or spores of bacteria.
Disinfectant	Agents are free infections that are not only chemical but also physical, such as UV light. As a result, pathogenic vegetative cells are killed with no necessary for killing spores.
Sanitizer	Substances can decrease the number of bacteria for prescription of safe levels. Typically they are applied only to inanimate objects.
Sterilization	Processes are used to get rid of all living forms, especially microorganisms.

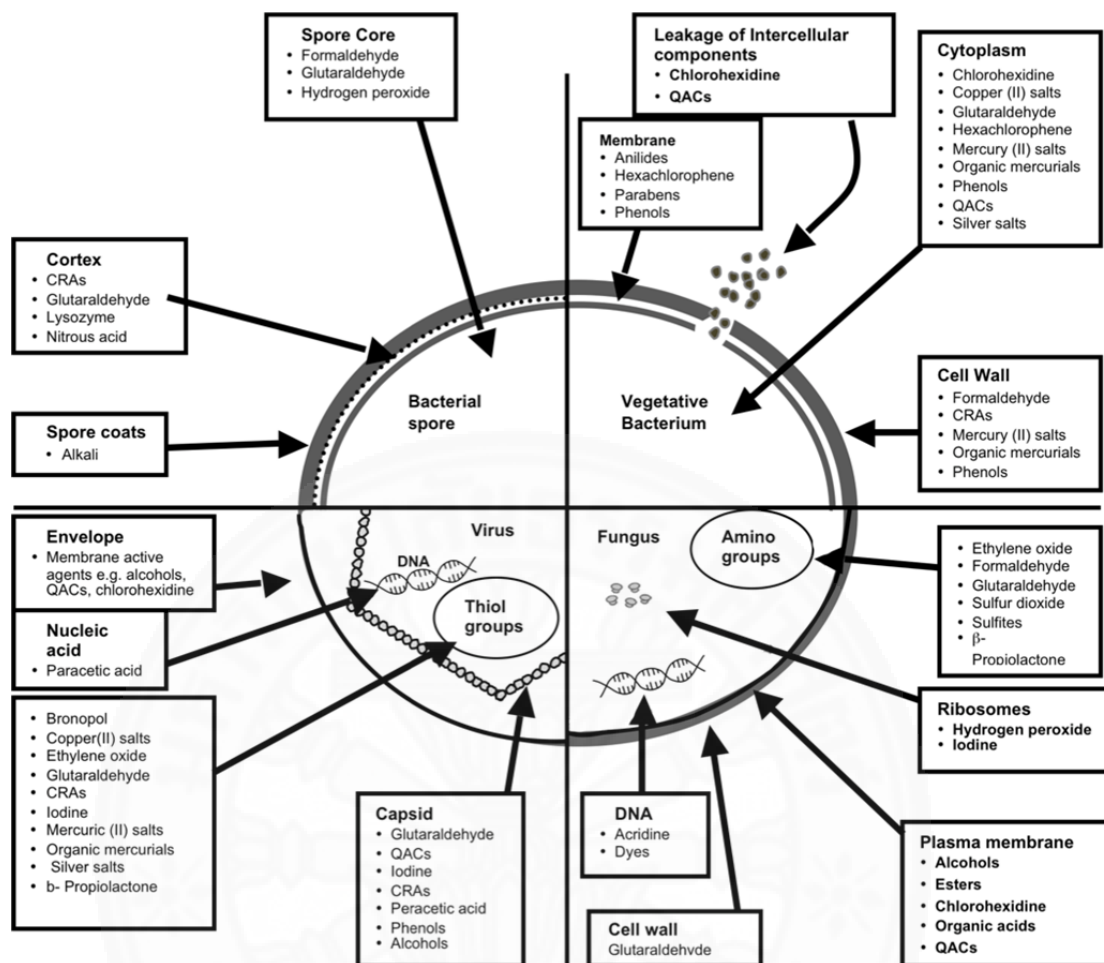


Figure 2.1 Action modes of various antibacterial agents on bacteria, spores, viruses and fungi. (Bshena, 2012)

2.1.1 Lower molecular weight of inorganic and organic antibacterial agents

Metals are known as antibacterial agents that is inorganic compounds with low molecular weight. They can be arranged according to their antibacterial properties as following: $Ag > Hg > Cu > Cd > Cr > Ni > Pb > Co > Zn > Fe > Ca$.

Organic-based antibacterial substances with a low molecular weight are major applied as disinfectants, antibacterial drugs and preservatives of food.

Quaternary ammonium compounds, known as quats, possess various spectrum of antibacterial activity and are utilized as disinfectants in hospitals. Their chemical structures, seen in Figure 2.2, compose of four substituents (R^1-R^4) of alkyl or heterocyclic groups, and a substitution of chloride, bromide or iodide.

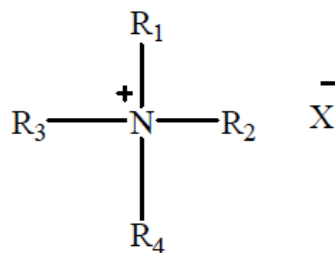


Figure 2.2 Common structure of quaternary ammonium compounds. (Bshena, 2012)

2.1.2 Higher molecular weight of antibacterial agents

Agents with a high molecular weight are mostly natural and synthetic polymeric material.

2.2 Synthetic antibacterial polymeric materials

Chemistry of polymer is designed and synthesized their antibacterial structure due to specific applications, such as medical fields, bandages, implants and filters.

Antibacterial polymeric materials are classified into two types. The first type consists of polymeric materials impregnated with antibacterial actives that are release in a period of time, or polymers employing metal ions to gradually diffuses from the polymeric matrix. Polymers, that antibacterial compound is release slowly in a low concentration, may cause an improvement of microorganism resistances. Regarding many products, in market, employing leachable antibacterial actives and antibiotic uses in disproportionation, a resistance rate is likely to develop. Given an example, excessive antibiotic uses in animal production have grown a risk of resistance improvement in animal and human pathogens. The second type of antibacterial polymers is polymers with inherent antiseptic and antibacterial properties. Such polymers enable to use or apply in various substrates, namely cellulosic materials, textiles, metals or plastics.

2.2.1 Antibacterial polymers

Antibacterial polymers with self-sterilizing are environmentally friendly mats that toxic chemicals are potentially not incorporated and cannot leach out. Moreover, in order to prevent adhesion of bacteria to their surface, they are easily

contained into fibers, electrospun into nanofibers, or extruded into fibers. Antibacterial polymers are produced via covalent bonding of biocidal functional groups in a post-polymerization modification, resulting in antiseptic and antibacterial properties. Modification by moieties of available reactive is either to bulk polymers or selectively to their surface. Another method of synthesis is a chemical modification of a biocidal molecule into a polymerizable substance that enable subsequently to polymerize or co-polymerized with another monomer. Both these modifications have been valuable in feasibility of establish for a concept of antibacterial polymers with non-leaching properties.

Among antibacterial actives investigated in polymer conjunctions are phosphonium and quaternary ammonium salts, and N-substituted halamines. Preparation of antibacterial polymeric materials based on quaternary salts is very attractive because of a fairly convenient modification of polymer that composes of reactive moieties, e.g. secondary or/and tertiary amino groups on the polymeric backbone. A biocidal activity of cationic substances is typically corresponded to a positively charged nature of their molecule. A surface membrane of bacteria cell is generally a negative charge, causing from a negative charge of phosphate groups in phospholipid heads of a bilayer. Therefore, a biocidal effect of polycations on bacterial cell is stronger, compared to one of low molecular weight of cations. In order word, polycations possess more adsorption a negatively charged surface of bacteria than monomeric cations.

2.2.2 Antibacterial surface modification

A research interest has recently been dedicated to an improvement of permanent, non-leaching, sterilizing-surface materials, especially for coating of surface materials. In a number of research, one end of a long chain of hydrophobic polycations employing antibacterial polymer is bonded covalently to the material surface, such as glass, cotton or plastic. A variety of uses of antibacterial surfaces is in a prevention of microbial infection in various medical and industrial settings.

2.3 Cellulose

Cellulose is the most abundant bio-based polymers. It is an important source for biocompatible and environmentally friendly materials due to its properties, i.e. renewability, non-toxicity, and biodegradability. Annually, a cellulose production from photosynthesis is approx. 10^{11} - 10^{12} ton. (Nechyporchuk, 2015)

2.3.1 Sources

Cellulose can be produced from various sources such as wood (softwood and hardwood), seed fibers (e.g. coir, cotton, and etc.), bast fibers (e.g. jute, flex, hemp, ramie, and etc.), grass (e.g. bamboo, bagasse, and etc.), marine animals (e.g. tunicate), fungi, algae, bacteria, and invertebrates. (Wang, 2005)

Commercially, content of cellulose presents in easily harvested sources as wood or highly pure source as cotton as illustrated in Table 2.2.

Sources of cellulose can be mainly classified into three types, as follows:

- Primary cellulosics, cellulose obtained from harvested plant such as cotton, timber, hay, etc.
- Agricultural waste cellulosics, cellulose obtained from residual plant materials after harvesting such as straw, corn, rice hulls, sugarcane etc.
- Municipal waste cellulosics, cellulose presenting in city wastes such as waste paper, yard debris, etc.

A vast industrial source of cellulose currently is wood. Beside cellulose in a wood composite, there are also hemicellulose, lignin, mineral substances, and a very small amount of extractives. Depending on anatomical feature of wood, their species can be divided into two categories- hardwood and softwood. Softwood is less heterogeneous and complex in structure than hardwood. Usually, fibers of hardwood is 3-4 times shorter than those of softwood; however, structure of hardwoods is more rigid than that of softwood. Therefore, hardwood requires more mechanical treatment than softwood in order to generate an equivalent fibrillation. (Nechyporchuk, 2015)

Table 2.2 Chemical composition of different cellulose resources (Hon, 1996).

Source	Composition (%)			
	Cellulose	Hemicellulose	Lignin	Extract
Wheat straw	30	50	15	5
Bagasse	40	30	20	10
Softwood	4-44	25-29	25-31	1-5
Hardwood	43-47	25-35	16-24	2-8
Flax (retted)	71.2	20.6	2.2	6.0
Jute	71.5	13.6	13.1	1.8
Henequen	77.6	4.8	13.1	3.6
Ramie	76.2	16.7	0.7	6.4
Cotton	95	2	0.9	0.4

2.3.2 Structure and chemistry

Cellulose is a major content of vascular plants. Additionally, it is a primary composition of structure to make a mechanical strength in plants. In such wood or plant, cellulose is a presence in a well organization of fibrillar elements containing in cells.

Each cell illustrate a fiber having a 10-50 μm of width, and a total thickness of cell wall is 1-5 μm , seen in Figure 2.3 presented a spruce wood. Due to a high lignin content, neighbouring cells is hold together by a middle lamella. A lumen is cells surrounding a central cavity. Cell wall is consisted of three layers- primary, secondary, and tertiary walls. Each wall composes of three major components: cellulose microfibrils, hemicelluloses, and a matrix that is generally pectin in primary wall, and lignin in secondary wall.

A primary cell wall is estimated to a 0.03-1.0 μm of thickness, containing a high content of lignin. Cellulose microfibrils in the primary cell wall are a location as a crosswise which forms a 50 nm of layer. In secondary cell wall, there are two layers with a thickness, ranging from 100 nm (for cotton) to 300 nm (for spruce pulp). Most cellulose mass is contained in the secondary cell wall. Microfrils in the layer are organized in parallel and densely packed in a flat helix. An inner layer closed to lumen of fiber is a tertiary cell wall. It is thin and composed of microfibril cellulose that are organized in a flat helix.

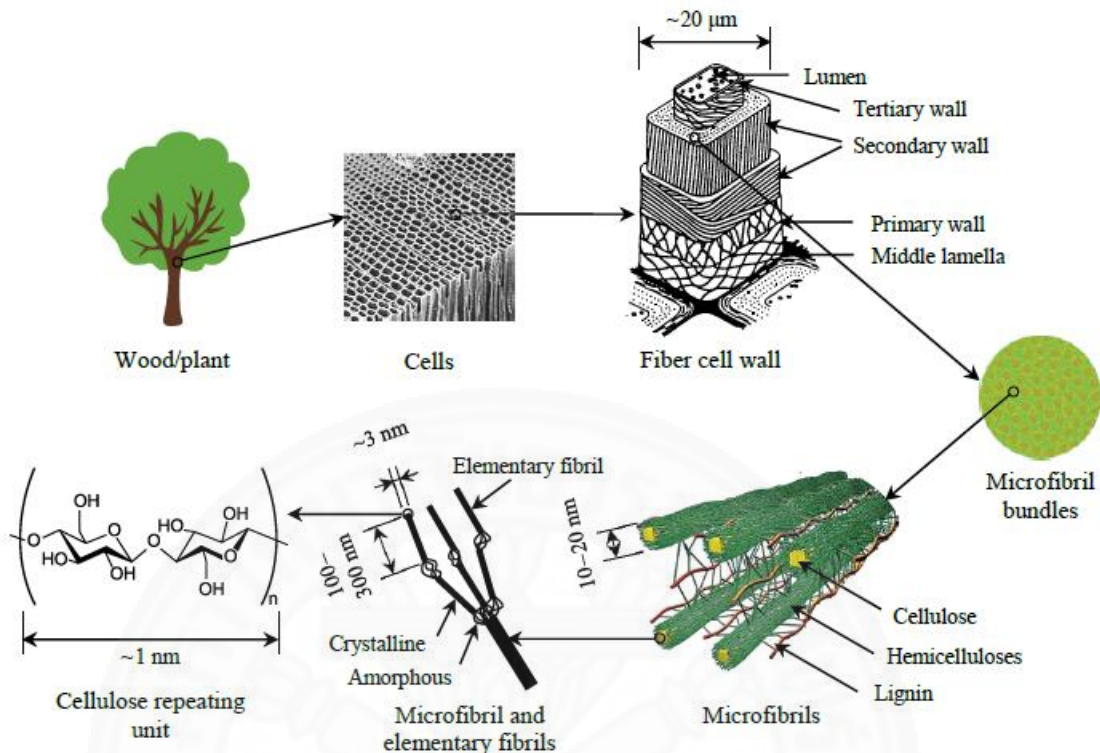


Figure 2.3 Structural composition of spruce wood (Nechyporchuk, 2015).

Cellulose molecule, represented in Figure 2.4, is a linear polymer of D-anhydroglucopyranose units which is linked together via β -1,4-glucosidic bonds. In other word, it is known as a β -1,4-D-glucan (polyglucose). The D-anhydroglucopyranose units are six carbons membered rings (i.e. pyranoses) with three hydroxyl groups at C-2, C-3, and C-6. A C-1 of one pyranose and a C-4 of neighbouring ring is joined by single oxygen atoms (acetal linkages), resulting a high degree of polymerization of cellulose molecule.

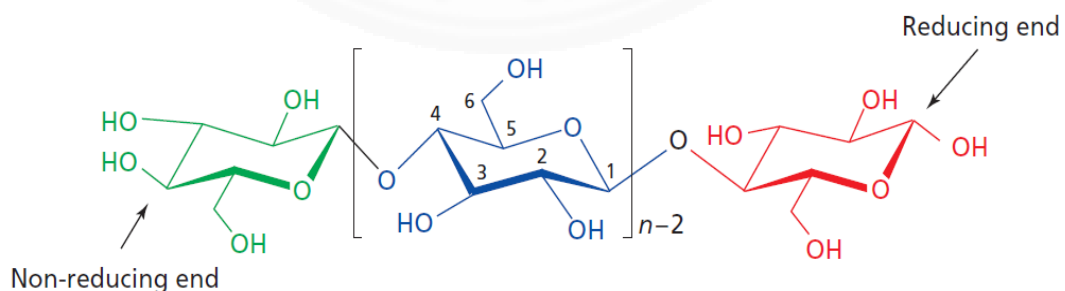


Figure 2.4 Molecular structure of cellulose (Wertz, Bédoué & Mercier, 2010).

2.3.2.1 Degree of polymerization

An average number of monomers is used to build up a polymer of cellulose, known as a degree of polymerization. A degree of polymerization of cellulose is due to source of cellulose (e.g. 44,000 in *Valonia*, 20,000 in cotton, 10,000 in native wood) and isolation and purification methods (e.g. 1,000 in bleached kraft pulp, and 200-500 in regenerated cellulose). For industrial purposes, a higher degree of polymerization is generally required, providing a higher tensile strength to products (Nechporchuk, 2015; Wang, 2005).

2.3.2.2 Crystalline index

Cellulose is a semi-crystalline polymer containing crystalline (i.e. ordered) and amorphous (i.e. disordered) regions. To indicate how much crystalline region compared to amorphous one is a crystalline index. Native cellulose, known as cellulose I, has a crystalline index varying from 5 to 90%, due to its sources and method used for calculation. A high level of crystalline leads to that cellulose cannot dissolve in most common solvent, resulting in much difficult process (Nechporchuk, 2015; Wang, 2005).

2.3.3 Reaction

2.3.3.1 General Consideration

Typically, cellulose modifications are etherification and esterification of hydroxyl groups. Preparation of most soluble cellulose derivatives by these substitution reaction allows dramatic changes in the original properties of cellulose. Other modifications consist of radical and ionic grafting, oxidation, deoxyhalogenation and acetalation. Usually, cellulose originated from wood and cotton pulps have carboxyl and aldehyde groups in quite small quantities, relying on the pulp purity. These minor groups are also target positions for chemical modification.

From one reaction to another, a relative reactivity of the hydroxyl groups varies. Normally, the reaction varies in the order of OH-6 \gg OH-2 $>$ OH-3 (Wang, 2005).

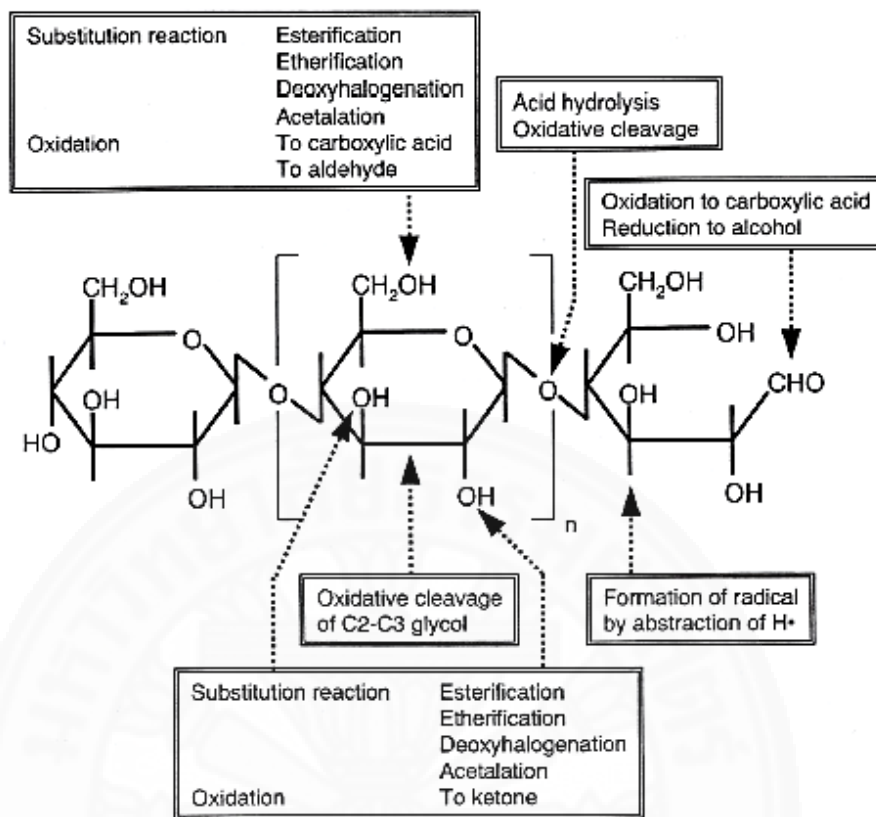


Figure 2.5 Positions in cellulose structure for chemical modification (Wang, 2005).

2.3.3.2 Etherification

In the early 1900s, there was patents disclosing cellulose ether preparation. Since that time, there have been significant process and reaction modification involved and this area have been continuously one of research from academia and industry. (Wang, 2005)

To prepare cellulose ethers, there are two reaction types. The most common is nucleophilic substitution. A reaction related to the study is quaternization of cellulose, presented in Figure 2.6.

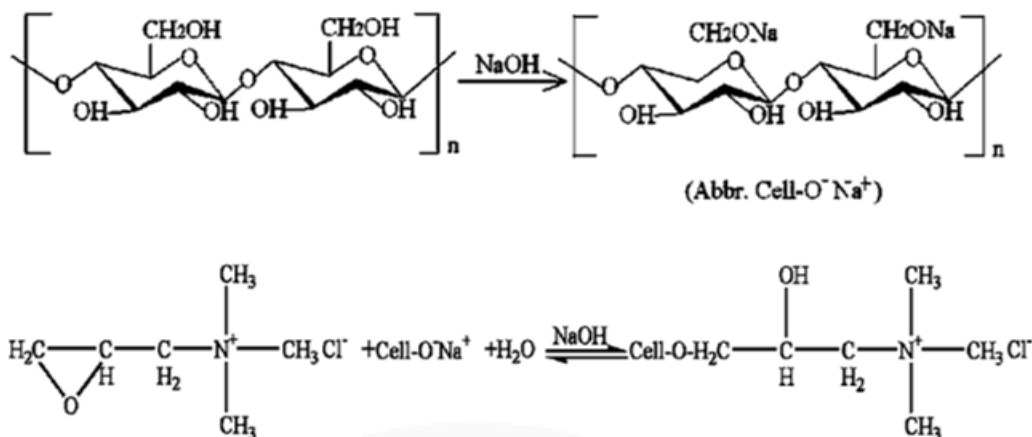


Figure 2.6 Quaternization of cellulose (Wang et al., 2009).

2.4 Nanocellulose

Nanocellulose is individual elements of cellulose with a diameter of less than 100 nm. As dimensions, properties, and composite, the nanocellulose can be separated into three main types: (1) cellulose nanocrystals (CNC) or whiskers; (2) cellulose nanofibrils (CNF) or cellulose microfibrils (CMF), or cellulose nano-/microfibrils; and (3) bacterial nanocellulose (BNC). (Nechporchuk, 2015)

CNC and CNF are generated via that cellulose fibers are disintegrated to nanomaterials, present in Figure 2.7. In contrast, BNC is produced by that sugars with low molecular weight are built up by an aerobic bacteria. Regarding nanocellulose, it displays a hydrophilicity, a wide range of potentials from a relatively large specific surface area to surface modification, and etc.

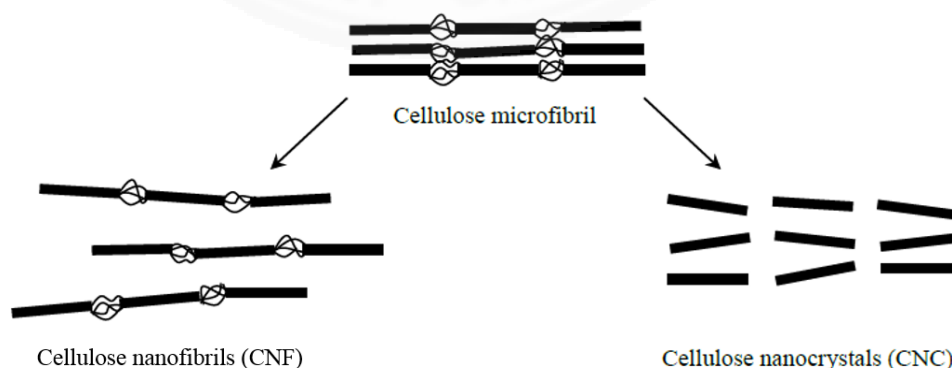


Figure 2.7 Cellulose nanocrystals (CNC) and cellulose nanofibrils (CNF) produced from a disintegration of cellulose microfibrils (Nechporchuk, 2006).

2.4.1 Cellulose nanocrystals (CNC)

CNC or cellulose nanowhiskers were generated by using an acid hydrolysis of cellulose fibers in an aqueous suspension. For this, commonly, a concentrated sulphuric acid (H₂SO₄) is applied to degrade amorphous regions and leave crystalline regions of cellulose. As a result, rod-like CNC with sulfate group on their surface are generated. Generally, CNC have a diameter range between 3 and 35 nm, and a length range from 0.05 to 4 μm.

2.4.2 Cellulose nanofibrils (CNF)

Softwood pulp is dispersed in water to obtain an aqueous suspension. The suspension is subsequently mechanically treated. Strongly entangled networks of CNF, containing both crystalline and amorphous regions, are generated during mechanical treatment. Consequently, they have a high aspect ratio and gel-like aqueous suspension with thixotropic and pseudoplastic properties. The cellulose fibers enable to disintegrate to obtain CNF with a lateral dimension of approx. 3 nm, or microfibrils with a dimension of 10 nm.

2.4.3 Bacterial nanocellulose (BNC)

BNC, or known as bacterial cellulose, is cellulose that possess a high purity. It is produced by strains of *Gluconacetobacter* bacteria in aqueous culture media consisting of sugar source. Such process spend time ranging between days and two weeks. BNC introduce a same chemical composition as plant cellulose; however, it possess free-functional groups other than hydroxyl group, e.g. carbonyl or carboxyl, which are normally presented in plant and wood-derived cellulose during a process of purification. Also, BNC is free of other polymers, i.e. hemicellulose, lignin, and pectin. BNC assembling into nanofibrils with hierarchical structures possess a width of 10 nm, and a length of more than 2 μm. Its degree of polymerization ranges from 3,000 to 9,000, and its crystallinity index ranges from 80 to 90%.

2.5 Microparticles

Microparticles are defined as particles with size ranging from 1 to 1,000 μm . The particles are utilized in a wide range of applications, from application in biochemical sciences for purification purposes as carrier materials, use as flow indicators, to use in medical field.

Microparticles can be produced from both polymeric and non-polymeric materials. Non-polymeric microparticles are normally generated by a simple method based upon particle formation in aqueous environment and then drying, and if needed, sintering (Saralidze et al., 2010).

Here, focusing on synthesis of polymeric microparticles, it can be mainly divided into two different methods, which are microparticles from linear polymers and those from radical polymerization.

2.5.1 Microparticles from linear polymers

Methods using linear polymers as precursor materials are also suited for microparticles generation from both polymers that are unable formed by radical polymerization, and naturally occurring polymers. The most common technique is a solvent evaporation.

Regarding a solvent evaporation, polymer is completely dissolved in a more or less volatile solvent, and subsequently dropped carefully into a solution of non-miscible fluid, called continuous phase. This phase consists of a stabilizer to form and maintain a particle shape, presented in Figure 2.8 (a). The solvent was evaporated. Consequently, remaining solid of polymeric microparticles was washed free of stabilizer. An example of microparticles, given in Figure 2.8 (d), is generated by a solvent evaporation.

A major advantage of microparticle synthesis via solvent evaporation is relatively simple method that polymers can be virtually completely dissolved, and obtained yields are high. The disadvantages is difficult to tailor particle size between different batches. Also, the solvent and surfactant used is mostly toxic and require to wash. The washing steps consume time, resulting in a large volume of wastewater. Moreover, during washing steps, active agent-loaded particles may lose some of the loaded active.

An alternative technique to the liquid-in-liquid solvent evaporation is spray drying. Polymers are dissolved in a volatile solvent, and a fine spray is produced under a pressure. It is dried under a high power heating, obtaining fine particles. The technique is easy, and enable to upscale. A disadvantage of the technique is obtained microparticles displaying high polydispersity. In addition, during spray drying process, relatively high temperature is required, and consequently more sensitive bioactive compounds enable to damage.

2.5.2 Microparticles synthesis from radical polymers

Methods of generating microparticles are derived from a mixture of monomers and polymerization initiator, forming into particles in a stabilizing non-miscible phase. The most common methods are suspension, emulsion, dispersion, and sedimentation polymerization.

According to Suspension polymerization, given in Figure 2.8 (b) and Table 2.3, a mixture of monomers and an initiator are dripped into a non-miscible phase, i.e. water, with detergents and surfactants as stabilizers, ensuring particle formation. The solution is then heated to induce an initiator activation, and start a reaction of radical polymerization. Microparticles are washed and collected after the polymerization reaction has been completed. The technique is obtained a wide range of particles size, ranging from 40 to 1,000 μm . A major disadvantage of suspension polymerization is obtained microparticles presenting high relatively polydispersity.

For emulsion polymerization, shown in Figure 2.8 (b) and Table 2.3, an initiator is dissolved in a solution of aqueous phase that consists of emulsifiers and stabilizers. Monomers are dissolved in a very low solid content in an oil phase, and then dripped in the aqueous phase to obtain a monomer emulsion. Due to a presence of the initiator in the water phase, an initial polymerization occur that free-oligomeric radicals is absorbed via micelles containing monomers, or is surrounded via dissolved surfactants and monomers. The polymerization reaction is completed when all monomers are used. The surfactants are subsequently washed away, generating microparticles with a size ranging from 0.1 to 10 μm , a low polydispersity, and high yields.

Another method of synthesis of microparticles is a dispersion polymerization, or called as a phase-separation polymerization. Due to the technique, in an oil phase, monomers are mixed and dissolved together with an initiator and a stabilizer. In an aqueous phase, a chosen solvent is a non-solvent of polymers. For polymerization, small polymer droplets are generated by that a stabilizer prevents a polymer-particle aggregation. Important parameters, i.e. a stirring speed, an exact composition of solvent mixture, and a heating, are required to result in a size of particles. The method is resulted in a relatively small particle with a size ranging from 1 to 10 μm .

A sedimentation polymerization, illustrated in Figure 2.8 (c), is a technique generating a large particle size (400-2,000 μm) with a low polydispersity. The mixture of monomers and an initiator is dripped into a heated-mineral oil column, and subsequently the droplets gradually sediment in the bottom of column. During the sedimentation, a polymerization reaction proceed, providing microparticles. The resulting particles are not aggregated due to applying an initial high temperature. A vital parameter for an integrity of particles is a composition of the monomers and the initiator. Due to time of droplets reaching the bottom, hardening and gelation of the microparticles should be fast enough to keep their shape. Needle size and dripping speed of monomer solution results in a monomer size, ranging between 400 and 2000 μm . The method is not popular due to a large size of particle and a low polydispersity. Also, it is difficult to upscale for a large production, causing from tailoring an aggregation of particles.

Table 2.3 Composition of a stirred solution and an additional solution for a different routes to synthesize microparticles (Saralidze et al., 2010).

Method	Stirred solution	Additional solution
Suspension polymerization	Surfactant	Monomers Initiator
Emulsion polymerization	Surfactant Initiator	Monomers
Dispersion polymerization	Surfactant Initiator Monomers	-

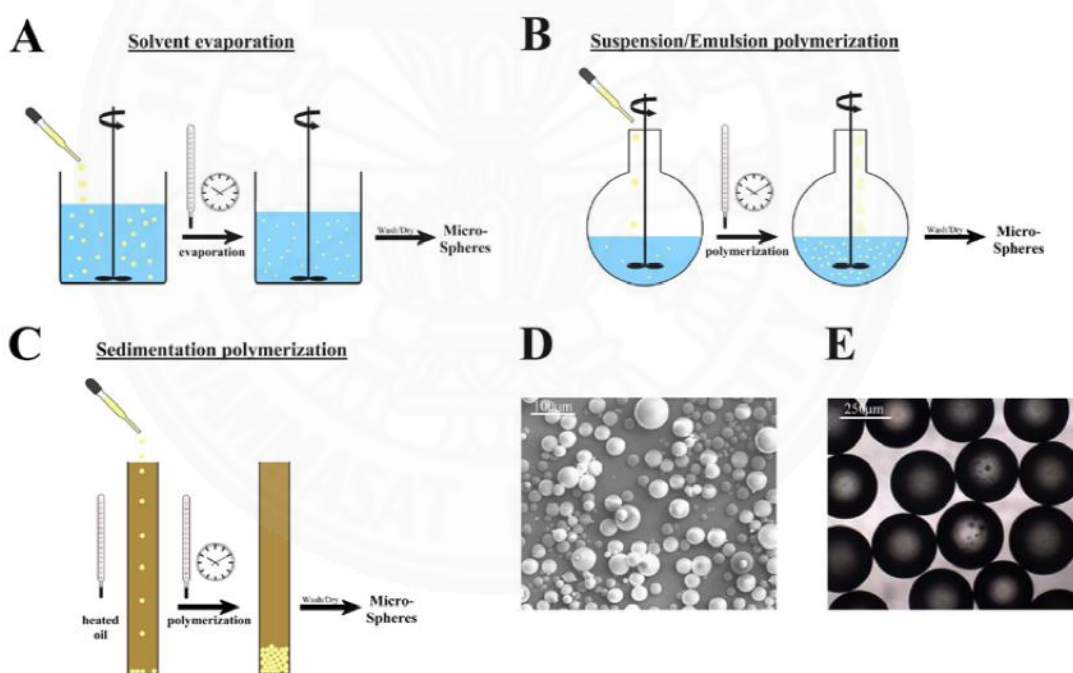


Figure 2.8 Different routes to synthesize microparticles: (a) Solvent evaporation; (b) Suspension or emulsion polymerization; (c) Sedimentation polymerization; (d) a SEM image of resulting microparticle via solvent evaporation; and (e) a phase contrast image of microparticles from suspension polymerization. (Saralidze et al., 2010)

2.6 Phase inversion emulsification (PIE)

Due to low energy consumption, PIE is an inexpensive method for production of oil droplets in miniemulsion polymerization, preparing micro/nano polymer particles with a narrow particle size distribution.

Basically, generation of oil droplets are stabilized by surfactant, forming at interface of oil-and-water when a dropwise addition of aqueous phase into oil phase. This forms firstly water-in-oil (W/O) emulsion. Subsequently, aqueous phase is added continuously until the amount of aqueous phase is higher than that of oil phase, forming oil-in-water emulsion. Therefore, it is called phase inversion emulsification.

This technique could decrease oil droplet coalescence, resulting from high adsorption rate of surfactant onto the oil-and-water interface than diffusion from aqueous media to the droplet interface (Chaiyasat et al., 2013).

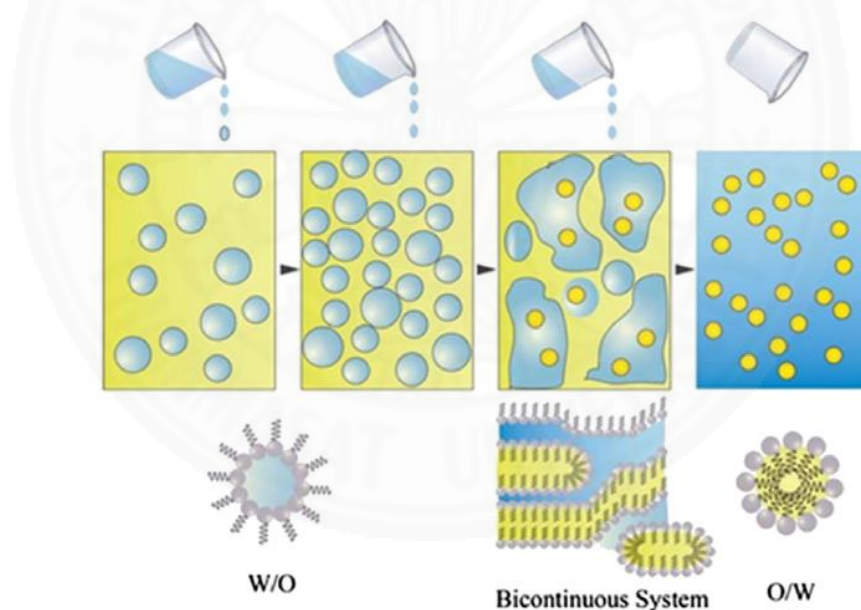


Figure 2.9 PIE Pathway from W/O to O/W emulsion (Perazzo et al., 2015).

2.7 Poly (lactic acid-co-glycidyl methacrylate) (PLLA-co-GMA) copolymers

In order to introduce functionality into PLA chains, lactide copolymerization with specific functionalized monomers is interested. Petchsuk et al. (2012) studied glycidyl methacrylate (GMA) incorporated into PLLA chains. There are two functional group in GMA monomer: methacrylic and epoxy groups. The

utilization of GMA as a compatibilizer in blending polymer, leading to graft to functionalize olefin copolymers and produce multifunction of acrylates. GMA incorporated into PLLA chains presents characterization of methacrylate funional groups as an active side forming crosslink network at C=C bonds (Petchsuk et al., 2012).

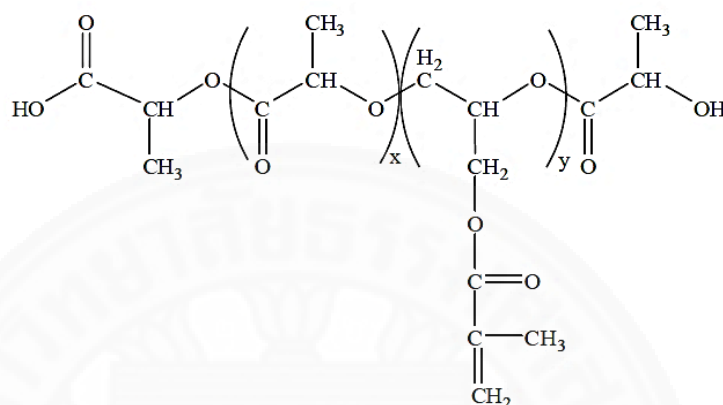


Figure 2.10 Chemical structure of PLLA-*co*-GMA copolymer (Petchsuk et al., 2012).

2.8 Electrospun nanofibers

Electrospinning is a method to use a strong electrostatic field, providing ultrafine fibers from a polymeric solution. Due to charge motion carriers presenting in the polymeric solution, the solution is accelerated towards the ground collectors. Electrospun nanofiber having high surface area-to-volume ratio and small pores are drawing interests in a wide range of applications such as filtration products, tissue engineering scaffolds, wound dressings, drug release materials, reinforced fiber composites, and protective clothing (Ibrahim & El-Zairy, 2015).

2.8.1 History of electrospinning

Electrostatic influence, in 1700s, was discovered on water behaviour and an electric charge influenced dielectric liquid excitation. This probably causes an invention of electrospinning producing ultrafiber by Cooley and Morton in early 1900s. Cooley used rotatory electrode in an electrospinning jet. Formhals, in 1930, patented a process and apparatus of yarn production via electrospinning without spinneret and in 1940, he patented a method producing composite fiber webs from multiple polymeric substrates via electroatracically spinning polymer fiber on a

movement of base substrate. Taylor, in 1969, studied a polymer droplet shape generated at a needle tip when applying an electric field and presented that it was a cone and an ejected jet from vortices of the cone, later referred as ‘Taylor cone’.

According to fiber industries, a major key of consideration is fiber production rate. Compared to popular industrial fiber spinning process, electrospinning has very low rate of production. A yarn from industrial dry spinning take-up a production rate of ranging from 200 to 1500 m/min whereas that from electrospinning take-up the rate of 30 m/min. Therefore, very little industrial research was interested in electrospinning, before 1990. Melt spinning is a preferred method for synthetic fiber production, making electrospun fiber using polymer melts. However, the melt spinning is a difficult method to encounter in fabrication of fiber with a nanometer diameters, resulting in little progress. Nonetheless, Dalton et al. (2006) have succeed recently in deposition of electrospun polymer melt fiber on to cells directly, forming layered tissue constructs for tissue engineering. This leads to elimination of cytotoxic solvent introduction into cell culture when the fiber was deposited. While, since the 1900s, there have been patents involved in set-ups of electrospinning, it is only in the last decade that there have been heavy studies in fabrication of nanofiber via electrospinning for a vast potential applications (Ibrahim & El-Zairy, 2015).

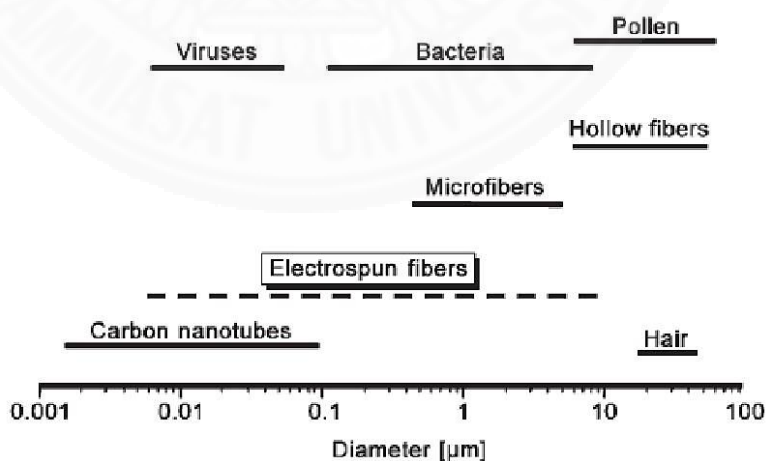


Figure 2.11 Diameter comparison of nanofiber, protein, viruses and bacterial cells (Greiner & Wendorff, 2007).

2.8.2 Fundamental Aspects

Figure 2.12 presents electrospinning of polymeric nanofiber. Basically, there are three main components in this process which are a high voltage supplier, a syringe with a small-diameter needle, and a screen collector. In electrospinning process, a high voltage is utilized to induce electrical charge in polymeric solution or melt, making a jet of the solution/melt out of a needle. Before the solution/melt jet reaches the collector, it evaporates or solidifies, and is collected as an interconnection of small fiber web. A positive electrode is connected to the needle and negative one attached to the collector, which, in the most case, the collection is simply grounded as indicated in Figure 2.12. The electric field is introduced to the end of needle containing the solution fluid held by its surface tension. This induces a charge on the liquid surface, causing mutual charge repulsion and contraction. This is resulted in a force opposite directly to the surface tension. With increasing intensity of the electric field, the hemispherical fluid surface at the needle elongates, forming a conical shape known as Taylor cone. Further increasing the electric field reach a critical value that the repulsion electrostatic force overcomes the surface tension and the charged fluid jet is subsequently ejected from the needle of the Taylor cone. The discharged jet of polymeric solution undergoes an elongation and instability process, allowing the jet to become very thin and long. Meanwhile, the evaporation of solvent leaves behind a charged polymeric fiber. In the case of melt, the discharge jet solidifies when travelling in the air.

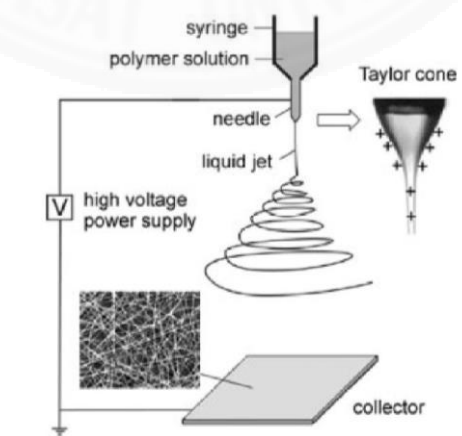


Figure 2.12 Electrospinning of polymeric nanofibers (Li & Xia, 2004).

In the open literature, there have been more than fifty different polymers which have been electrospun successfully into ultrafine fiber with a diameter ranging from below 3 nm to over 1 mm (Huanga et al., 2003).

2.8.3 Parameter studies

There are various parameters affecting electrospinning process. These parameters affected morphology of nanofiber can be classified into three major factors: solution, process and ambient parameters as summary in Table 2.4.

Table 2.4 Electrospinning parameter affected fiber morphology (Bhardwaj & Kundu, 2010).

Parameters	Effect on fiber morphology
Solution parameters	
Viscosity	<ul style="list-style-type: none"> - Low viscosity produces beads - High viscosity leads to increasing fiber diameter and disappearance of beads
Concentration	Diameters of fiber increase with increasing concentration of polymer solution.
Molecular weight of polymer	Decrease in the number of bead formation with increasing molecular weight.
Conductivity	Decrease in diameters of fiber with increasing conductivity.
Surface tension	Instability of polymeric solution jet appearing with high surface tension
Processing parameters	
Applied voltage	Decrease in diameters of fiber with increasing in voltage.
Spinning distance	<ul style="list-style-type: none"> - Bead Formation with too small and too large distance - Minimum distance required for uniform fibers

Table 2.4 (cont'd)

Parameters	Effect on fiber morphology
Flow rate	<ul style="list-style-type: none">- Decrease in diameters of fiber with decreasing flow rate- Bead generation with too high flow rate
Ambient parameters	
Humidity	High humidity resulting in circular pores on the fibers
Temperature	Increase in temperature resulting in decreasing fiber diameter.

2.8.4 Techniques of electrospinning for controlling location of active agents

In order to specific uses for biomedical application, a rate at active agents released from a mats enables to control via housing the active agents in either outside or inside of fibers (Rieger et al., 2013). The electrospun mats can design strategically by various electrospinning techniques, as displayed in Figure 2.13.

2.8.4.1 Blend electrospinning

An active agents are blended into polymeric solution and implemented with traditional electrospinning, as illustrated in Figure 2.13 (a). The resulting electrospun mats can consist of the agents that are dispersed both inside and outside of the fibers.

Ojha et al. (2008) demonstrated that blend electrospun fibers display a high release rate of the agents because of accumulation of active agents along the fibers' surface. A high initial release rate, known as a burst release, is suitable for use of antibiotic at a wound site to eliminate bacteria. While, a resultant of slow release rate is desirable for drug aids in an infection preventing.

2.8.4.2 Coaxial electrospinning

Core-shell fibers are generated by employing a coaxial nozzle, which consists of an outer and an inner channel to separate two or more solution, as presented in Figure 2.13 (b).

Coaxial electrospinning is applied for tailoring location of active agents in either core or shell due to their purposes, i.e. for antibacterial agents, the actives should locate in shell layer, while for controlling drug release, the actives should be in core layers. Additionally, non-spinnable mats such as inorganic nanomaterials, is enable to be electrospun by utilizing a polymeric solution in an outer channel to carry the mats through the process.

2.8.4.3 Emulsion electrospinning

An emulsion is employed as a precursor solution to achieve a core-sheath morphology. A surfactant, additionally, is applied to separate phases between oil and aqueous, as shown in Figure 2.13 (c).

The use of emulsion electrospinning allows for DNA, protein, and peptides by developing a stable release, eliminating an initial burst release, and protecting the active from harsh solvents.

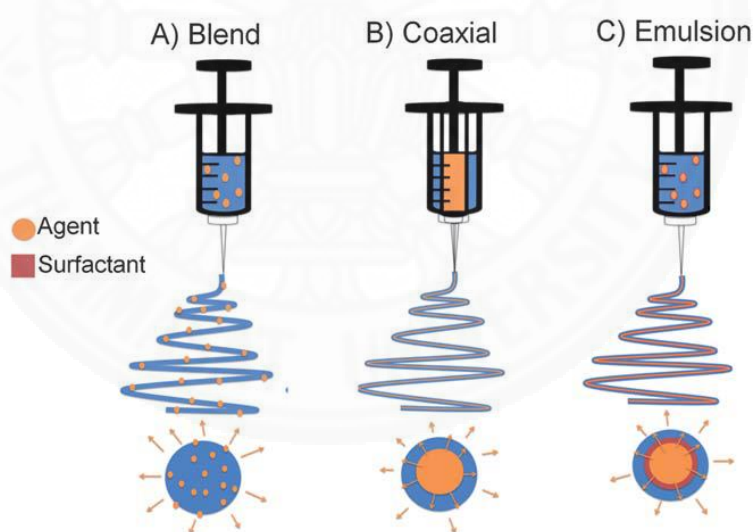


Figure 2.13 Schematic of electrospinning techniques controlling active agent locations: (A) blend, (B) coaxial, and (C) emulsion electrospinning (Rieger et al., 2013).

2.9 Polylactic acid (PLA)

PLA is produced from lactic acid (2-hydroxy propionic acid) as a basic monomer. It is manufactured by chemical synthesis or fermentation of carbohydrate. Lactic acid has a hydroxyl acid with an asymmetric carbon, which has two optically active configurations, L- and D- isomer, seen in Figure 2.14. Generally, lactic acid is produced from petroleum-based source or a renewable source (e.g. glucose and maltose from corn or potato, sucrose from cane or beat sugar etc.) (Lopina et al., 1996; Popelka et al., 2007)



Figure 2.14 Chemical structure of lactic acid isomers (Garrison et al., 2016).

PLA has two types: poly (L-lactic acid) PLLA and poly (D-lactic acid) (PDLA). Both types are well known as biodegradable synthetic polymer due to lactic acid itself occurring in metabolism process (Narayanan et al., 2004)

Chapter 3

Experimental Approach

Overview of experimental approach in this research is illustrated in Figure 3.1. It can be divided into three main sections: (1) preparation of quaternized cellulose, (2) preparation of microparticles of PLLA-*co*-GMA copolymers and quaternized cellulose, and (3) preparation of electrospun nanofiber of polylactide and quaternized cellulose.

3.1 Materials

All materials and chemicals used in the first part of the study are listed in Table 3.1.

Table 3.1 List of materials and chemicals used in the study.

Name of chemicals	Grade	Supplier
Section I: Preparation and characterization of quaternized cellulose		
De-starch cassava pulp (DCP)	-	Cholcharoen Group, Thailand
Sodium hydroxide pellets (NaOH)	AR grade	Quality Reagent Chemical
Sodium Chlorite (NaClO ₂)	Technical grade, 80%	Sigma-Aldrich
Acetic acid	Analytical grade	Carloerba
Glycidyl trimethyl ammonium chloride (GTMAC)	Technical grade, ≥90%	Sigma-Aldrich
Ethanol	ACS reagent, ≥99%	CARLO ERBA Reagents

Table 3.1 (cont'd)

Name of chemicals	Grade	Supplier
Section II: Preparation and characterization of microparticles of PLLA-co-GMA copolymers and quaternized cellulose		
Poly(lactic acid-co-glycidyl methacrylate) (PLLA-co-GMA)	-	Synthesized by MTEC according to the methodology reported from Petchsuk et al. (2012)
Benzyl peroxide (BPO)	72-77%	Sigma-Aldrich
Camphorquinone (CQ)	97%	Sigma-Aldrich
Poly(vinyl alcohol) (PVA)	Hydrolyzed, 87-90%	Sigma-Aldrich
Sodium dodecyl sulfate (SDS)	ACS reagent, $\geq 99\%$	Sigma-Aldrich
Chloroform	CHCl ₃	ACI Labscan
Section III: Preparation and characterization of electrospun nanofiber of polylactide and quaternized cellulose		
Poly (L-lactic acid) pellet (PLLA)	Ingeo™ Grade 4043D, Density = 1.24 g cm ⁻³	Nature Works LLC
N, N-dimethyl formamide (DMF)	Analytical Grade	CARLO ERBA Reagents
and Tetrahydrofuran (THF)	Analytical Grade	CARLO ERBA Reagents
Poly(vinyl alcohol) (PVA)	Hydrolyzed, 95-97%	Ajax Finechem Pty Ltd

3.2 Methodology

Section I: Preparation and characterization of quaternized cellulose

1. Preparation of cellulose from de-starched cassava pulp (DCP)

There are three main steps for cellulose preparation: (1) alkali treatment, (2) bleaching treatment, and (3) Spray drying process.

1.1 Alkali Treatment

In order to isolate all hemicellulose and some lignin from DCP, methodology of Alkali treatment was employed modified from that of Deepa et al. (2011). 15 g of DCP (particle size = 250 μm) were treated with 375 mL of 4%wt sodium hydroxide solution in an Erlenmeyer flask. The mixture was autoclaved as sterilized liquid at 120°C for 1 hr (TOMY SX-700, Japan). The sediment from the mixture was collected by filtration and washed with distilled water until the supernatant was clear, and the pH decreased to 6-7. The solid residue, called de-lignified DCP was transferred into a bag and kept in the refrigerator for a subsequent step, bleaching process.

1.2 Bleaching treatment

In order to isolate all lignin from the obtained de-lignified DCP samples, a bleaching treatment was used by modifying from that of LaCourse et al. (1994). De-lignified DCP was soaked in 750 mL of 1% sodium chlorite solution. The pH of the mixture was adjusted (SUNTEX SP-2200, Microprocessor pH meter, Taiwan) to 5 ± 0.2 with 4% acetic acid solution, and then stirred in a water bath at 80°C for 24 hr, with magnetic stirrer (IKA RCT basic, Malaysia). After stirring for 1 day, the mixture color became cloudy white. The solid residue from the mixture was filtered and neutralized with distilled water. The white solid residue, i.e. cellulose, was transferred into a bag and kept in a refrigerator.

1.3 Spray drying

To recover the solid product, a spray drying process was employed. The cellulose samples obtained from the bleaching process was added into 1500 mL of distilled water, and homogenized by a high speed homogenizer (IKA T-25 ULTRA-TURRAX Digital High-Speed Homogenizer) for 30 min. The conditions for spray drying (MOBILE MINOR™ Spray Dryer, GEA process engineering co. ltd) were: an air pressure of 5 bar, a feed flow rate of 20 mL/min and an inlet air temperature of 130 °C. The final products, cellulose, were in the form of snowy white powder.

2. Preparation of quaternized cellulose nanofibrils (QCNF)

There are 2 main steps to fabricate QCNF: (1) Optimization of GTMAC contents for preparation of quaternized cellulose under a semi-dry process, and (2) Nanofibrillation of quaternized cellulose by a microfluidizer (M-110P Microfluidizer Processor).

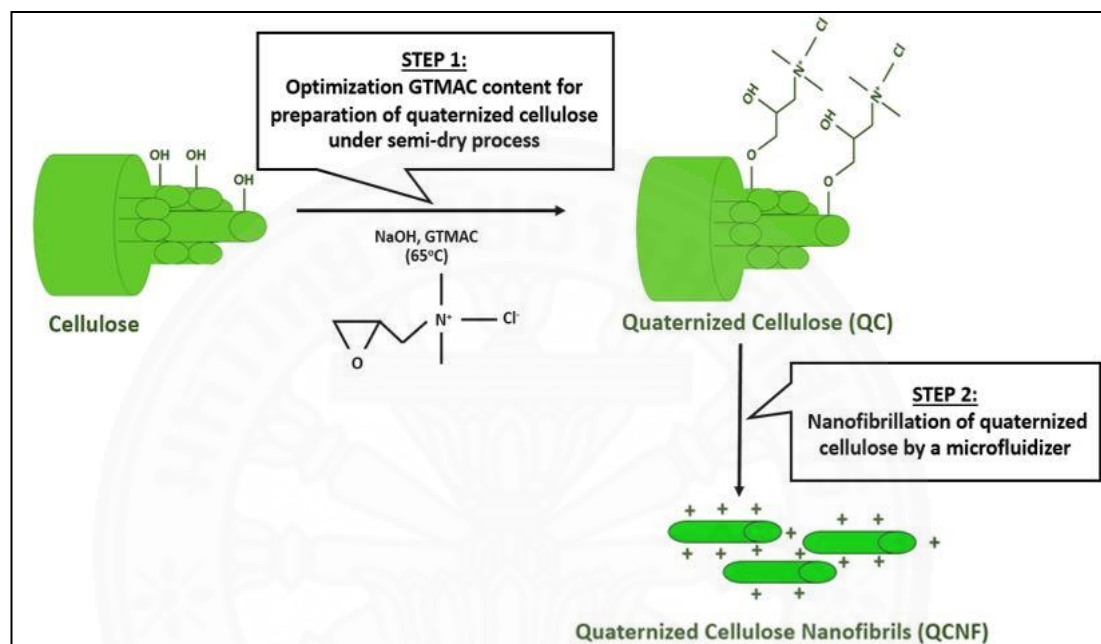


Figure 3.1 Schematic of preparation of quaternized cellulose nanofibrils.

2.1 Optimization GTMAC contents for preparation of quaternized cellulose (QC) under a semi-dry process

The preparation of QC was modified from a previous method by Zaman et al. (2012). 1000 mg of cellulose and 50 mg of sodium hydroxide powder was mixed using a mortar and pestle for 5 min. The solid mixture was transferred into a polypropylene bag and then distilled water was added to make a 36% water content. This step is called a semi-dry process. Subsequently, glycidyl trimethyl ammonium chloride (GTMAC) was dropped into the solid mixture as a quaternization reagent at various GTMAC-to-Anhydroglucose unit (AGU) molar ratios, ranging from 1 to 3. Then, the solid mixture was hand kneaded to generate uniform mixture. The mixture was kept in a thermostated ultrasonication (Crest Ultrasonics, USA) at 65°C for 4 hr with the application of hand kneading every 15 min. After 4 hr, the reaction was

stopped and residues of any unreacted reagents, i.e. sodium hydroxide and unreacted GTMAC, were removed by centrifugation (TOMY MX-305 High speed refrigerated micro centrifuge) in 95% ethanol at a temperature of 10°C with a rotational speed of 11,000 G for 10 min. After centrifugation, the obtained sediment, quaternized cellulose, was finally filtered and oven dried (BINDER, Germany) at 45°C overnight.

2.2 Nanofibrillation of QC by a microfluidizer

The methodology for QC nanofibrillation was adapted from that of Pei et al. (2013). The QC at an optimal GTMAC content was dispersed in distilled water to produce QC suspension at a solid content of 0.5% (w/v), and then agitated with magnetic stirring at 600 rpm for 24 hr. The QC suspension was then passed through a microfluidizer (M-110P Microfluidizer Processor) equipped with Z chamber, at room temperature and a pressure of 1600 bar. The final product in a form of gel-like suspension of quaternized cellulose nanofibrils (QCNF) was obtained.

3. Characterization of DCP, cellulose and QC

3.1 Fourier transform infrared spectroscopy (FTIR)

Chemical Structures of all samples were characterized by an FTIR spectrometer (NICOLET 6700, Thermo Scientific, USA). The sample was grinded with a mortar and pestle, and compressed into disks with a concentration of 2% (w/w) in KBr. The FTIR spectra were recored in a region of 400-4000 cm^{-1} , using 32 scans at a nominal resolution of 4 cm^{-1} .

3.2 Solid-state CP/MAS ^{13}C NMR spectroscopy

Chemical Structure of cellulose and QC was characterized by Solid-state CP/MAS ^{13}C NMR (Cat. No. 03-339-21D, Fischer Scientific).

3.3 X-ray diffraction (XRD) analysis

X-ray diffractogram was obtained with a 2θ angular range from 5° to 30° at a scanning speed of 0.05° min^{-1} . The $\text{CuK}\alpha$ radiation ($\lambda = 1.5418\text{\AA}$) was operated at 45 kV and 40 mA (Bruker D8 Advance) (Salajkova' et al., 2012). By using Fityk

software, crystallinity index (CrI) was determined using a peak intensity method (Ciolacu et al., 2010), by employed the following equation:

$$\text{CrI} = \frac{A_c}{A_t} \times 100\% \quad (3.2)$$

Where, A_c is area of crystalline peak

A_t is total area

3.4 Nitrogen contents

Nitrogen contents (N%) of the samples were investigated by an elemental analyzer (Series CHNS-628, LECO instruments co. ltd, Thailand). Degree of substitution (DS) and Cationization Reaction Efficiency (CRE) of quaternary ammonium groups was determined by considering nitrogen contents and calculated by using the following equations (Wang et al, 2009; Zaman et al., 2012):

$$\text{DS} = 162 \times \text{N\%} / (1400 - 151.5 \times \text{N\%}) \quad (3.1)$$

Where, N% is nitrogen content in quaternized cellulose

162 is molecular weight of anhydroglucose unit

151.5 is molecular weight of glycidyltrimethylammonium chloride (GTMAC)

$$\% \text{CRE} = \text{DS} \times 100 / (\text{GTMAC-to-AGU molar ratio}) \quad (3.2)$$

3.5 Antibacterial activity evaluation

The antibacterial activity of the optimal QC was test against both Gram positive; *S. aureus* (ATCC 6538), and Gram negative; *E. coli* (ATCC 8739) using standard test method of CLSI M7-A9: Methods for dilution antimicrobial susceptibility tests for bacteria that grow aerobically (MIC).

The optimal QC was dissolved in distilled water to provide a 2% w/v suspension as a stock dilution. The QC aqueous suspension was sterilized in an autoclave at a temperature of 121°C for 15 min. After incubation at a temperature of 37°C for 24 h, the visual turbidity was measured and obtained the minimal inhibitory concentration (MIC) values. The test procedure was extend further to evaluate the minimal bacterial concentration (MBC), or the lowest concentration that 99.9% of cells was killed. In this test, the sample without visible microbial growth were

transferred and plated on agar. The MBC is determined the lowest concentration of antibiotic that there is no bacteria growth on the agar.

3.6 Scanning electron microscopy (SEM)

Surface morphology of powder of QC at molar ratio of 2, and resulting QCNF from freeze drying were observed from scanning electron microscope (HITACHIS-3400N SEM, Illinois, USA). The samples were mounted on a stub, and gold coated by an ion sputter (Hitachi E-1010) prior at a current of 15 mA for 90 s before SEM imaging.

Section II: Preparation and characterization of microparticles of PLLA-co-GMA copolymers and quaternized cellulose

1. Preparation of microparticles by a suspension curing process

1.1 Microparticle formation

There are 2 main experimental approaches for preparation of PLLA-co-GMA copolymers and quaternized cellulose.

1.1.1 Microparticle formation from QC powder via a phase inversion emulsification (PIE) method

The microparticles were prepared via a suspension curing process of PLLA-co-GMA copolymer droplets generated by PIE method, modified from that of Chaiyasat et al. (2013). The oil and aqueous phases were separately prepared. For the oil phase, PLLA-co-GMA copolymers were dissolved in chloroform at a concentration of 25% (w/w), and then mixed with Benzyl peroxide (BPO) initiator (8% w/w of copolymer) and Poly(vinyl alcohol) (PVA) surfactant (4% w/w of the total solution). Subsequently, the QC powder obtained from section I at an optimal GTMAC content (2.5% w/w of the total solution), was added into the oil phase suspension. The obtained oil phase suspension was transferred to a round-bottom schlenk flask. After that, 50 mL of 12.5% (w/w) Sodium dodecyl sulfate (SDS) surfactant as the aqueous phase was gradually dropped into the oil phase suspension at a rate of 2 mL/min under mechanical stirring at a speed ranging from 250 to 500 rpm, at a polymerization temperature of 80°C for 2 hr.

In the early stage of aqueous phase addition into the oil phase, water-in-oil (W/O) system was formed by the surfactant adsorption at the droplet interface. When the amount of aqueous medium increased until higher than the amount of the oil phase, an oil-in-water emulsion (O/W) was formed. Therefore, the process is called a phase inversion process.

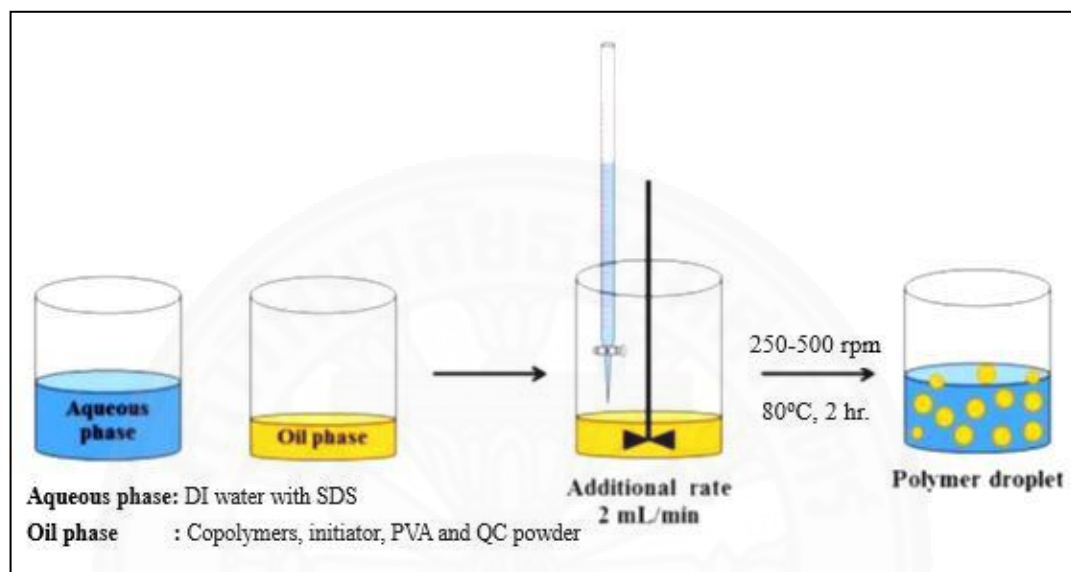


Figure 3.2 Schematic of microparticle formation by PIE method.

1.1.2 Microparticle formation from QC or QCNF suspension via phase inversion emulsification (PIE) method and microfluidizer

To improve uniformity in particle size and reduce the average size the particles, microfluidizer was employed with the PIE process. PLLA-*co*-GMA copolymer droplets were first prepared via PIE method, in which 5 mL of QC or QCNF suspension was mixed with the aqueous phase. After O/W emulsion formation, the emulsion were divided into two routes:

Route 1: The O/W emulsion was stirred with a mechanical stirring at 500 rpm and a polymerization temperature of 80°C for 2 hr.

Route 2: DI water was added into the O/W emulsion to obtain a total volume of 400 mL and then kept overnight. Subsequently, the emulsion was passed through a microfluidizer (M-110P Microfluidizer Processor) and underwent polymerization reaction, under magnetic stirring at 500 rpm, at 80°C for 2 hr.

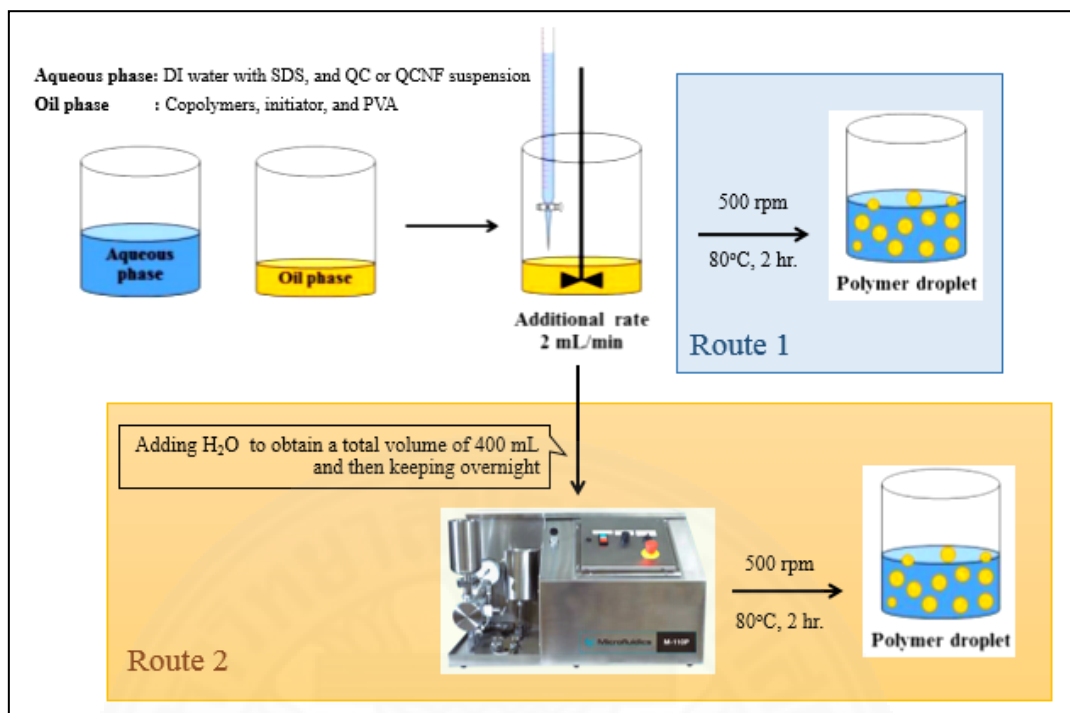


Figure 3.3 Schematic of microparticle formation from QC or QCNF suspension via PIE method and microfluidizer.

1.2 Washing process

After polymerization reaction was completed, the obtained emulsion was transferred to a beaker and left overnight. The emulsion was separated into 2 layers: an oil phase as the bottom layer and an aqueous phase as the top layer. The microparticles were washed with DI water for several times, before oven drying overnight at a temperature of 50°C.

2 Characterization of the microparticles

2.1 Fourier transform infrared spectroscopy (FTIR)

Chemical structures of the samples were characterized by FTIR spectroscopy (Thermo Scientific, iD5) in an attenuated total reflectance (ATR) mode. The spectra were obtained using 32 scans, at a resolution of 2 cm⁻¹.

2.2 Scanning electron microscopy (SEM)

Surface morphology of the particle products was observed from scanning electron microscope (HITACHIS-3400N SEM, Illinois, USA). The resulting microparticles were mounted on a stub, and gold coated by an ion sputter (Hitachi E-1010) prior at a current of 15 mA for 90 s before SEM imaging.

2.3 Laser Scattering Particle Size Distribution Analyzer

Particle size distributions of microparticles were examined by a mastersizer (Laser Scattering Particle Size Distribution Analyzer LA-950, Horiba). The samples were dispersed into diluted water. Before testing, an refractive index was set at 1.47.

Section III: Preparation and characterization of electrospun nanofibers of polylactide and quaternized cellulose

1. Preparation of electrospun nanofibers of neat PLA and blending electrospun nanofiber composites of PLA and QC

PLA pellets were dissolved in a mixture of tetrahydrofuran (THF) and N, N-dimethyl formamide (DMF) with a weight ratio of 3:1) under magnetic stirring at a temperature of 60°C, obtaining a PLA suspension at a concentration of 12% (w/w). Subsequently, QC powder was dispersed into the solution with a solid content of 10% (w/w) based on the amounts of PLA.

Nanofibers from PLA suspension (with or without addition of QC) were fabricated by horizontal electrospinning. The suspension was filled into a 5 mL syringe, connected to a circular-shaped metal needle of a 0.7 mm inner diameter. A high DC voltage power supply was employed to provide a high voltage of 9 kV to the needle and a rotary collector covering with an aluminum foil. The suspension was electrospun at a flow rate of 1 mL/hr, and a spinning distance of 10 cm.

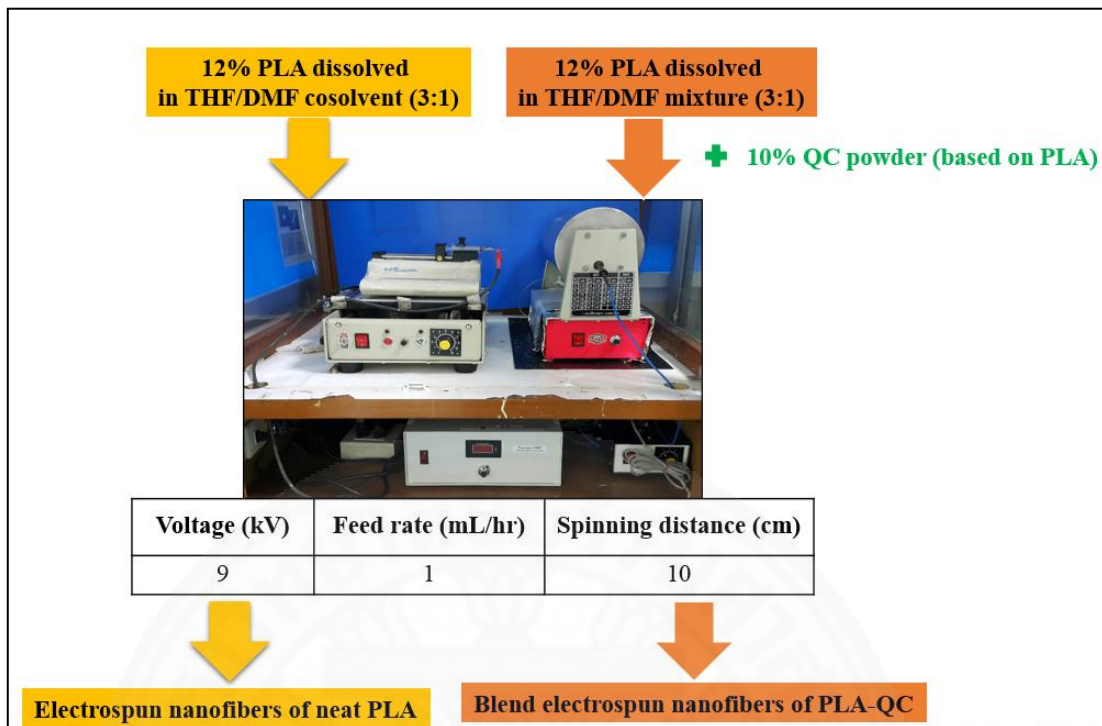


Figure 3.4 Schematic of electrospun nanofibers of neat PLA, and blending electrospun nanofiber composites of PLA and QC.

2. Preparation of coaxial electrospun nanofiber composites of PLA and QCNF

PLA and QCNF were fabricated via coaxial electrospinning process. The core solution is 12% (w/w) PLA suspension in THF-DMF with a weight ratio of 3-to-1. Regarding preparation of shell solution, PVA pellets were firstly dissolved in distilled water under magnetic stirring at a temperature of 120°C. Subsequently, 0.5% w/w of QCNF suspension were added and mixed by magnetic stirring. The resulting shell solution consisted of PVA (3% w/w of total solution), and QCNF (0.25% of a solid content in the total solution).

A dual concentric nozzle consisted of inner and outer ones. The inner nozzle had 0.35 mm of an inner diameter, and 0.65 mm of an outer diameter. While, the outer nozzle had inner and outer diameters of 1.05 mm and 1.45 mm, respectively. Both the core and shell solution were independently fed with two separate syringe pumps. The core feed rate was set to 1.1 mL/h, while the shell feed rate was 0.4 mL/h. The spinning distance and applied voltage were set at 10 cm and 12 kV. The electrospun nanofibers were collected in aluminium foil covered above rotary drum. Vastly, all

electrospinning processes were carried out at a temperature of approx. 25°C and a humidity of higher than 65%.

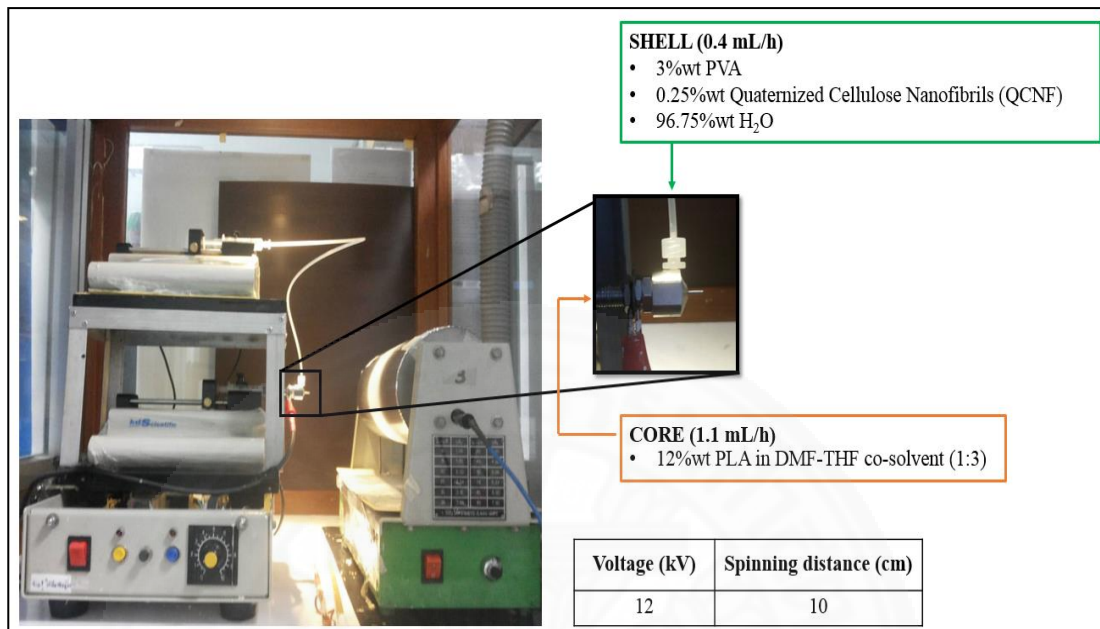


Figure 3.5 Schematic of coaxial electrospun nanofiber composites of PLA and QCNF.

3. Characterization of the nanofibers

3.1 Fourier transform infrared spectroscopy (FTIR)

Chemical structure was characterized by FTIR spectroscopy (Thermo Scientific, iD5) in both Attenuated Total Reflectance (ATR) and transmission modes. The spectra were obtained using 32 scans, at a resolution of 2 cm⁻¹.

3.2 Scanning electron microscopy (SEM)

Surface morphology of the resulting electrospun fibers was observed from SEM (HITACHIS-3400N SEM, Illinois, USA). Aluminum foil with the resulting nanofibers was mounted on a stub, and an ion sputter coated (Hitachi E-1010) with gold prior at a current of 15 mA for 90 s before SEM imaging. Average diameters of fibers were measured from 80 fibers by using ImageJ software.

3.3 Water contact angle measurements

Surface wettability of the fibers was measured by using a water contact meter (Dataphysics, Germany) with water droplets volume of approx. 5 μ L. Each sample was evaluated in five times. Apparent contact angle were recorded over a duration of 30 min with evaluating every 5 min (Dufficy et al., 2015).

3.4 Evaluation of antibacterial activity

The antibacterial activity was evaluated against both Gram positive; *S. aureus* (ATCC 6538), and Gram negative; *E. coli* (ATCC 8739) based on JIS Z 2801-2010: Antimicrobial product – Test for antimicrobial activity and efficacy.

To prepare samples, the nanofibers were peeled aluminum foil off and cut into a size of 5 cm x 5 cm. Under test, 3 replicated samples of electrospun nanofibers of PLA-QCNF and 6 replicated untreated samples of neat PLA electrospun nanofibers were used. A cell suspension of either *E. coli* (1.85×10^6 CFU/ml) or *S. aureus* (1.54×10^6 CFU/ml) is prepared. An aliquot with a volume of 0.3 ml was inoculated onto surface of the material, and then a sterile polyethylene film (4 cm x 4 cm) was covered on a test piece in order to hold in intimate contact. The incubation was at 35°C at saturation humidity for 24 hr. After incubation, the sample was washing with 10 ml of soya casein digest lecithin polysorbate (SCDLP) broth using stomacher mechanical agitation. Surviving bacteria were counted to determine the antibacterial activity as following equations:

$$R = \log (B/C) \quad (3.3)$$

$$\% \text{ Reduction} = \log [(C-B) / B] \quad (3.4)$$

Where, R = value of antibacterial activity

B = average number of viable bacterial cells on untreated sample after 24 hr

C = average number of viable bacterial cells on sample after 24 hr

Chapter 4

Results and Discussion

4.1 Characterization of quaternized cellulose (QC)

Physical appearance of cellulose product and its raw materials are examined, as illustrated in Figure 4.1. De-starch cassava pulp (DCP), a by-product from cassava starch production, is brown powder. Cellulose product extracted from the DCP is white cloudy powder, as a result from the extraction and bleaching steps. The cellulose extraction yield in this study was 17.5%.



Figure 4.1 Physical appearance of de-starched cassava pulp (DCP) (a), and cellulose products (b).

The chemical structures and properties of DCP, cellulose, and QC are examined. FTIR spectra of all samples are illustrated in Figure 4.2. A strong band at around 3400 cm^{-1} was assigned to the O-H stretching mode of hydroxyl groups which form intramolecular hydrogen bonding, on C-2 and C-6 of the pyranose rings. The absorbance mode at 2903 cm^{-1} was corresponded to the C-H stretching mode (Nazir et al., 2013; Saelee et al., 2014; Mariño et al., 2015). A sharp band at 897 cm^{-1} was assigned to C-O-C stretching at β -glycosidic linkage between the glucose units (Fang et al., 2000; Nazir et al., 2013; Saelee et al., 2014; Raeisi et al., 2015). When de-starch cassava pulp (DCP) was extracted to form cellulose, a disappearance of the vibrational mode at 1739 cm^{-1} (acetyl and ester group of hemicellulose and carbonyl ester of the p-coumaric monomeric lignin unit) (Fang et al, 2000; Nazir et al., 2013;

Mariño et al., 2015; Raeisi et al., 2015), 1250 cm^{-1} (C-O stretching vibration of hemicellulose) (Fang et al., 2000; Periera et al., 2011; Mariño et al., 2015) and 1515 cm^{-1} (C=C stretching of aromatic ring in lignin) (Saelee et al., 2014; Raeisi et al., 2015) is observed, indicating a removal of hemicellulose and lignin components. The corresponding FTIR spectrum of quaternized cellulose after the incorporation of GTMAC shows a distinct mode at 1479 cm^{-1} , assigned to asymmetrical stretching of C-H in methyl groups of GTMAC (Gorshkova et al., 2011; Zaman et al., 2012; Sajjan et al., 2013; Sajjan et al., 2015; Tang et al., 2016). The intensity of this band increases with the increase in the GTMAC contents. Moreover, the intensity of a band at around 3400 cm^{-1} , corresponding to hydroxyl groups of cellulose, decreases with the increasing of the GTMAC contents. These results provide firm evidences of successful grafting of GTMAC on the cellulose's structures.

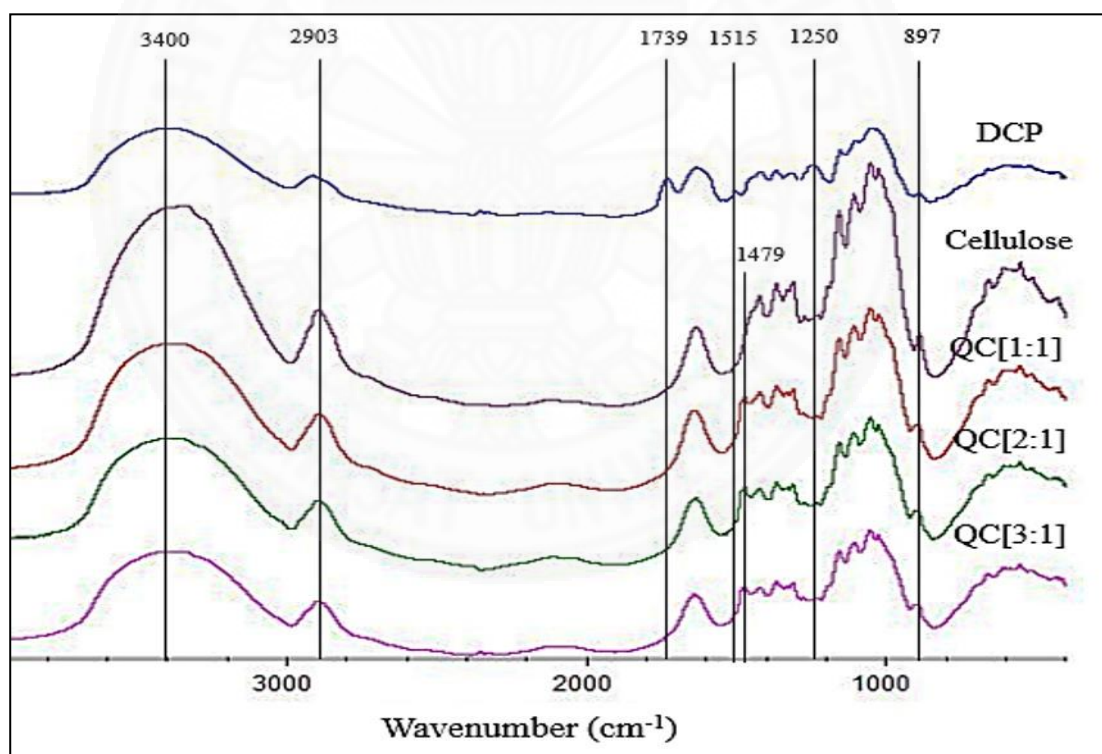


Figure 4.2 FTIR spectra of de-starch cassava pulp (DCP), cellulose, and quaternized cellulose (QC) at various GTMAC-to-AGU molar ratios, from 1 to 3.

The crystal structure of all samples were investigated by XRD, as presented in Figure 4.3. All samples illustrate semi-crystalline characteristics, including amorphous and crystalline regions. There are characteristic signals at 15°, 17°, 21°, and 23° in all samples as typical diffraction pattern of cellulose I or native cellulose (Neto et al., 2013). The pattern of cellulose is narrower and sharper, compared to that of DCP. This is because the amorphous domains from non-cellulosic compound were removed after the alkaline treatment and the bleaching process (Pereira et al., 2011). Results on calculated CI values of cellulose (59.93%) show slight higher values than that of DCP, with CI of 33.33%. The CI values of QC at various molar ratios of 1, 2 and 3 are 49.36%, 49.46%, and 48.32%, respectively. This is also reflected by a decrease in the peak intensity of QC with an increasing GTMAC content. This is because GTMAC substitution causes H-bond deformation in hydroxyl groups of cellulose, leading to lower crystalline contents. However, the partial crystalline region available in QC would lead to water insoluble (Wang et al., 2009).

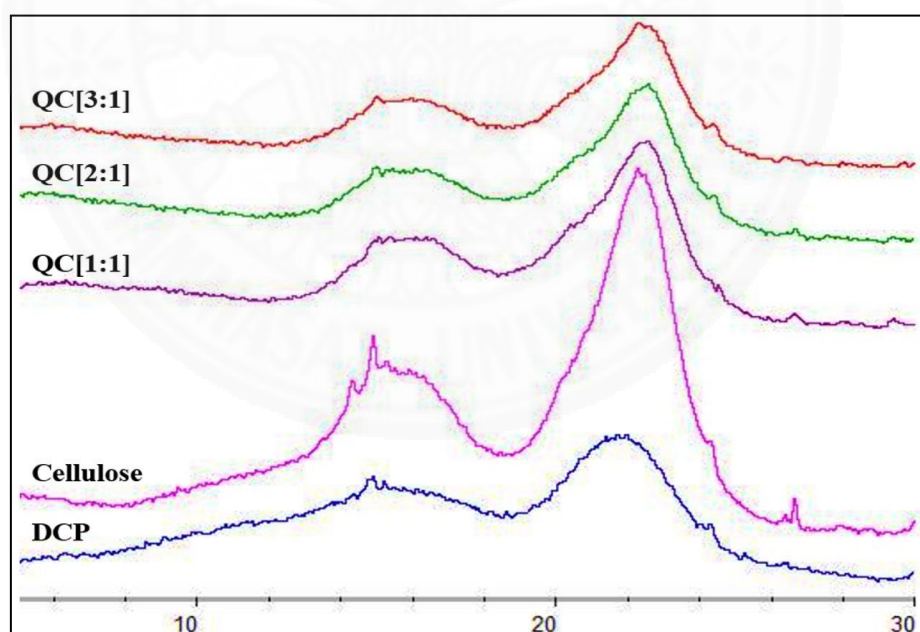
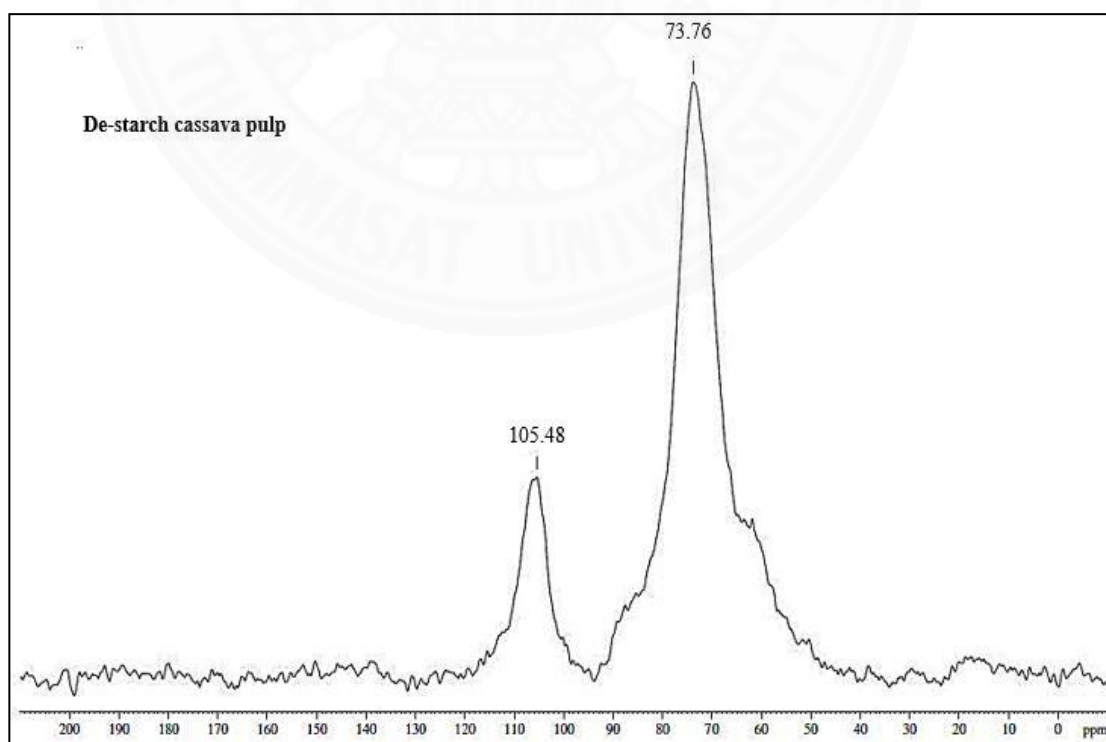


Figure 4.3 XRD patterns of de-starch cassava pulp (DCP), cellulose, and quaternized cellulose (QC) at various GTMAC-to-AGU molar ratio, from 1 to 3.

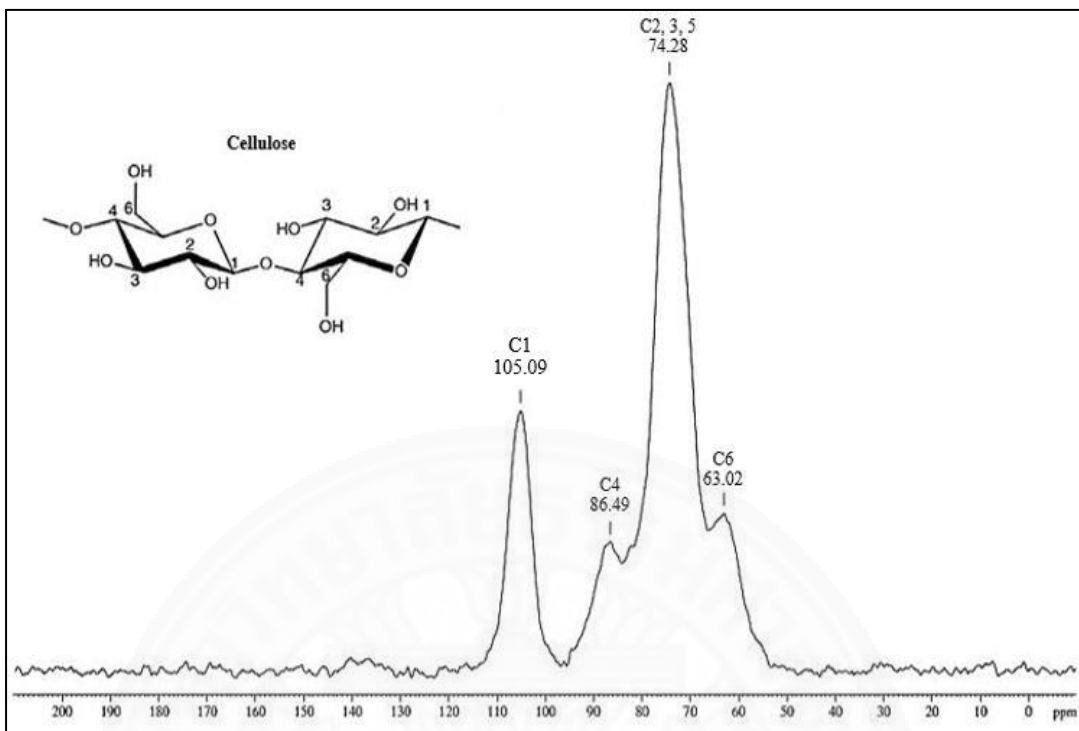
As results of Solid-state ^{13}C NMR, they were verified the FTIR and XRD results. Solid-state ^{13}C NMR spectra of DCP, cellulose, and QC, at various GTMAC

contents are shown in Figure 4.4. There are two significant signals (105.48 and 73.76 ppm) in the NMR spectrum of DCP. After alkaline treatment and bleaching process, the obtained cellulose has 4 distinctive peaks. The signal at 105.09 and 63.02 ppm were assigned to C1 and C6, respectively. The peaks appearing at around 64 and 67 ppm are assigned to those of C8 and C9, leading to a new signal around 65 ppm (C6'). The strong signal at about 74 ppm was attributed to C2, C3, C5 and C7. Obviously, there was a new signal at 55 ppm, attributing to N⁺ (CH₃) (C10) functional. Moreover, a peak at around 86 ppm was corresponded to C4 (Song et al., 2008; Song et al., 2010; Li et al., 2015). All results from FTIR and NMR spectroscopy demonstrate that GTMAC was introduced successfully onto the cellulose chains via a semi-dry process.

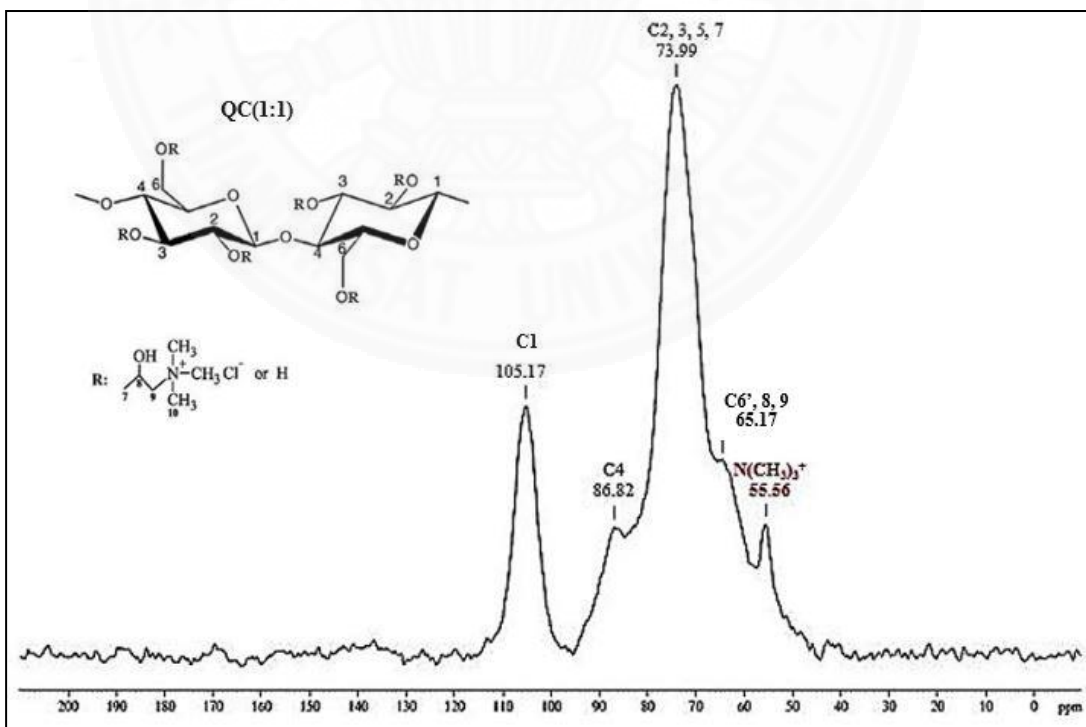
The CI values calculated from the NMR C4 peak separation method (Appendix D) show that DCP has CI of 22.73%. After alkaline treatment and bleaching process, CI of the obtained cellulose increases to 34.56%. QC at various molar ratios of 1, 2 and 3 have CI of 31.84%, 31.51%, and 30.91%, respectively. This also confirms that higher degree of GTMAC substitution, leading to lower CI values.



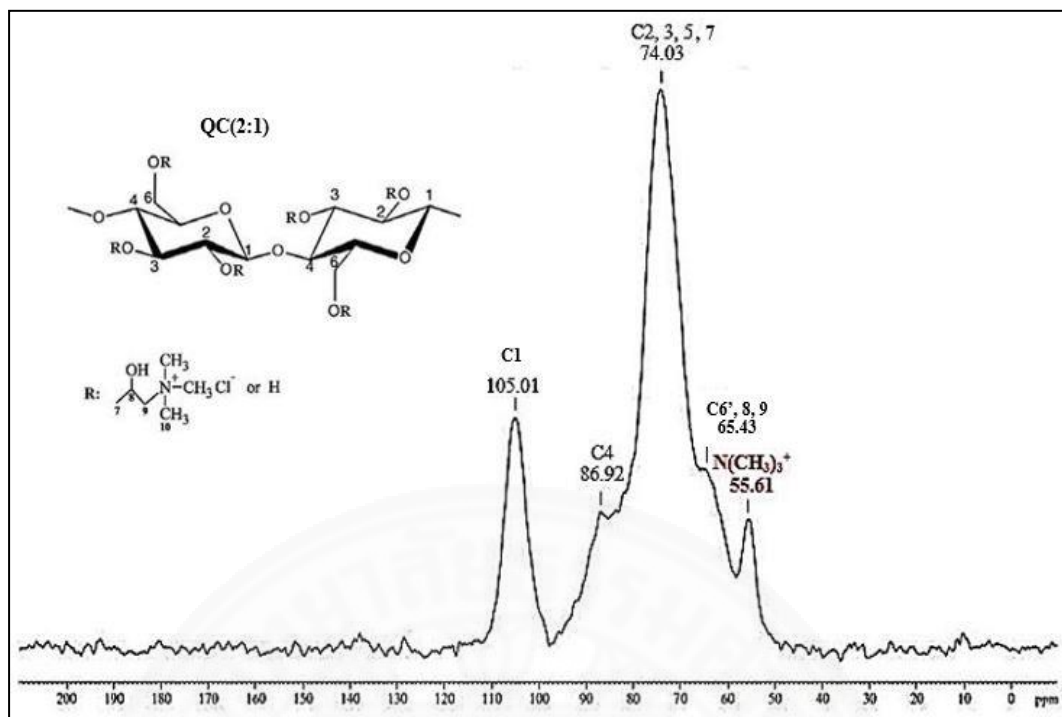
(a) De-starch cassava pulp (DCP)



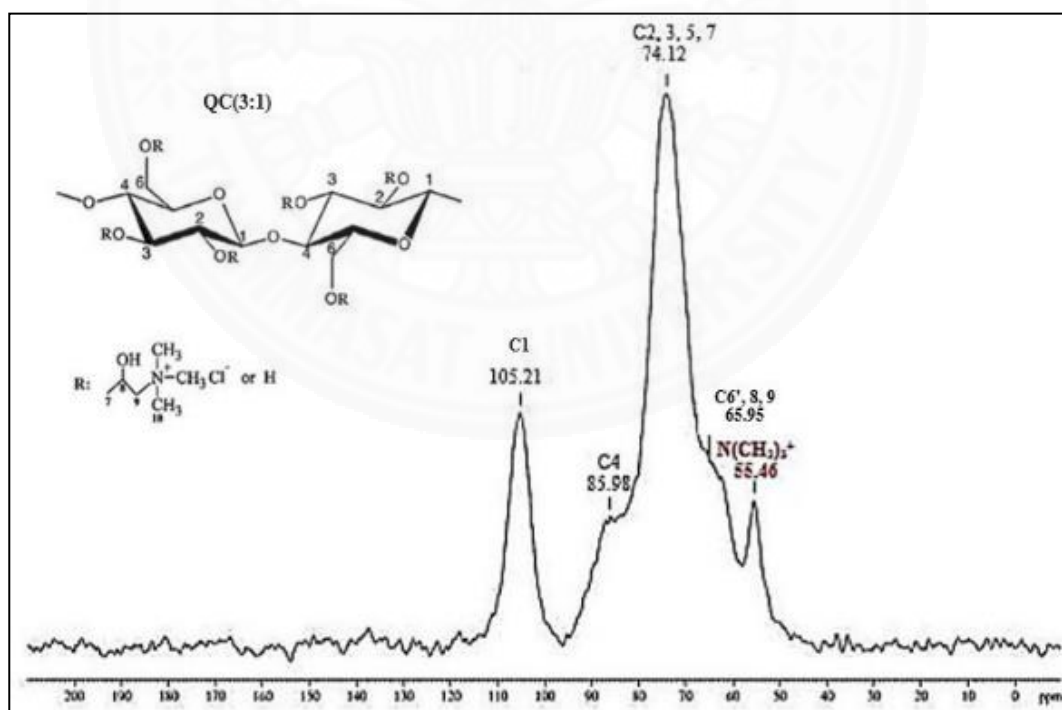
(b) Cellulose



(c) QC at molar ratio of 1



(d) QC at molar ratio of 2



(e) QC at molar ratio of 3

Figure 4.4 ¹³C NMR spectra of de-starch cassava pulp (DCP), cellulose, and quaternized cellulose (QC), at various GTMAC-to-AGU molar ratios, from 1 to 3.

The nitrogen contents of DCP, cellulose, and QC are summarized in Table 4.1. DCP has 0.5% nitrogen content, indicating that some nitrogen components are observed which are crude protein and non-protein (nitrate, nitrite, cyanogenic compound), in this materials (Montagnac et al., 2009). After alkaline treatment and bleaching process, the protein constituents in DCP samples were removed, causing a decrease in the nitrogen content to 0.11%. The nitrogen contents of QC is higher than that of cellulose. The increases in the nitrogen content of QC confirms that GTMAC is grafted onto the cellulose's surface. On the effect of molar ratio of GTMAC-to-AGU, the results show that the nitrogen contents increase with increasing of the molar ratio. The nitrogen content of QC is used to calculate the degree of substitution and cationization reaction efficiency.

Figure 4.5 shows results on effect of GTMAC-to-AGU molar ratios on the degree of substitution and the cationization reaction efficiency. The degree of substitution has an upward trend while the cationization reaction efficiency shows a downward trend, when the molar ratio of GTMAC-to-AGU is increased. This is likely because at lower GTMAC contents, there is limited GTMAC availability to substitute hydroxyl groups in cellulose, resulting in low degree of substitution (Zaman et al. 2012). In contrast, the higher GTMAC contents lead to higher degree of substitution. To determine the cationization reaction efficiency, percentages of GTMAC consumption in the cationization of cellulose are measured. At higher GTMAC contents, higher GTMAC consumption is observed in the GTMAC hydrolysis reaction. This is an undesirable reaction, which causes low cationization reaction efficiency. In the contrast, at lower GTMAC contents, an excessive hydroxyl groups in cellulose is available for GTMAC substitution, leading to an increase in the cationization reaction efficiency. From the results of degree of substitution and cationization reaction efficiency, it is important to note that a molar ratio of 2:1 is an optimal GTMAC content. The degree of substitution of 0.26 and the cationization reaction efficiency of 12.28% is obtained at this molar ratio.

Table 4.1 Results on the nitrogen contents of DCP, cellulose, and QC samples

Sample	Nitrogen content (%)
DCP	0.51 ± 0.03
Cellulose	0.11 ± 0.01
QC[1:1]	1.56 ± 0.02
QC[2:1]	1.89 ± 0.03
QC[3:1]	1.93 ± 0.02

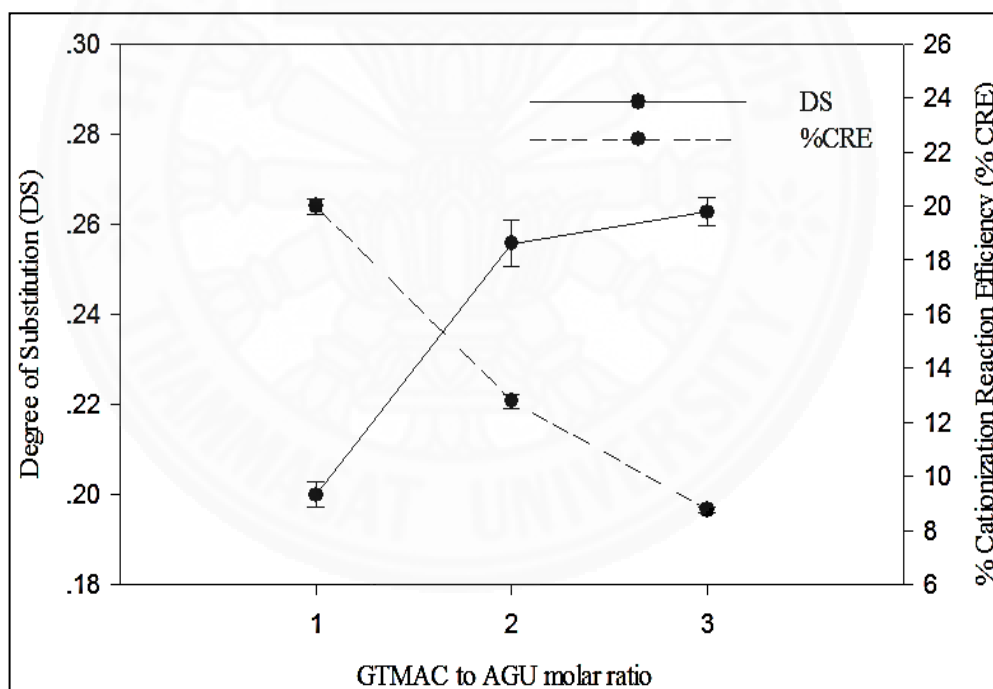


Figure 4.5 Effect of GTMAC: AGU molar ratio on the degree of substitution and the cationization reaction efficiency.

Table 4.2 presents minimum inhibitory concentration (MIC) and minimum bactericidal concentration (MBC) of QC at molar ratio of 2. The QC sample exhibited effective antibacterial activity against both Gram-negative (*E. coli*) and Gram-positive (*S. aureus*) bacteria with the MIC values of 0.5% (w/v) and 0.0078% (w/v), respectively. In addition, the MBC values against *E. coli* and *S. aureus* of the QC sample are 2% (w/v) and 0.0078% (w/v), respectively. Interestingly, both the MIC and MBC results can be concluded that the QC samples presented less effective inhibition and bactericide against *E. coli* than *S. aureus*. This may be corresponded to their difference in cell wall. *S. aureus* is a Gram-positive bacterium in which the cell wall is derived from peptide polyglycogen having a pore structure. Consequently, the foreign molecules can pass through the cell wall easily. Whereas, *E. coli* (Gram-negative bacterium) has its cell wall that is composed of a thin membrane of peptide and an outer membrane made up of lipoprotein, lipopolysaccharide, and phospholipids. The outer membrane is utilized as a potential barrier against foreign molecules such as antibacterial agents (Song et al., 2010).

Regarding typically accepted mechanism for antibacterial action of such quaternary ammonium salts, positive-charged polycations of QC interact electrostatically to negative-charged phospholipids and proteins represent on the surface of bacterial cell. These interactions consequently defect a membrane permeability of cytoplasm. It causes the loss of cytoplasmic components and the death of microorganisms (Roy et al., 2008).

Table 4.2 Minimum inhibitory concentration (MIC) and minimum bactericidal concentration (MBC) of QC at molar ratio of 2 against *E. coli* (ATCC 8739) and *S. aureus* (ATCC 6538) for 24 hours of incubation period

	MIC (w/v)	MBC (w/v)
Gram-negative bacteria: <i>E. coli</i> (ATCC 8739)	0.5%	2%
Gram-positive bacteria: <i>S. aureus</i> (ATCC 6538)	0.0078%	0.0078%

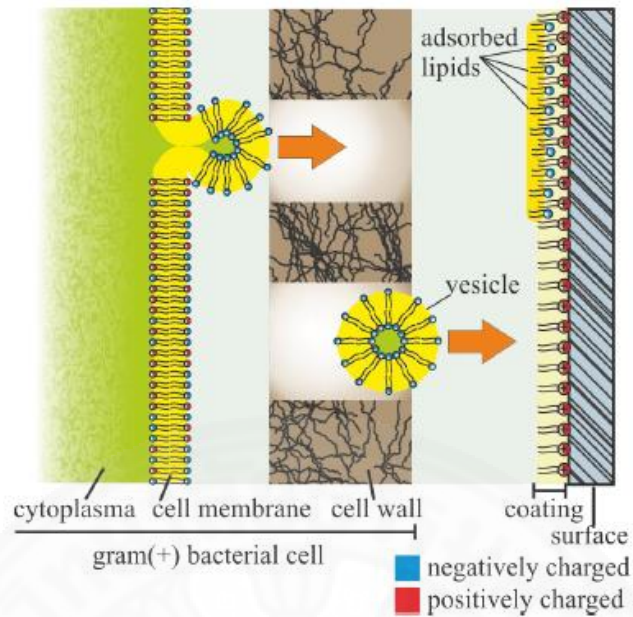


Figure 4.6 Mechanism of antibacterial action of quaternized cellulose (Siedenbiedel & Tiller, 2012).

QC powder obtained from the optimal conditions was used as raw materials to produce quaternized cellulose nanofibrils (QCNF). The QC suspension, shown in Figure 4.7, with a solid content of 0.5% (w/w) was magnetic stirred at 600 rpm for 24 hr, resulting swollen QC fibers). After pre-agitation, the QC suspension was passed through a microfluidizer. The obtained suspension was optically transparent and gel-like aqueous suspension of QCNF, generated from disintegration of the swollen fibers into nanofibrils. The visible transparent suspension indicated a good level of QCNF dispersion in water and generation of colloidal suspension (Pei et al., 2013).

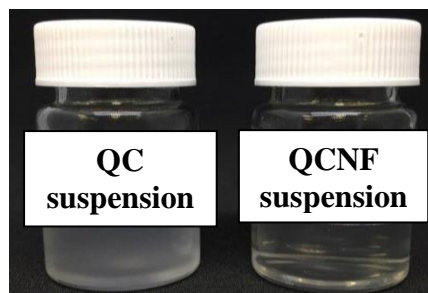


Figure 4.7 Appearances of quaternized cellulose (QC) and quaternized cellulose nanofibrils (QCNF) suspension.

Figure 4.8 presented SEM images of QCNF compared to QC. The QC fragments present agglomeration of macrofibrils, shown in Figure 4.8 (a). After passing through a microfluidizer, the resulting QCNF illustrates an aggregation of nanofibrils, presented in Figure 4.8 (b). Individual nanofibrils have a diameter of approx. below 1 μm .

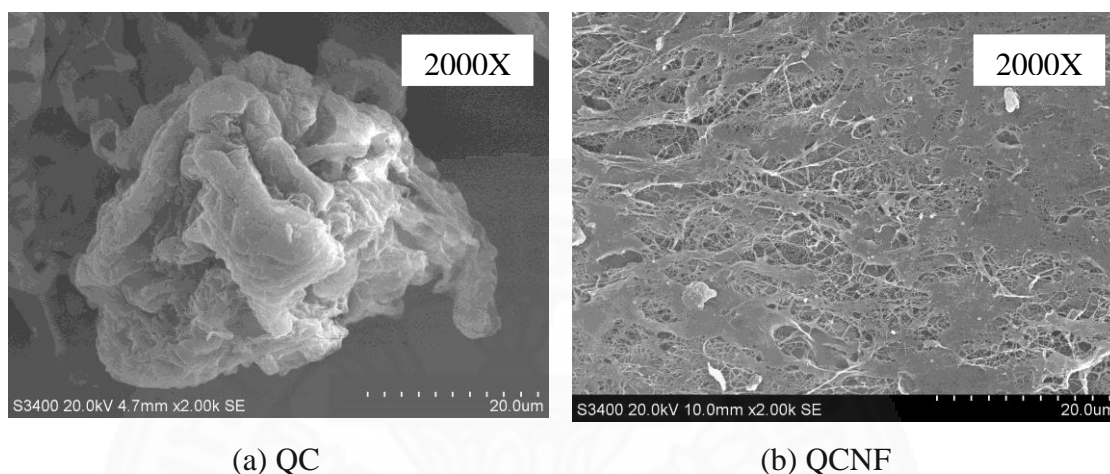


Figure 4.8 SEM images of quaternized cellulose (QC) (a), and quaternized cellulose nanofibrils (QCNF) (b).

4.2 Characterization of microparticles of PLLA-*co*-GMA copolymers and quaternized cellulose

Chemical structures and properties of microparticles are investigated. Figure 4.9 presents ATR-FTIR spectra of neat P(PLLA-*co*-GMA) copolymers, QC at an GTMAC content of 2, and microparticle samples containing QC via different experimental approaches. Vibrational modes located at 1760 and 1720 cm^{-1} are assigned to the C=O stretching modes of PLLA and GMA, respectively. The C=C stretching modes of GMA are at 1640 and 817 cm^{-1} (Petchsuk et al., 2012). In the spectra of microparticle, a disappearance of bands 1640 or 817 cm^{-1} is observed, reflecting a formation of crosslinked network by utilizing the double bonds. All spectra of microparticles containing QC powder, QC suspension, and QCNF suspension via PIE method show a characteristic signal of CH₃ blending modes at 997 cm^{-1} , indicating the presence of cellulose on the microparticles' surface. On the other hand, this signal at 997 cm^{-1} does not present in all spectra employing QC suspension and QCNF suspension via PIE method and then passing through microfluidizer. This

is likely because that before passing through the microfluidizer, oil-in-water emulsion obtaining from PIE method was kept overnight, leading phase separation.

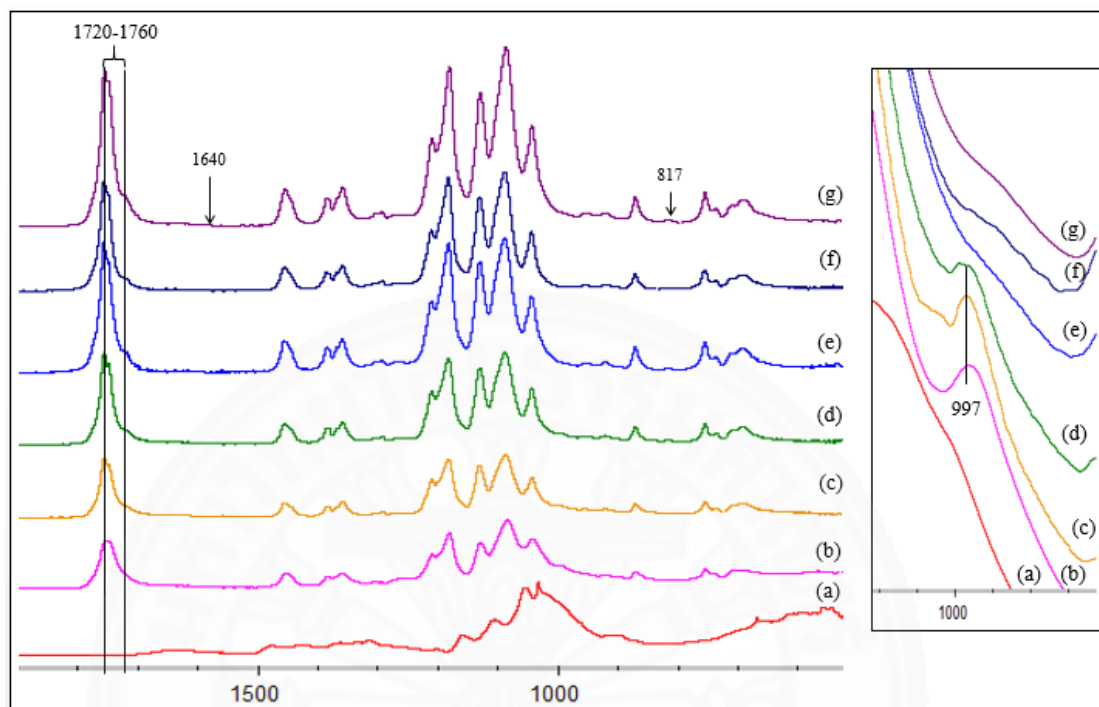
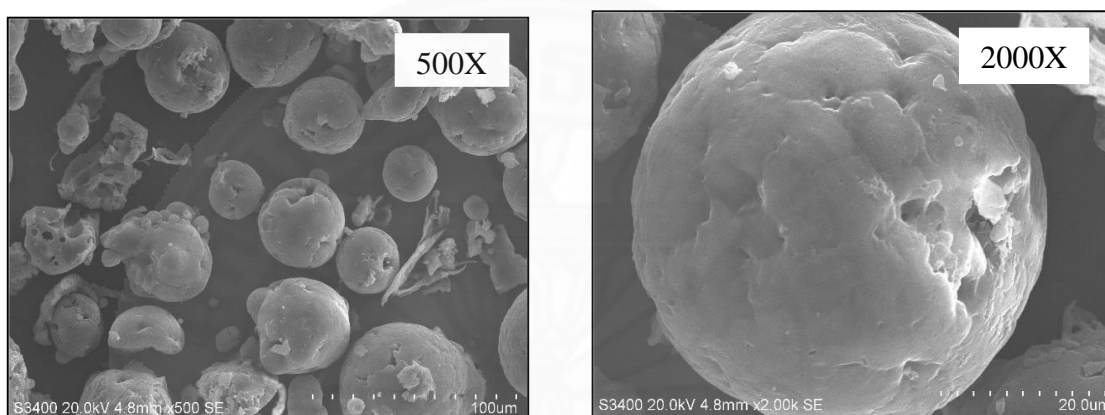


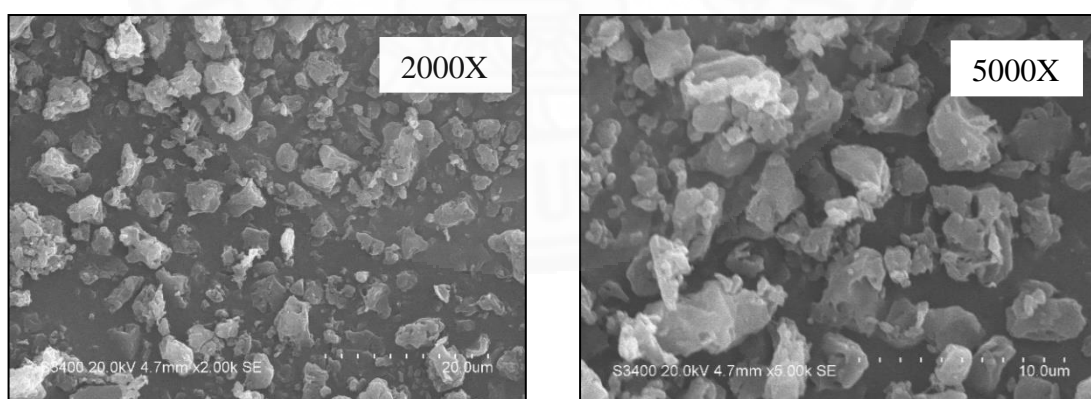
Figure 4.9 FTIR-ATR spectra of microparticles containing QC via different experimental approaches and their raw materials: (a) QC at molar ratio of 2, (b) Microparticles from QC powder via PIE, (c) Microparticles from QC suspension via PIE, (d) Microparticles from QCNF suspension via PIE, (e) Microparticles from QC suspension via PIE-Microfluidizer, (f) Microparticles from QCNF suspension via PIE-Microfluidizer, and (g) PLLA-*co*-GMA copolymers.

Surface morphology of microparticles fabricated via different experimental approaches are compared in Figure 4.10. The microparticles prepared from QC powder via PIE method show in Figure 4.10 (a). Certain amount of QC was successfully incorporated into the microparticles, forming spherical shape. However, residual QC which was not incorporated into the microparticles during the suspension curing process, presenting as irregular shape. Microparticles prepared from either QC or QCNF suspension via a PIE method present irregular shape with roughness surface, in which QC and QCNF fragments are clearly observed on their surface, as

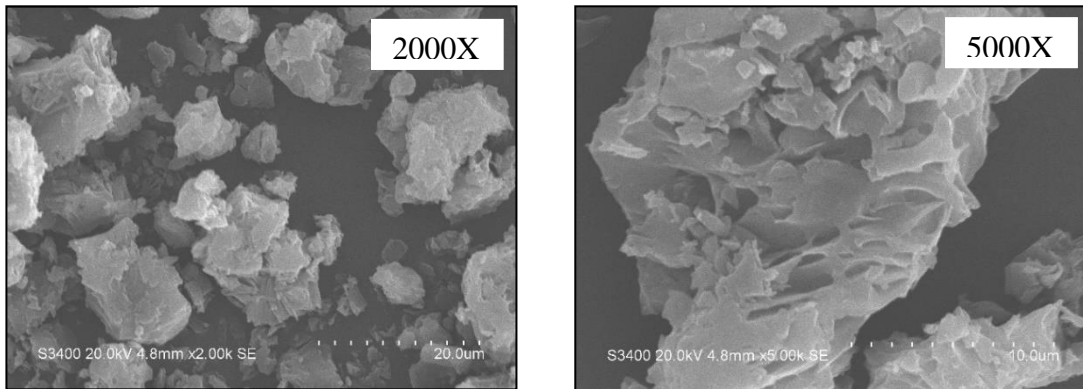
illustrated in Figure 4.10 (b) and (c) respectively. This is because of surface charge on cellulose, leading to the fact that some surfactants are spoiled instead of stabilizing to form polymer droplets. On the other hand, microparticles from either QC or QCNF suspension via PIE method and then passing through microfluidizer, illustrated in Figure 4.10 (d) and (e) respectively, is resulted in spherical shapes of microparticles because microfluidizer have small size of hole. This makes no effect of microfluidizer on stabilizing polymer droplets.



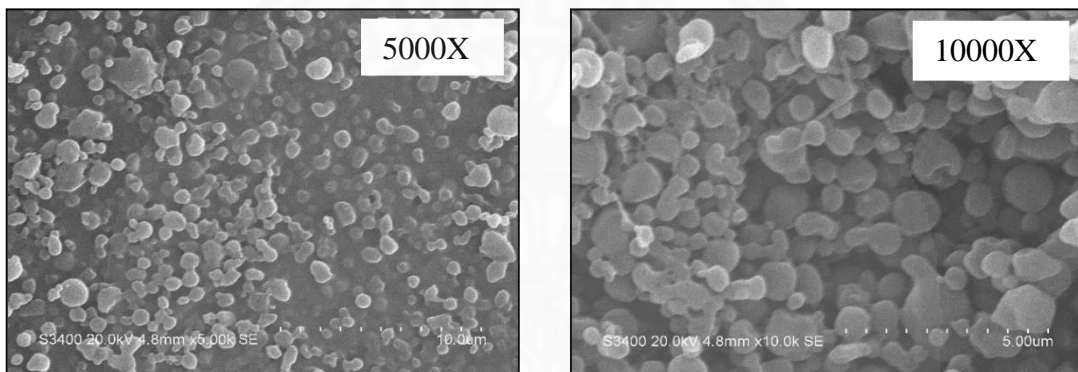
(a) Microparticles employing QC powder via PIE method



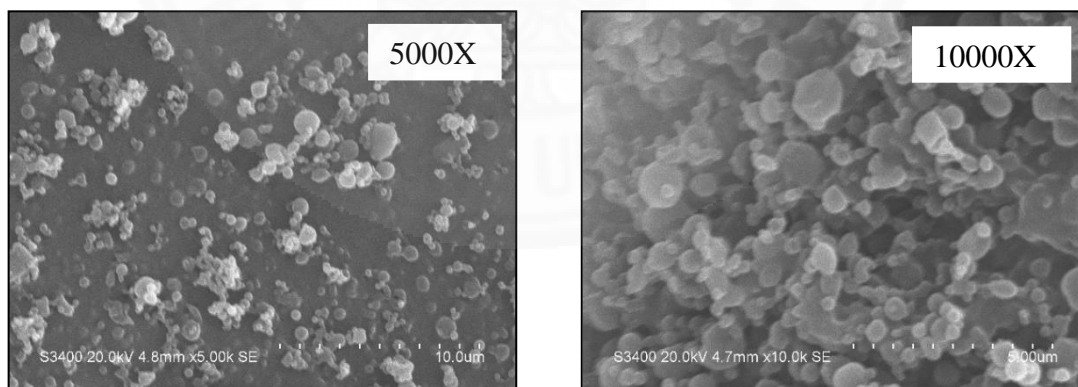
(b) Microparticles from QC suspension via PIE method



(c) Microparticles from QCNF suspension via PIE method



(d) Microparticles from QC suspension via PIE method and microfluidizer



(e) Microparticles from QCNF suspension via PIE method and microfluidizer

Figure 4.10 SEM images of microparticles obtained from different experimental approaches.

Results on the particle size distribution (PSD) of all microparticles are shown in Figure 4.11. Microparticles employing QC powder via PIE method exhibit a PSD curve with bimodal feature, whose median diameter is 39.78 μm . The PSD curves of microparticles employing both QC and QCNF suspension via PIE method show in multi-modal pattern, with median diameters of 37.74 and 24.08 μm , respectively. The corresponding particles obtained via PIE method and then passing through microfluidizer, from either QC or QCNF suspension show PSD curves with bimodal pattern, whose median diameters are 1.08 and 0.52 μm , respectively. It is clearly seen that the mean diameter of microparticles prepared by PIE method and then passed through microfluidizer is smaller, compared to those of microparticles prepared via only PIE method.

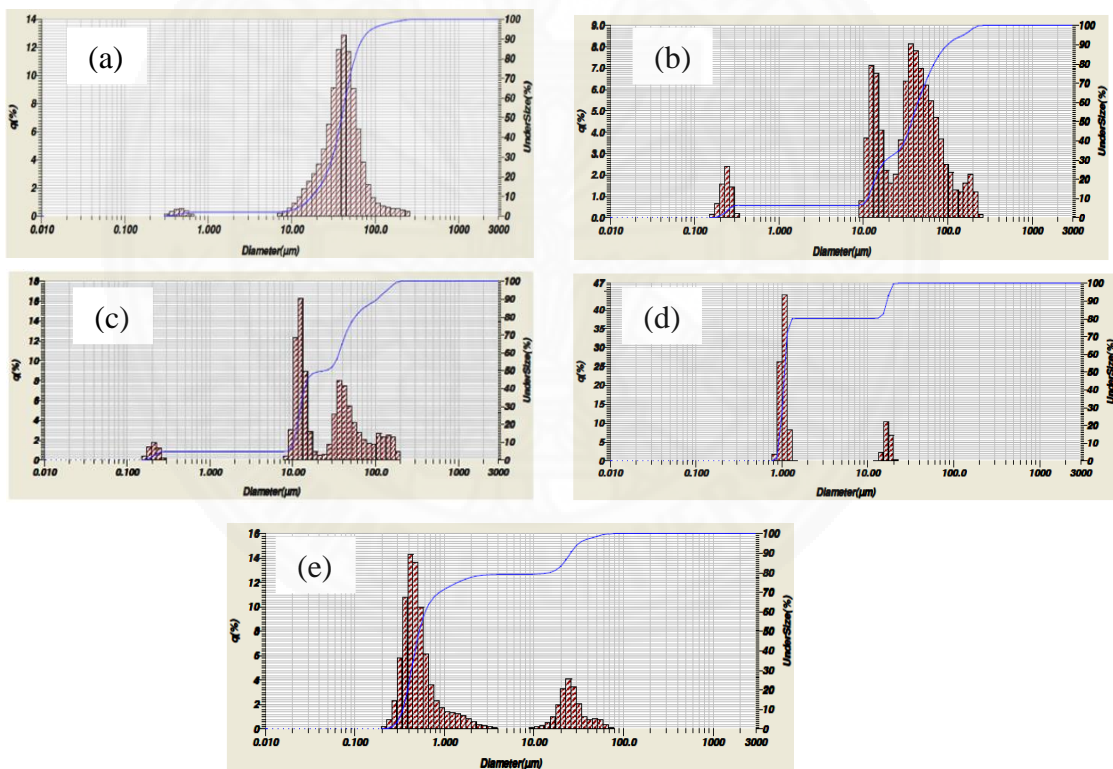


Figure 4.11 Particle size distributions of microparticles obtained from different experimental approaches: (a) Microparticles from QC powder via PIE method, (b) Microparticles from QC suspension via PIE method, (c) Microparticles from QCNF suspension via PIE method, (d) Microparticles from QC suspension via PIE method and microfluidizer, and (e) Microparticles from QCNF suspension via PIE method and microfluidizer.

4.3 characterization of electrospun nanofibers of polylactide and quaternized cellulose

Properties and surface morphology of the resulting electrospun nanofibers are examined. Chemical structure of the resulting electrospun nanofibers are characterized by FTIR spectroscopy in both ATR and transmission modes, as illustrated in Figures 4.12 and 4.13. Bands near 3000 cm^{-1} are assigned to various C-H stretching modes (Seyedjafari et al, 2011; Mashhadikhan et al., 2015). A strong band of carbonyl stretching (C=O) is observed at 1754 cm^{-1} (Seyedjafari et al., 2010; Seyedjafari et al, 2011; Chen et al., 2013; Mashhadikhan et al., 2015). The band at 1083 cm^{-1} is attributed to C-O stretching (Seyedjafari et al, 2011). In addition, in spectra of PLA composite nanofibers employing either QC or QCNF, a new band appears at 1215 cm^{-1} , corresponding to interaction between hydroxyl group of QC and ester group of PLA. The C-H stretching mode of PVA, exhibited at 2923 cm^{-1} (Costa et al., 2007), can be found in the FTIR spectra of coaxial electrospun nanofiber composites of PLA and QCNF.

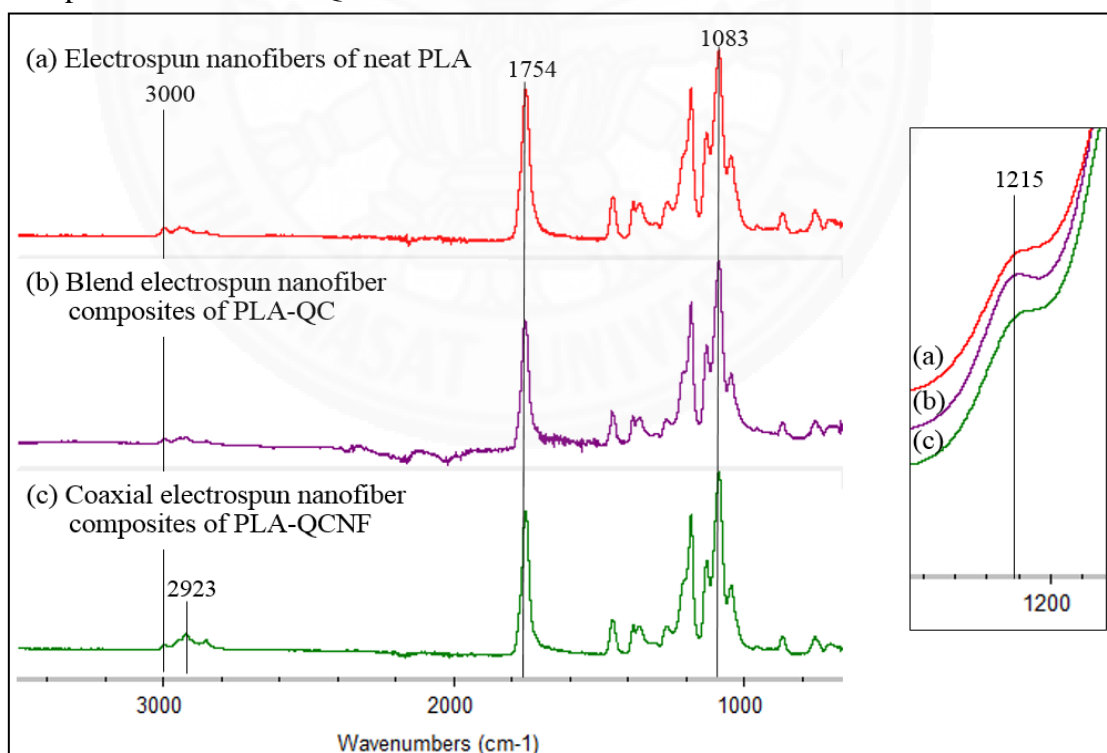


Figure 4.12 ATR-FTIR spectra of electrospun nanofibers of neat PLA, blend electrospun nanofiber composites of PLA-QC, and coaxial electrospun nanofiber composites of PLA-QCNF.

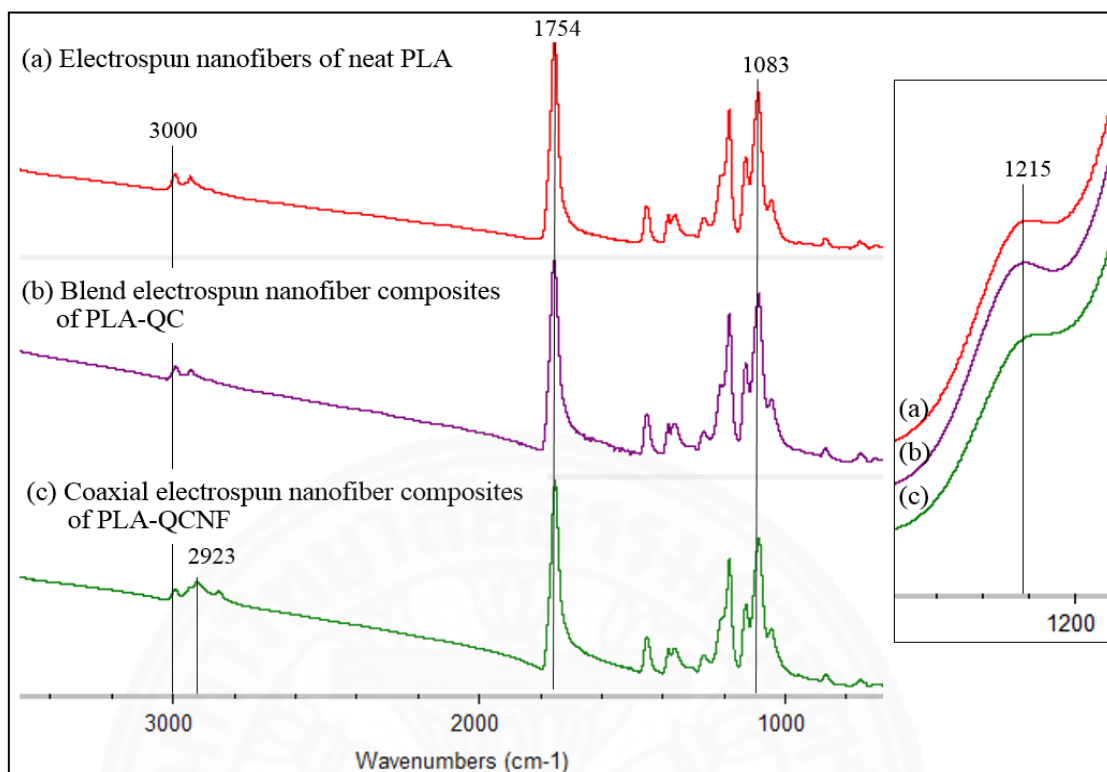


Figure 4.13 FTIR spectra in transmission mode of electrospun nanofibers of neat PLA, blend electrospun nanofiber composites of PLA-QC, and coaxial electrospun nanofiber composites of PLA-QCNF.

Figure 4.14 (a) shows that neat PLA nanofibers possess a smooth surface morphology with an average diameter of 1.145 μm . Bead defects are not observed in this neat PLA nanofibers. However, Figure 4.14 (b) shows that many fibers are fused together. This is due to an insufficient evaporation rate of the solvents during electrospinning (Ding, B. & Yu, J. (Eds.), 2014).

Regarding blend electrospun nanofibers of PLA-QC, where the QC powder was added as a loaded component at a solid content of 10% (w/w), a smooth surface morphology of composite nanofibers is also observed. The results show that QC fragments presents at both outside and inside of PLA nanofibers. The morphology of the filaments in regions where QC are located both inside (Figure 4.15a) and outside (Figure 4.15b) of PLA nanofibers. This is likely because this consists of a portion of QC with particle sizes smaller and larger than that of the composite nanofibers. The composite nanofibers by blend electrospinning have an

average diameter of $0.964\ \mu\text{m}$. With comparison of SEM images between neat PLA and the blend electrospun nanofiber composites of PLA and QC, the porosity of composite nanoweb is dramatically higher than that of neat PLA nanoweb. This may affect a surface wettability or a deposition of water droplets in the nanoweb.

Likely, coaxial electrospun nanofiber composites of PLA-QCNF (Figure 4.16) present a smooth surface morphology with an average diameter of $1.019\ \mu\text{m}$. As a result, there is a presence of splitting droplet particles with spherical shape attached on the composite nanofibers. This may be attributed to the fact that the solvent of core is non-solvent of shell. Consequently, particles of splitting droplets are formed when the solvents meet.

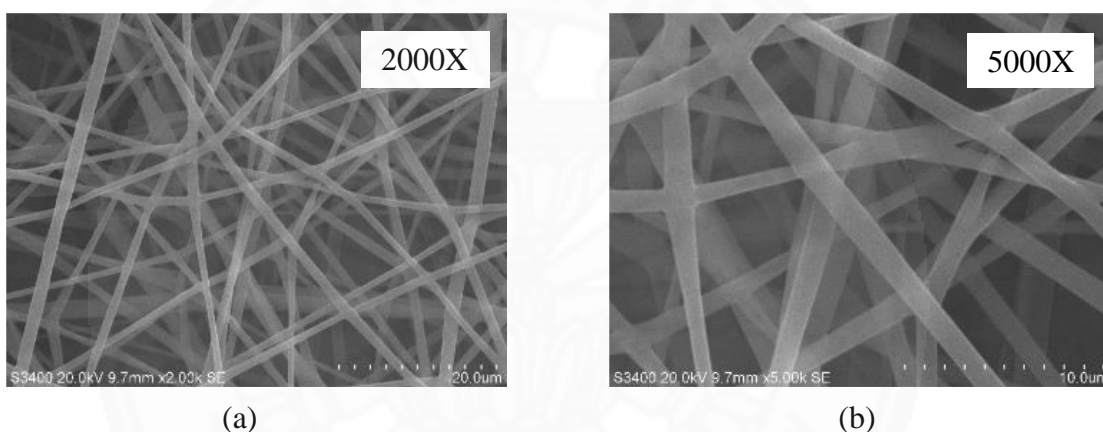


Figure 4.14 SEM images of electrospun nanofibers of neat PLA.

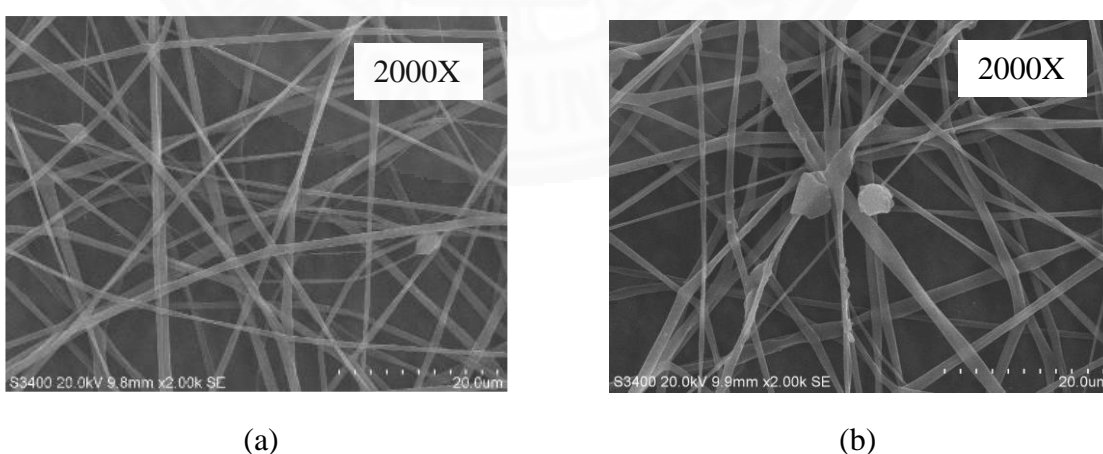


Figure 4.15 SEM images of blend electrospun nanofiber composites of PLA-QC.

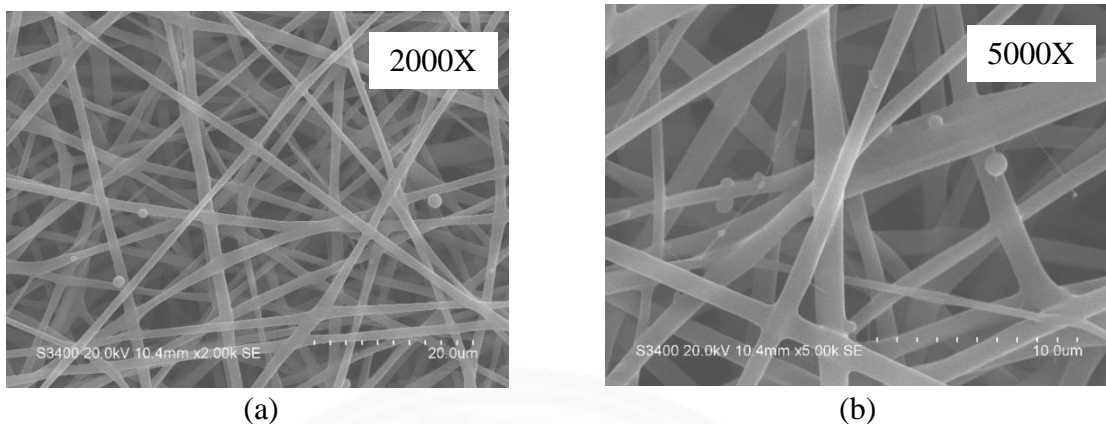


Figure 4.16 SEM images of coaxial electrospun nanofiber composites of PLA-QCNF

Surface wet behaviors of all sample (Figure 4.17) display hydrophobicity, causing that on the top surface of neat PLA and PLA composite nanofibers employing either QC or QCNF illustrate water droplets remained with an average apparent contact angle of $134\pm 1.97^\circ$, $134.85\pm 2.66^\circ$, and $132.10\pm 4.28^\circ$, respectively. Interestingly, there are no significant statistical difference in apparent contact angle of between neat PLA and PLA composite nanofibers employing either QC or QCNF. This is because of a combination of (1) roughness surface of the nanofibers causing from incorporated of QC particles, and splitting droplets of PLA and QCNF as presented in SEM results, and (2) hydrophobic nature of PLA (Dufficy et al., 2015; Oliveira et al., 2016).

To further verify repellent characterizations of all resulting nanofibers, water contact angles were also recorded over a time period of 30 min (Figure 4.18). At an initial deposition, all nanofiber samples display hydrophobicity. Apparent contact angles of all sample decrease over a duration of 30 min with different rates. With comparison of a $0.78^\circ/\text{min}$ decreasing rate of neat PLA nanofibers, the composite nanofibers presenting either QC or QCNF are slightly higher with a rates of $1.12^\circ/\text{min}$ and $0.90^\circ/\text{min}$, respectively. This may be corresponded to hydrophilicity of a presence of either QC or QCNF in nanofibers. In addition, the nanofiber composites employing QC shows the highest value of decreasing rate due to the fact that there is a lot of porosity in its nanoweb as illustrated in SEM results.



Figure 4.17 Surface wetting behavior of electrospun nanofibers of neat PLA, blend electrospun nanofiber composites of PLA-QC, and coaxial electrospun nanofiber composites of PLA-QCNF.

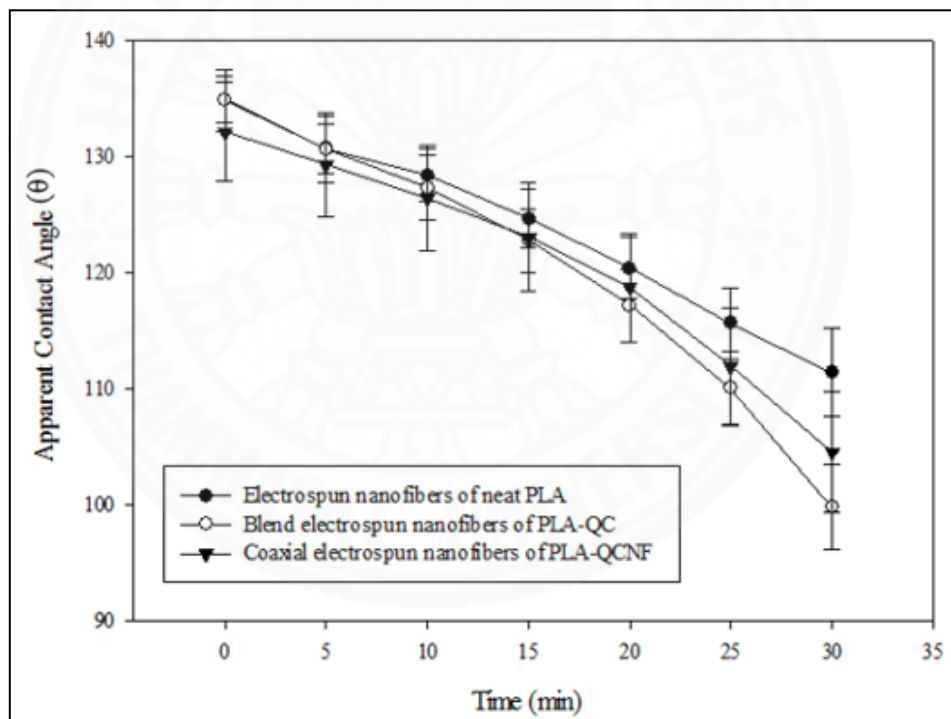


Figure 4.18 Apparent contact angle of electrospun nanofibers of neat PLA, blend electrospun nanofiber composites of PLA-QC, and coaxial electrospun nanofiber composites of PLA-QCNF over a duration of 30 min.

As summarized in Table 4.3, surface antibacterial activity and efficacy of coaxial electrospun nanofibers of PLA-QCNF were tested against *S. aureus* and *E. coli* under testing standard of JIS Z 2801-2010, i.e. membrane adhering method. The neat PLA electrospun nanofibers were evaluated as an untreated sample. It was found that the values of antibacterial activity and percent knockdown against *E. coli* are 0.01 and 2.94%, respectively, while those values against *S. aureus* are 0.10 and 21.01%, respectively. This agrees with previous results of MBC tests for QC suspensions, i.e. the value of MBC against *S. aureus* (0.0078% w/v) is noticeably higher than that against *E. coli* (2% w/v). However, the antibacterial activity cannot be judged to be effective, causing from that antibacterial activity is less than 2. This is because of 2 combination reasons: (1) a low content of QCNF in the fibers, and (2) the method evaluated antibacterial activity of surface of the materials, meaning that QC fragments incorporated in the nanoweb have no effect.

Table 4.3 Antibacterial activity and efficacy of electrospun nanofibers of neat PLA and coaxial electrospun nanofibers of PLA-QCNF against *S. aureus* (ATCC 6538) and *E.coli* (ATCC 8739), based on JIS Z 2801-2010

Sample	Test organism	
	<i>E. coli</i>	<i>S. aureus</i>
Untreatment sample: Electrospun nanofibers of neat PLA Number (CFU/cm ²)	6.38 x 10 ⁴	8.23 x 10 ³
Sample: Coaxial electrospun nanofibers of PLA-QC Number (CFU/cm ²)	6.19 x 10 ⁴	6.50 x 10 ³
Antimicrobial activity	0.01	0.10
% Reduction	2.94	21.01

Chapter 5

Conclusions and Recommendations

5.1 Research conclusions

De-starch cassava pulp (DCP) was utilized by an extraction of cellulose. The obtained cellulose was further surface modified via quaternization, resulting in quaternized cellulose (QC) as antibiotic agent. In order to use its property for specific use in biomedical applications, the QC was incorporated with polylactic acid (PLA) biocompatible plastics via various techniques, generating microparticles and nanofibers. This research can be summarized as follows:

5.1.1 Characterization of quaternized cellulose

After each treatment and modification processes, DCP, cellulose, and QC at various GTMAC content present different characteristics and properties. In terms of chemical structure, the extracted cellulose does not present peaks of hemicellulose and lignin components. All FTIR and NMR spectra of QC show distinct signals of methyl group of GTMAC, providing evidences of successful GTMAC grafting on the surface of cellulose. Results of crystalline index calculated from XRD and solid-state NMR spectra indicate that cellulose has higher value of crystalline index than DCP, due to the removal of amorphous domains from non-cellulosic compounds. QC with higher degree of GTMAC substitution exhibits lower values of crystalline index. Results of degree of substitution and cationization reaction efficiency of QC identify that an optimal molar ratio of GTMAC-to-AGU is 2:1. The optimal QC presents antibacterial activity against both Gram-positive and –negative bacteria. After passing QC aqueous suspension through a microfluidizer, QC was disintegrated and resulted in optically transparent and gel-like suspension of quaternized cellulose nanofibrils (QCNF).

5.1.2 Characterization of microparticles of PLLA-co-GMA copolymers and quaternized cellulose

Microparticles obtained from QC powder via a phase inversion emulsification (PIE) method show that certain amount of QC was successfully

incorporated into the microparticles, which present as spherical shape particles. However, irregular-shaped residual QC is also observed in the system. However, microparticles prepared from either QC or QCNF suspension via a PIE method possess irregular shape, in which QC and QCNF fragments are clearly observed on their surface. In contrast, microparticles prepared from either QC or QCNF suspension via PIE method and passing through a microfluidizer show a spherical shape of microparticles. In terms of particle size distributions, all microparticles prepared by PIE method and then passing through a microfluidizer present uniform particle size distribution, having smaller size, compared to the microparticles prepared by only PIE method.

5.1.3 Characterization of electrospun nanofibers of polylactide and quaternized cellulose

Electrospun nanofibers of neat PLA present a smooth surface morphology of fibers that many fibers are fused together. Compared with the neat PLA electrospun nanofibers, blending electrospun nanofibers of PLA and QC have a smooth fibers with a higher porosity of nanoweb and a presence of QC in both inside and outside of fibers. Coaxial electrospun nanofibers of PLA and QC have a smooth fiber's surface with spherical shape particles of splitting droplet attached on the composite fibers. All resulting nanofibers display surface's hydrophobicity. However, the coaxial electrospun nanofibers have no antibacterial activity.

5.2 Recommendations

5.2.1 Microparticles of PLLA-co-GMA copolymers and quaternized cellulose

To improve the property of microparticles, the obtained oil-in-water emulsion from PIE method should be passed through a microfluidizer immediately to prevent phase separation of the 2 components.

5.2.2 Electrospun nanofibers of polylactide and quaternized cellulose

In the coaxial electrospinning of PLA and QCNF process, hexane-fluoro ethanol should be applied to improve miscibility between organic and

non-organic solvents. In addition, antibacterial activity of coaxial electrospun nanofibers could be improved by loading higher QCNF contents in the fibers.



References

- Brettmann, B. K., Tsang, S., Forward, K. M., Rutledge, G. C., Myerson, A. S. & Trout, B. L. (2012). Free surface electrospinning of fibers containing microparticles. *Langmuir*, 28, 9714-9721.
- Bhardwaj, N. & Kundu, S. C. (2010). Electrospinning: a fascinating fiber fabrication technique. *Biotechnology advance*, 28(3), 325-347.
- Bshena, O. E. S. (2012). Synthesis of permanent non-leaching antibacterial polymer nanofibers. Retrieved April 25, 2017, from <http://scholar.sun.ac.za/handle/10019.1/20160>
- Chaiyasat, P., Islam, Md. Z. & Chaiyasat, A. (2013). Preparation of poly(divinylbenzene) microencapsulated octadecane by microsuspension polymerization: oil droplets generated by phase inversion emulsification. *RSC Advances*, 3, 10202–10207.
- Chen, L., Bai, Y., Liao, G., Peng, E., Wu, B., Wang, Y., Zeng, X. & Xie, X. (2013). Electrospun Poly(L-lactide)/Poly(ϵ -caprolactone) Blend Nanofibrous Scaffold: Characterization and Biocompatibility with Human Adipose-Derived Stem Cells. *PLoS One*, 8(8). Doi: 10.1371/journal.pone.0071265.
- Ciolacu, D., Ciolacu, F. & Popa, V. I. (2010). Amorphous cellulose - structure and characterization. *Cellulose Chemistry and Technology*, 45(1-2), 13-21.
- Costa, V. C., Costa, H. S. & Vasconcelos, W. L. (2007). Preparation of hybrid biomaterials for bone tissue engineering. *Materials Research*, 10, 21-26.
- Dalton, P.D., Klinkhammer, K., Salber, J., Klee, D. & Möller, M. (2006). Direct in vitro electrospinning with polymer melts. *Biomacromolecules*, 7(3), 686-690.
- Deepa, B., Abraham, E., Cherian, B. M., Bismarck, A., Blaker, J. J., Pothen, L. A. & Kottaisamy, M. (2011). Structure, morphology and thermal characteristics of banana nano fibers obtained by steam explosion. *Bioresource Technology*, 102, 1988-1997.
- Ding, B. & Yu, J. (Eds.). (2014). *Electrospun Nanofibers for Energy and Environmental Applications*, Nanostructure Science and Technology.

- Dufficy, M. K., Geiger, M. T., Bonino, C. A. & Khan, S. A. (2015). Electrospun ultrafine fiber composites containing fumed silica: from solution rheology to materials with tunable wetting. *Langmuir*, 31, 12455-12463.
- Fang, J. M., Sun, R. C. & Tomkinson, J. (2000). Isolation and characterization of hemicelluloses and cellulose from rye straw by alkaline peroxide extraction. *Cellulose*, 7, 87-107.
- Garrison, T. F., Murawski, A. & Quirino, R. L. (2016). Bio-based polymers with potential for biodegradability. *Polymer*, 8 (7), 262. Doi: 10.3390/polym8070262
- Gräsvik, J. (2013). Ionic liquids in bio-refining Synthesis and applications. Retrieved May 18, 2016, from <http://www.diva-portal.org/smash/get/diva2:619365/fulltext01.pdf>
- Greiner, A. & Wendorff, J. H. (2007). Electrospinning: fascinating method for the preparation of ultrathin fibers. *Angewandte Chemie International Edition*, 5670-5703.
- Gorshkova, M. Y., Volkova, I. F., Alekseeva, S. G., Molotkova, N. N., Skorikova, E. E. & Izumrudov, V. A. (2011). Water soluble modified chitosan and its interaction with a polystyrenesulfonate anion. *Polymer Science*, 53, 57-66.
- Hegde, R. R., Dahiya, A. & Kamath, M. G. (2005). Nanofiber nonwovens. Retrieved May 17, 2016, from <http://www.engr.utk.edu/mse/Textiles/Nanofiber%20Nonwovens.htm>
- Hon, DN-S. (1996). *Chemical modification of cellulose*. New York, Basel, Hong Kong: Marcel Dekker.
- Huanga, Z-M, Zhangb, Y.-Z., Kotakic, M. & Ramakrishna, S. (2003). A review on polymer nanofibers by electrospinning and their applications in nanocomposites. *Composites Science and Technology*, 63, 2223-2253.
- Huda, M. S., Mohanty, A. K., Drzal, L. T., Schut, E. & Misra, M. (2005). “Green” composites from recycled cellulose and poly(lactic acid): Physico-mechanical and morphological properties evaluation. *Journal of materials science*, 40, 4221-4229.
- Ibrahim, H. M. & El-Zairy E.M.R. (2015). Chitosan as a Biomaterial - Structure, Properties, and Electrospun Nanofibers. Retrieved May 18, 2016, from

<http://www.intechopen.com/books/concepts-compounds-and-the-alternatives-of-antibacterials/chitosan-as-a-biomaterial-structure-properties-and-electrospun-nanofibers>

- Kenawy, E., El-Shanshoury, A. R., Shaker, N. O., El-Sadek, B. M., Khattab, A. H. B. & Badr, B. I. (2011). Biocidal polymers: Synthesis, antimicrobial activity, and possible toxicity of poly (hydroxystyrenecomethylmethacrylate) derivatives. *Wiley Online Library*.
- Khalil, K. A., Fouad, H., Elsarnagawy, T. & Almajhdi, F. N. (2013). Preparation and characterization of electrospun PLGA/silver composite nanofibers for biomedical applications. *International Journal of Electrochemical Science*, 8, 3483-3493.
- LaCourse, N. L., Chicalo, K., Zallie, J. P. & Altieri, P. A. (1994). United State Patent No.
- Lee, J. W., Lee, H. Y., Park, S. H., Park, J. H., Kim, J. H., Min, B. H. & Kim, M. S. (2016). Preparation and evaluation of dexamethasone-loaded electrospun nanofiber sheets as a sustained drug delivery system. *Materials*, 9, 175. Doi: 10.3390/ma9030175.
- Li, D. & Xia, Y. (2004). Electrospinning of nanofibers: reinventing the wheel. *Advanced materials*, 15(14), 1151-1170.
- Li, G., Fu, Y., Shao, Z., Zhang, F. & Qin, M. (2015). Preparing cationic cellulose derivation in NaOH/urea aqueous solution and its performance as filler modifier. *BioResources*, 10(4), 7782-7794.
- Lopina, S. T., Wu, G., Merrill, E.W. & Griffith-Cima, L. (1996). Hepatocyte culture on carbohydrate-modified star polyethylene oxide hydrogels. *Biomaterials*. 17, 559-569.
- LaCourse, N. L., Chicalo, K., Zallie, J. P. & Altieri, P. A. (1994). United State Patent No.
- Mashhadikhan, M., Soleimani, M., Parivar, K. & Yaghmaei, P. (2015). ADSCs on PLLA/PCL Hybrid Nanoscaffold and Gelatin Modification: Cytocompatibility and Mechanical Properties. *Avicenna Journal of Medical Biotechnology*, 7 (1), 32-38.

- Mariño, M., Silva, L. L. D., Durán, N. & Tasic, L. (2015). Enhanced Materials from Nature: Nanocellulose from Citrus Waste. *Molecules*, 20, 5908-5923.
- Montagnac, J. A., Devis, C. R. & Tanumihardjo, S. A. (2009). Nutritional value of cassava for use as a staple food and recent advances for improvement. *Comprehensive reviews in food science and food safety*, 8, 181-194.
- Nazir, M. S., Wahjoedi, B. A., Yussof, A. W. & Abdullah, M. A. (2013). Eco-friendly extraction and characterization of cellulose from oil palm empty fruit bunches. *Bioresources*, 8(2), 2161-2172.
- Nechporchuk O. (2015) Cellulose nanofibers for the production of bionanocomposites. Retrieved April 25, 2017, from <https://tel.archives-ouvertes.fr/tel-01244186/document>
- Neto, W. P. F., Silvério, H. A., Dantas, N. O. & Pasquini, D. (2013). Extraction and characterization of cellulose nanocrystals from agro-industrial residue – Soy hulls. *Industrial Crops and Products*, 42, 480-488.
- Narayanan, N., Roychoudhury, P. K. & Srivastava, A. (2004). L(+) lactic acid fermentation and its product polymerization. *Electronic journal of biotechnology*, 7, 167-U162.
- Ojha, S. S., Stevens, D. R., Hoffman, T. J., Stano, K., Klossner, R., Scott, M. C., Krause, W., Clarke, L. I. & Gorga, R. E. (2008). Fabrication and characterization of electrospun chitosan nanofibers formed via templating with polyethylene oxide. *Biomacromolecules*, 9 (9). doi: 10.1021/bm800551q
- Oliveira, J. E., Mattoso, L. H. C., Orts, W. J. & Medeiros, E. S. (2013). Structural and morphological characterization of micro and nanofibers produced by electrospinning and solution blow spinning: a comparative study. *Advances in Materials Science and Engineering*, 2013, 14. Retrieved May 11, 2016, from <http://www.hindawi.com/journals/amse/2013/409572/>
- Park, D., Finlay, J. A., Ward, R. J., Weinman, C. J., Krishnan, S., Paik, M., Sohn, K. E., Callow, M. E., Callow, J. A., Handlin, D. L., Willis, C. L., Fischer, D. A., Angert, E. R., Kramer, E. J. & Ober, C. K. (2010). Antimicrobial behavior of semifluorinated-quaternized triblock copolymers against airborne and marine microorganisms. *ACS Applied Materials and Interfaces*, 2(3), 703-711.

- Pei, A., Butchosa, N., Berglund, L. A. & Zhou, Q. (2013). Surface quaternized cellulose nanofibrils with high water absorbency and adsorption capacity for anionic dyes. *Journal of Soft Matter*, 9(6), 2047-2055.
- Pereira, P. H. F., Voorwald, H. C. J., Cioffi, M. O. H., Mulinari, D. R., Luz, S. M. D. & Silva & M. L. C. P. D. (2011). Sugarcan bagasse pulping and bleaching: thermal and chemical characterization. *BioResource*, 6(3), 2471-2482.
- Petchsuk, A., Submark, W. & Opaprakasit, P. (2012). Development of crosslinkable poly (lactic acid-co-glycidyl methacrylate) copolymers and their curing behaviors. *Polymer journal*, 45(4), 406-412.
- Perazzo, A., Preziosi, V. & Guido S. (2015). Phase inversion emulsification: Current understanding and applications. *Advances in Colloid and Interface Science*, 222, 581-599.
- Popelka, S. Machová, L. K. & Rypáček, F. (2007). Adsorption of poly (ethylene oxide)-block-poly lactide copolymers on polylactide as studied by ATR-FTIR spectroscopy. *Journal of colloid Interface Science*, 308, 291-299.
- Puoci, F., Iemma, F., Spizzirri, U. G., Cirillo, G., Curcio, M. & Picci, N. (2008). Polymer in Agriculture: a Review. *American Journal of Agricultural and Biological Sciences*, 3(1), 299-314.
- Oliveira, J. E., Mattoso, L. H. C., Orts, W. J. & Medeiros, E. S. (2013). Structural and morphological characterization of micro and nanofibers produced by electrospinning and solution blow spinning: a comparative study. *Advances in Materials Science and Engineering*. Retrieved May 11, 2016, from <http://www.hindawi.com/journals/amse/2013/409572/>
- Raeisi, S., M., Tabatabaei, M., Ayati, B., Ghafari, A. & Mood, S., H. (2015). A novel combined pretreatment method for rice straw using optimized EMIM [Ac] and mild NaOH. *Waste biomass Valor*. DOI: 10.1007/s12649-015-9437-5.
- Rieger, K. A., Birch, N. P. & Schiffman, J. D. (2013). Design electrospun nanofiber mats to promote wound healing - a review. *Journal of Materials Chemistry B*, 1, 4531-4541.
- Roy, D., Knapp, J. S., Guthrie, J. T. & Perrier, S. (2008). Antibacterial cellulose fiber via RAFT surface graft polymerization. *Biomacromolecules*, 9, 91-99.

- Saelee, K., Yingkamhaeng, N., Nimchua, T. & Sukyai, P. (2014). Extraction and characterization of cellulose from sugarcane bagasse by using environmental friendly method. *The 26th Annual Meeting of the Thai Society for Biotechnology and International Conference*, 162-168.
- Sajjan, A. M., Kumar, B. K. J., Kittur, A. A. & Kariduraganavar M. Y. (2013). Development of novel grafted hybrid PVA membranes using glycidyltrimethylammonium chloride for pervaporation separation of water–isopropanol mixtures. *Journal of Industrial and Engineering Chemistry*, 19, 427-437.
- Sajjan, A. M., Premakshi, H. G. & Kariduraganavar, M. Y. (2015). Synthesis and characterization of GTMAC grafted chitosan membranes for the dehydration of low water content isopropanol by pervaporation. *Journal of Industrial and Engineering Chemistry*, 25, 151-161.
- Salajkova', M., Berglund, L. A., & Zhou, Q. (2012). Hydrophobic cellulose nanocrystals modified with quaternary ammonium salts. *Journal of Materials Chemistry*, 22, 19798-19805.
- Saralidze, K., Koole, H., L. & Knetsch, L.W. M. (2010). Polymeric microspheres for medical applications. *Materials*, 3, 3537-3564.
- Seyedjafari, E., Soleimani, M., Ghaemi, N. & Sarbolouki, M. N. (2011). Enhanced osteogenic differentiation of cord blood-derived unrestricted somatic stem cells on electrospun nanofibers. *J Mater Sci: Mater Med*, 22, 165-174.
- Seyedjafari, E., Soleimani, M., Ghaemi, N., & Shabani, I. (2010). Nanohydroxyapatite-Coated Electrospun Poly(L-lactide) Nanofibers Enhance Osteogenic Differentiation of Stem Cells and Induce Ectopic Bone Formation. *Biomacromolecules*, 11, 3118-3125.
- Song, Y., Sun, Y., Zhang, X., Zhou, J. & Zhang, L. (2008). Homogeneous quaternization of cellulose in NaOH/urea aqueous solutions as gene carriers, *Biomacromolecules*, 9, 2259-2264.
- Song, Y., Zhang, J., Gan, W., Zhou, J. & Zhang, L. (2010). Flocculation properties and antimicrobial activities of quaternized celluloses synthesized in NaOH/urea aqueous solution. *Ind. Eng. Chem. Res.*, 49, 1242-1246.

- Siedenbiedel, F. & Tiller, J. C. (2012). Antimicrobial polymers in solution and on surfaces: overview and functional principles. *Polymers*, 4, 46-71.
- Tang, R., Zhang, Y., Zhang, Y. & Yu, Z. (2016). Synthesis and characterization of chitosan based dye containing quaternary ammonium group. *Carbohydrate Polymers*, 139, 191-196.
- Wang, W. (2005). A study on the absorption properties of quaternized cellulose. Retrieved May 18, 2016, from https://etd.auburn.edu/bitstream/handle/10415/829/WANG_WEIJUN_40.pdf?sequence=1
- Wang, Y., Shi, W., Yu, Yun & Chen, X. (2009). Synthesis and characterization of properties of quaternary ammonium cationic cellulose. *IEEE*.
- Wertz, J.-L., Bédué, O. & Mercier, J. P. (2010). *Cellulose science and technology*. Swiss: EPFL Press.
- Xue, Y., Xiao, H. & Zhang, Y. (2015). Antimicrobial polymeric materials with quaternary ammonium and phosphonium salts. *International Journal of Molecular Sciences*, 16(2), 3626-3655.
- Yu, Y., Kong, L., Li, L., Li, N. & Yan, P. (2015). Antitumor activity of doxorubicin-loaded carbon Nanotubes Incorporated poly(Lactic-Co-Glycolic Acid) electrospun composite nanofibers. *Nanoscale Research Letter*. Doi: 10.1186/s11671-015-1044-7
- Zamana, M., Xiaoa, H., Chibanteb, F. & Ni, Y. (2012). Synthesis and characterization of cationically modified nanocrystalline cellulose. *Carbohydrate Polymers*, 89, 163-170.



Appendices

Appendix A

Calculation of GTMAC-to-AGU molar ratio

Molecular weight of Anhydroglucose unit (AGU) is 162 g/mol

Properties of glycidyltrimethylammonium chloride (GTMAC) solution:

- Molecular weight is 151.63 g/mol
- Concentration is 90% (w/w)
- Density is 1.13 g/mL

1. Calculation of the amount of AGU in 1000 mg of cellulose

$$\begin{aligned}\text{The amount of AGU} &= \frac{1000 \times 10^{-3} \text{ g}}{162 \text{ g/mol}} \\ &= 6.1728 \times 10^{-3} \text{ mol}\end{aligned}$$

2. Calculation of the amount of GTMAC using in quaternary ammonium cationic cellulose preparation

- Converting from 6.1728×10^{-3} mol of GTMAC to mass
GTMAC mass = $(6.1728 \times 10^{-3} \text{ mol}) (151.63 \text{ g/mol})$
= 0.9360 g

For molar ratio of [1:1] between GTMAC and AGU,

$$\begin{aligned}\text{The amount of GTMAC added} &= \frac{(0.9360 \text{ g})}{\left(1.13 \frac{\text{g}}{\text{mL}}\right)(0.9)} \\ &= 0.9203 \text{ mL} \\ &= 920.3 \mu\text{L}\end{aligned}$$

For molar ratio of [2:1] between GTMAC and AGU,

$$\begin{aligned}\text{The amount of GTMAC added} &= 920.3 \times 2 \\ &= 1840.7 \mu\text{L}\end{aligned}$$

For molar ratio of [3:1] between GTMAC and AGU,

$$\begin{aligned}\text{The amount of GTMAC added} &= 920.3 \times 3 \\ &= 2760.9 \mu\text{L}\end{aligned}$$

Appendix B

Proof equation of degree of substitution

Molecular weight of GTMAC = 151.5 g

Molecular weight of Anhydroglucose unit (AGU) is 162 g/mol

Assumption: Weight of sample = 100 g

Therefore, weight of nitrogen in sample is %N

Step 1: To determine GTMAC content in sample (%GTMAC)

1 mol of GTMAC having one atom of nitrogen means that

GTMAC 151.5 g have Nitrogen 14 g

100 g of sample having nitrogen (%N) means that

$$\%GTMAC = \frac{151.5}{14} \times (\%N) \quad (B.1)$$

To determine mole of GTMAC in 100 g of sample:

$$\text{Mole of GTMAC} = \frac{\%GTMAC}{\text{Molecular weight of GTMAC}} \quad (B.2)$$

Instead of 'Equation (B.1) in 'Equation (B.2)'

$$\text{Mole of GTMAC} = \left(\frac{151.5}{14} \times (\%N) \right) \times \frac{1}{151.5}$$

$\text{Mole of GTMAC} = \frac{\%N}{14} \quad (B.3)$

Step 2: To determine AGU in sample (%AGU)

$$\%AGU = (100 \text{ g sample}) - (\%GTMAC) \quad (B.4)$$

Instead of 'Equation (B.1) in 'Equation (B.4)'

$$\%AGU = (100 \text{ g sample}) - \left(\frac{151.5}{14} \times (\%N) \right) \quad (B.5)$$

To determine mole of GTMAC in 100 g of sample:

$$\text{Mole of AGU} = \frac{\%AGU}{\text{Molecular weight of AGU}} \quad (B.6)$$

Instead of 'Equation (B.6) in 'Equation (B.6)'

$\text{Mole of AGU} = (100 \text{ g sample}) - \left(\frac{151.5}{14} \times (\%N) \right) \times \frac{1}{162} \quad (B.7)$

Step 3: To determine degree of substitution (DS)

$$DS = \frac{\text{mole of GTMAC}}{\text{mole of AGU}} \quad (\text{B.8})$$

Instead of 'Equation (B.3) and (B.7)' in 'Equation (B.8)'

$$DS = \frac{\%N}{14} \times \frac{1}{(100 \text{ g sample}) - \left(\frac{151.5}{14} \times (\%N)\right) \times \frac{1}{162}}$$

$DS = \frac{162 (\%N)}{1400 - 151.5 (\%N)}$



Appendix C

Crystalline indices from X-ray diffractogram

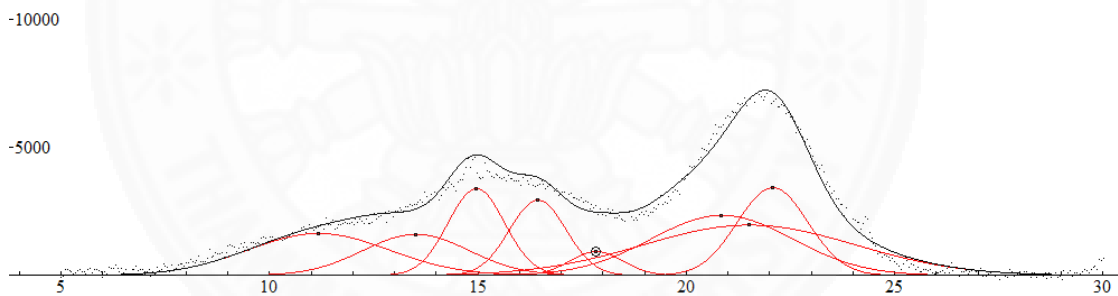
The crystallinity index (CI) of all samples were calculated as the ratio of crystalline area to the entire area via peak de-convolution method (Park et al, 2010).

$$CI (\%) = \left[\frac{\text{Crystalline Area}}{\text{Total Area}} \right] \times 100$$

Peak de-convolution method is a separation of amorphous and crystalline regions to diffractogram by a curve-fitting process (Fityk software). There are two main assumptions in the method:

- (1) Gaussian function are used for de-convolution of diffractogram
- (2) Amorphous region is predicted to be broad peaks, and peak at around 21.5°

De-starch cassava pulp (DCP)

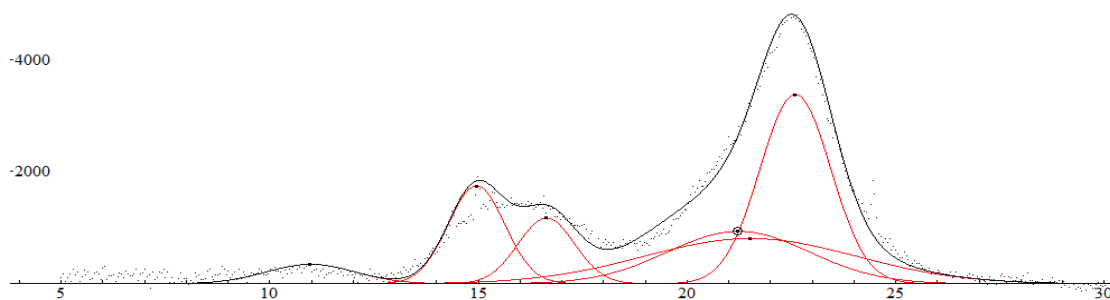


Amorphous		Crystalline	
Peak (°)	Area	Peak (°)	Area
11.2	6982.90	15.0	5773.67
13.5	5131.68	16.4	5017.75
17.8	1488.86	22.1	7302.24
20.8	10008.70		
21.5	12582.00		
Total Area	36194.14	Total Area	18093.66

$$CI (\%) = \frac{18093.66}{18093.66 + 36194.14} \times 100 = 33.33 \%$$

Figure C-1 X-ray diffractogram of DCP

Cellulose

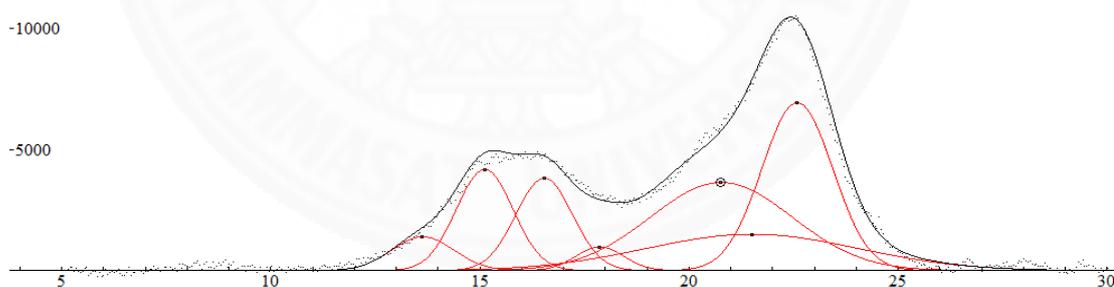


Amorphous		Crystalline	
Peak (°)	Area	Peak (°)	Area
11.0	920.425	22.6	7184.41
21.0	3902.21	14.9	2970.29
21.5	5139.57	16.6	1990.68
Total Area	9962.205	Total Area	12145.38

$$CI (\%) = \frac{12145.38}{12145.38 + 9962.21} = 54.94 \%$$

Figure C-2 X-ray diffractogram of cellulose

QC [1:1]

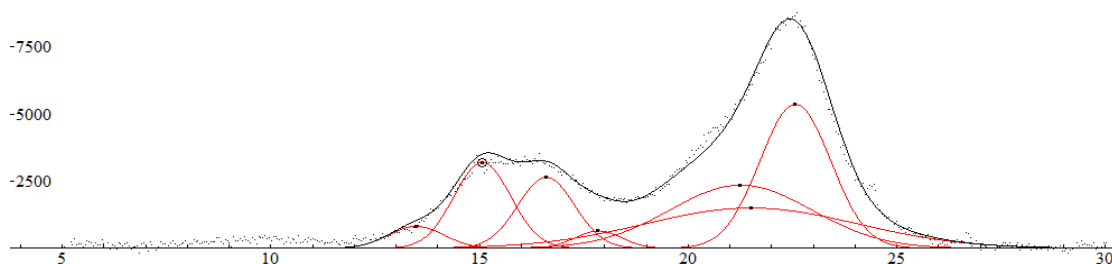


Amorphous		Crystalline	
Peak (°)	Area	Peak (°)	Area
13.6	2606.46	15.1	7102.12
17.9	1406.92	16.53	6488.99
20.8	15478.50	22.6	14742.70
21.5	9580.20		
Total Area	29072.08	Total Area	28333.81

$$CI (\%) = \frac{28333.81}{28333.81 + 29072.08} = 49.36 \%$$

Figure C-3 X-ray diffractogram of QC [1:1]

QC [2:1]

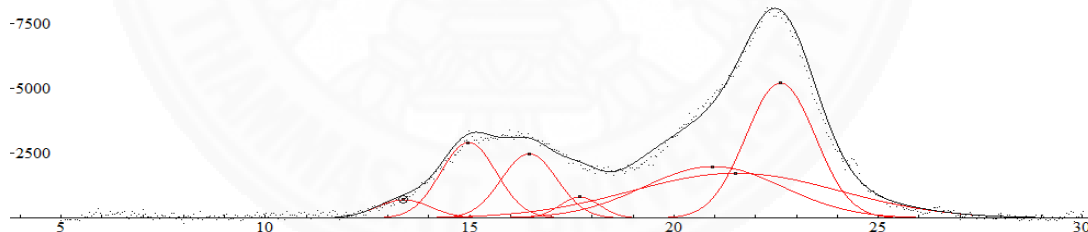


Amorphous		Crystalline	
Peak (°)	Area	Peak (°)	Area
13.5	1350.67	15.1	5450.07
17.8	896.25	16.59	4510.24
21.3	10023.60	22.6	11424.60
21.5	9580.20		
Total Area	21850.72	Total Area	21384.91

$$CI (\%) = \frac{21384.91}{21384.91 + 21850.72} = 49.46 \%$$

Figure C-4 X-ray diffractogram of QC [2:1]

QC [3:1]



Amorphous		Crystalline	
Peak (°)	Area	Peak (°)	Area
13.4	1168.19	15.0	4965.75
17.7	1000.36	16.45	4227.75
21.0	8473.16	22.6	11088.90
21.5	11049.20		
Total Area	21690.91	Total Area	20282.40

$$CI (\%) = \frac{20282.40}{20282.40 + 21690.91} = 48.32\%$$

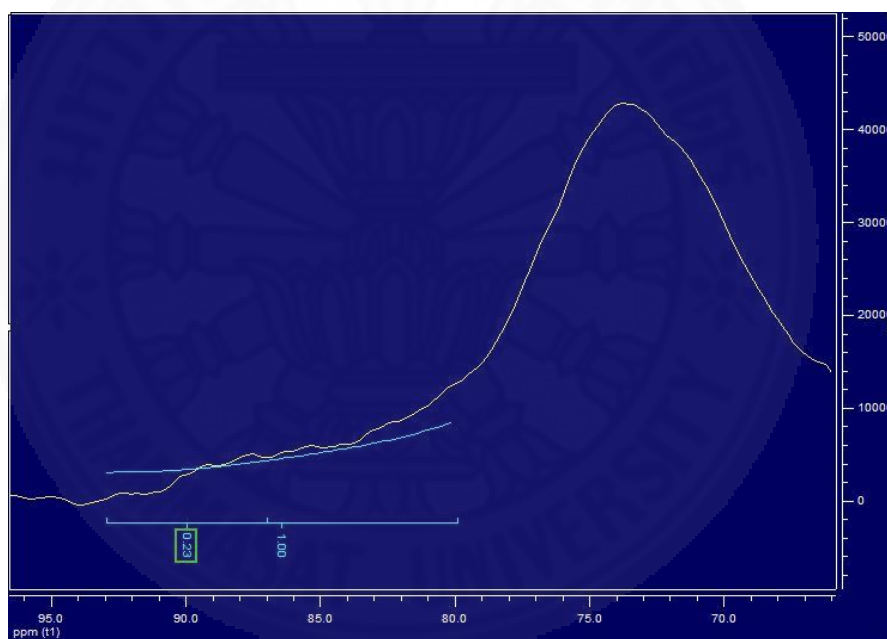
Figure C-5 X-ray diffractogram of QC [3:1]

Appendix D

Crystalline Indices from NMR

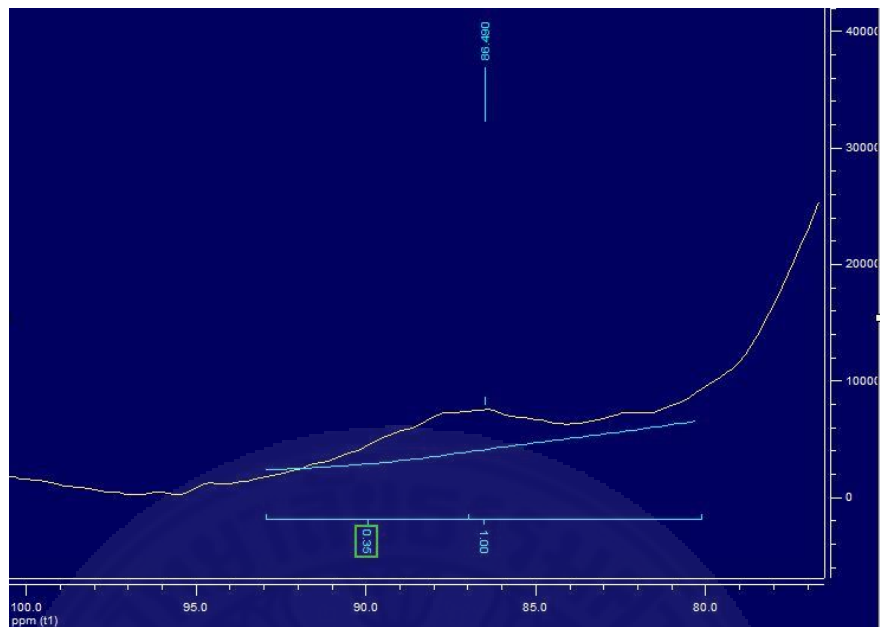
The CI is calculated via the NMR C4 peak separation method. The method is that the peak at 89 ppm is attributed to the C4 carbon in crystalline region of cellulose whereas the C4 carbon in amorphous region of cellulose attribute at 84 ppm (Park et al., 2010).

$$\text{CI (\%)} = \frac{\text{Area of the crystalline peak (integrating the peak from 87 to 93 ppm)}}{\text{Total area (integrating the peak from 80 to 93 ppm)}} \times 100$$



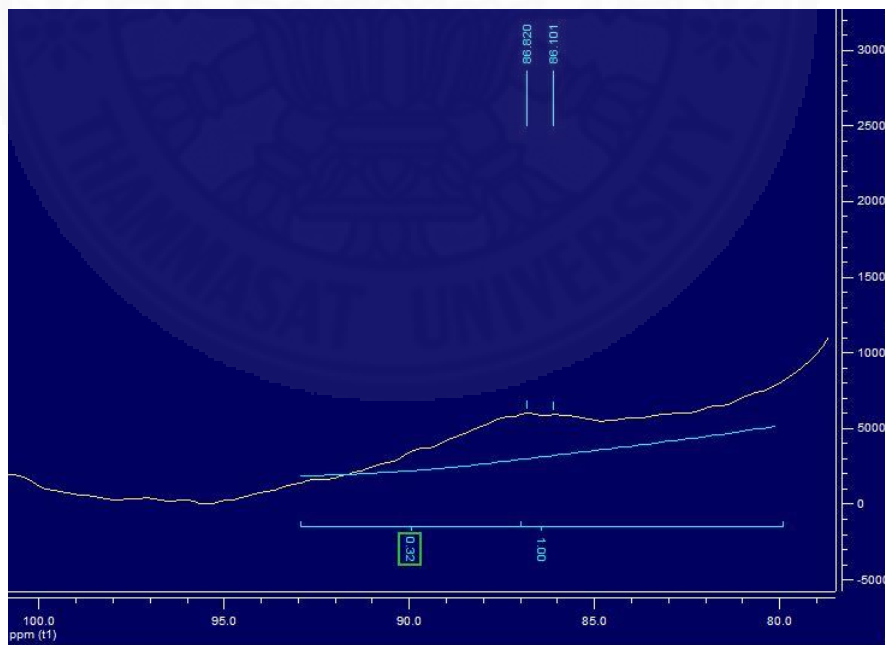
Crystalline Area	Total Area	CI (%)
0.2273	1.00	22.73

Figure D-1 NMR spectrum of DCP



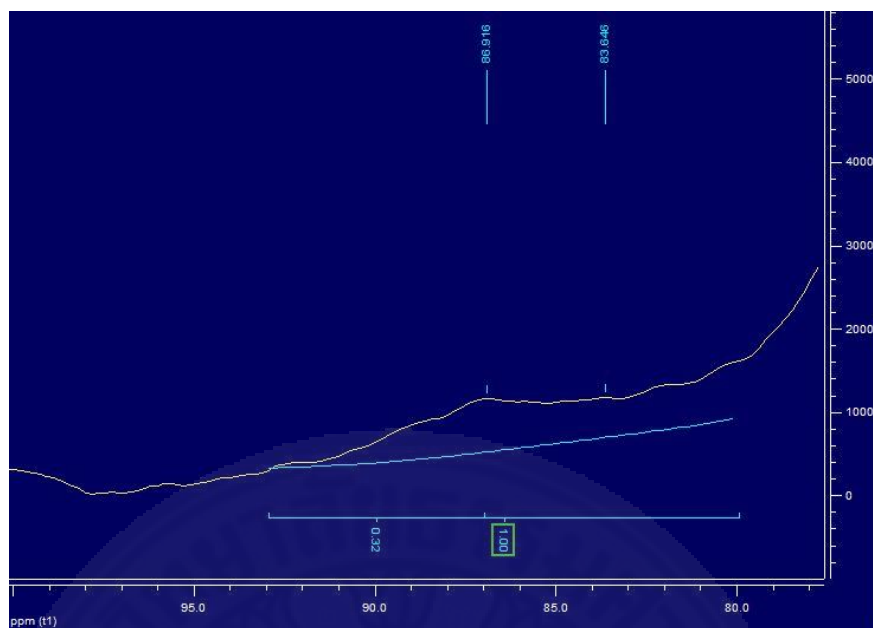
Crystalline Area	Total Area	CI (%)
0.3456	1.0000	34.56

Figure D-2 NMR spectrum of cellulose



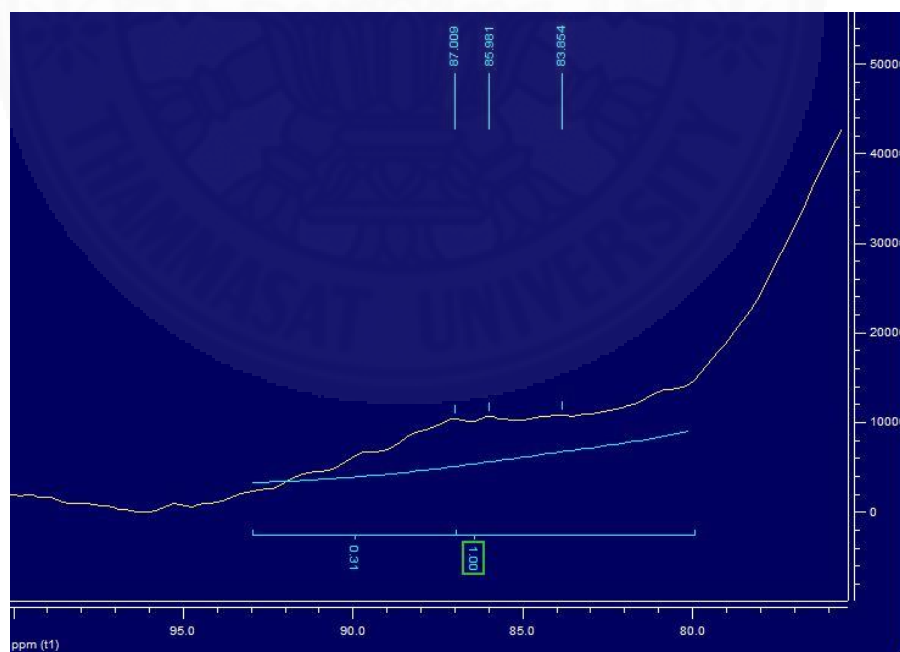
Crystalline Area	Total Area	CI (%)
0.3184	1.0000	31.84

Figure D-3 NMR spectrum of QC [1:1]



Crystalline Area	Total Area	CI (%)
0.3151	1.00	31.51

Figure D-4 NMR spectrum of QC [2:1]



Crystalline Area	Total Area	CI (%)
0.3091	1.00	30.91

Figure D-5 NMR spectrum of QC [3:1]

Appendix E
Particle size distribution of microparticles

Table E-1 Summary of particle size distribution of microparticles via different experimental approaches.

Samples	D10 (μm)	D50 (μm)	D90 (μm)	Median (μm)	Span ((D90-D10)/D50)
Microparticles employing QC powder via PIE method	17.59	39.78	70.99	39.78	1.34
Microparticles employing QC suspension via PIE method	11.18	37.33	99.77	37.34	2.37
Microparticles employing QCNF suspension via PIE method	10.30	24.08	104.56	24.08	3.91
Microparticles employing QC suspension via PIE method and Microfluidizer	0.92	1.08	16.70	1.08	14.67
Microparticles employing QCNF suspension via PIE method and Microfluidizer	0.34	0.52	25.58	0.52	48.08

Appendix F

Measured diameters of nanofibers from ImageJ software

Table F-1 Measured diameter of electrospun nanofibers of neat PLA

No.	Diameter (μm)	No.	Diameter (μm)	No.	Diameter (μm)
1	1.229	32	0.893	63	0.887
2	0.702	33	1.404	64	1.073
3	0.744	34	0.993	65	1.211
4	0.993	35	0.772	66	1.012
5	1.404	36	1.241	67	1.068
6	1.123	37	1.299	68	0.853
7	0.983	38	1.042	69	1.211
8	1.263	39	0.912	70	1.091
9	0.772	40	1.053	71	0.848
10	1.199	41	1.334	72	1.243
11	1.191	42	1.489	73	1.161
12	1.290	43	1.241	74	0.992
13	1.737	44	0.943	75	1.096
14	1.290	45	1.141	76	1.021
15	0.893	46	1.588	77	1.382
16	0.912	47	1.184	78	0.977
17	1.263	48	1.168	79	1.012
18	1.638	49	1.061	80	0.794
19	1.404	50	0.912		
20	1.787	51	1.253		
21	1.184	52	1.093		
22	0.983	53	1.201		
23	0.842	54	0.948		
24	1.544	55	1.544		
25	0.844	56	1.191		
26	0.842	57	1.053		
27	1.123	58	1.935		
28	1.241	59	1.390		
29	1.191	60	1.193		
30	0.993	61	0.627		
31	1.787	62	1.190		

Table F-2 Measured diameter of blend electrospun nanofiber composites of PLA-QC

No.	Diameter (μm)	No.	Diameter (μm)	No.	Diameter (μm)
1	2.251	32	0.527	63	0.476
2	0.58	33	1.189	64	1.231
3	2.042	34	0.884	65	0.795
4	1.22	35	0.759	66	0.871
5	1.364	36	0.909	67	0.867
6	1.129	37	0.811	68	0.848
7	1.403	38	0.625	69	0.826
8	1.216	39	1.287	70	1.01
9	1.046	40	0.407	71	0.249
10	1.142	41	1.191	72	0.884
11	1.631	42	0.905	73	0.676
12	0.871	43	1.321	74	0.891
13	1.071	44	0.982	75	0.365
14	1.379	45	1.035	76	0.662
15	0.52	46	0.422	77	0.912
16	0.909	47	1.746	78	0.448
17	0.714	48	0.966	79	0.677
18	1.386	49	0.986	80	1.114
19	1.567	50	1.23		
20	1.061	51	0.59		
21	1.055	52	1.475		
22	1.463	53	1.402		
23	0.442	54	0.505		
24	0.976	55	0.601		
25	1.008	56	0.665		
26	1.852	57	1.079		
27	0.395	58	1.057		
28	0.672	59	0.758		
29	1.013	60	1.1		
30	0.482	61	0.992		
31	0.704	62	0.339		

Table F-3 Measured diameter of coaxial electrospun nanofiber composites of PLA-QCNF

No.	Diameter (μm)	No.	Diameter (μm)	No.	Diameter (μm)
1	1.195	32	1.261	63	0.983
2	1.247	33	0.791	64	0.894
3	0.732	34	0.900	65	1.202
4	0.986	35	0.869	66	1.152
5	0.933	36	0.712	67	1.135
6	0.705	37	1.011	68	1.100
7	0.817	38	1.362	69	1.035
8	1.236	39	1.117	70	1.154
9	1.034	40	1.083	71	1.310
10	0.877	41	1.087	72	1.146
11	1.105	42	1.162	73	1.176
12	1.176	43	1.109	74	1.196
13	0.817	44	1.369	75	1.036
14	1.290	45	0.974	76	1.145
15	1.150	46	0.513	77	1.572
16	0.840	47	1.095	78	1.044
17	1.096	48	0.665	79	1.060
18	1.199	49	1.082	80	0.629
19	0.958	50	0.987		
20	1.050	51	0.605		
21	1.196	52	0.855		
22	0.906	53	0.766		
23	1.112	54	0.841		
24	1.173	55	0.883		
25	1.011	56	1.048		
26	1.050	57	0.900		
27	0.700	58	1.443		
28	1.006	59	0.703		
29	0.828	60	1.370		
30	0.982	61	0.892		
31	1.261	62	0.771		

Appendix G

Coaxial electrospinning of PLA-QCNF with various shell feed rates

Table G-1 Results of coaxial electrospinning of PLA-QCNF with various shell feed rates.

Feed rate (mL/h)		Observation results during electrospinning process	Causes
Core	Shell		
1.1	> 0.4	Polymer solution attached at the tip of needle	Excess feed rate is not match to applied high voltage
1.1	≤ 0.4	Perfect nanofibers	-

Core solution: 12% (w/w) PLA solution in THF-DMF co-solvent; Shell solution: 3% (w/w) PVA, and 0.25% (w/w) QCNF in water

Fixed parameter:

Applied voltage = 12 kV; Spinning distance = 10 cm

Temperature ~ 25°C

Humidity ≥ 65%